Optimization Approaches for Parameter Estimation and Maximum Power Point Tracking (MPPT) of Photovoltaic Systems

Thesis submitted in accordance with the requirements of
the University of Liverpool for the degree of Doctor in Philosophy
by
Jieming Ma

August 2014

Declaration

1. Candidate's declarations:

I, Jieming Ma, hereby certify that this thesis, which is approximately 36,000 words in length, has been written by me, that it is the record of work carried out by me and that it has not been submitted in any previous application for a higher degree.

Date: November 9, 2014. Signature: Jieming Ma.

2. Supervisor's declarations:

I hereby certify that the candidate has fulfilled the conditions of the Resolution and Regulations appropriate for the degree of Doctor in Philosophy in the University of Liverpool and that the candidate is qualified to submit this thesis in application for that degree.

Date: November 9, 2014. Signature: Ka Lok Man.

Acknowledgement

I have been blessed to do my doctoral research in a privileged place. I would like to take this opportunity to thank those who have helped me in some way or another. Without their help, it would not have been possible for me to complete this thesis.

First of all, I would like to express my special thanks of gratitude to my supervisors, Dr. Ka Lok Man, Dr. Prudence W.H. Wong and Prof. Sheng-Uei Guan, who gave me the golden opportunity to do this project. Throughout the supervision process, I have not only learned the technical knowledge, but also acquired the attitude and spirit of research.

My heartfelt appreciation also goes to my examiners for their insightful comments and suggestions. My sincere gratitude also goes to Dr. Tiew On Ting and Dr. Nan Zhang for their excellent advice, inspiration, encouragement, and help throughout the duration of my PhD studies. My special thanks extend to my fellow research students and associates at University of Liverpool and Xi'an Jiaotong-Liverpool University. They are Dr. Yungang Zhang, Dr. Ting Wang, Dr. Chili Li, Dr. Xiangmeng Huang, Dr. Jie Ren, Dr. Chun Zhao, Dr. Jimin Xiao and Mr. Jude-Thaddeus Ojiaku. I highly appreciate their encouragement and help. I will treasure our friendship forever.

Last but not least, my deepest gratitude goes out to my parents, for their support, encouragement and patience during my pursuit of the Doctorate in Computer Science, and also to my dearest wife Chun Liu, who provided much support. It is to them that I dedicate this thesis.

Publications

1. Jieming Ma, Ka Lok Man, Tiew On Ting, Nan Zhang, Sheng-Uei Guan, and Prudence W. H. Wong, Approximate Single-Diode Photovoltaic Model for Efficient I-V Characteristics Estimation, *The Scientific World Journal*, vol. 2013, no. 230471, pp. 1-7, 2013.

2. Jieming Ma, Tiew On Ting, Ka Lok Man, Nan Zhang, Sheng-Uei Guan, and Prudence W. H. Wong, Parameter Estimation of Photovoltaic Models via Cuckoo Search, *Journal of Applied Mathematics*, vol. 2013, no. 362619, 1-8, 2013.

3. Jieming Ma, Ka Lok Man, Tiew On Ting, Nan Zhang, Sheng-Uei Guan, Prudence W. H. Wong, Eng Gee Lim, T. Krilaviius, D. Sauleviius, and Chi-Un Lei, Simple Computational Method of Predicting Electrical Characteristics in Solar Cells, *Electronics and Electrical Engineering*, vol. 20, no. 1, pp. 41-44, 2014.

4. Jieming Ma, Ka Lok Man, Tiew On Ting, Nan Zhang, Sheng-Uei Guan, Prudence W. H. Wong, Eng Gee Lim, T. Krilaviius, J. Kapoit-Dzikien, and Chi-Un Lei, Improving Power-Conversion Efficiency via a Hybrid MPPT Approach for Photovoltaic Systems, *Electronics and Electrical Engineering*, vol. 19, no. 7, pp. 57-60, 2013.

5. Ka Lok Man, Chi-Un Lei, Hemangee K. Kapoor, T. Krilaviius, Jieming Ma, and Nan Zhang, PAFSV: a Formal Framework for Specification and Analysis of SystemVerilog, *The Journal Computing and Informatics*, accepted for publication, 2014.

6. Jieming Ma, Ka Lok Man, Tiew On Ting, Nan Zhang, Sheng-Uei Guan, and Prudence W.H. Wong, DEM: Direct Estimation Method for Photovoltaic Maximum Power Point Tracking, *Procedia Computer Science*, vol. 17, pp. 537-544, 2013.

7. Jieming Ma, Ka Lok Man, Tiew On Ting, Nan Zhang, Sheng-Uei Guan, and Prudence W.H. Wong, Accelerating Parameter Estimation for Photovoltaic Models

via Parallel Particle Swarm Optimization, *IEEE International Symposium on Computer, Consumer and Control*, pp. 175-178, 2014.

8. Jieming Ma, Ka Lok Man, Tiew On Ting, Nan Zhang, Sheng-Uei Guan, and Prudence W.H. Wong, Estimation and Revision: A Framework for Maximum Power Point Tracking on Partially Shaded Photovoltaic Arrays, *IEEE International Symposium on Computer, Consumer and Control*, pp. 162-165, 2014.

9. Jieming Ma, Ka Lok Man, Tiew On Ting, Nan Zhang, Chi-Un Lei, and Ngai Wong, Low-Cost Global MPPT Scheme for Photovoltaic Systems under Partially Shaded Conditions, in *Proceedings of IEEE International Symposium on Circuits and Systems*, pp. 245-248, 2013.

10. Jieming Ma, Ka Lok Man, Tiew On Ting, Nan Zhang, Chi-Un Lei, and Ngai Wong, A Hybrid MPPT Method for Photovoltaic Systems via Estimation and Revision, in *Proceedings of IEEE International Symposium on Circuits and Systems*, pp. 241-244, 2013.

11. Jieming Ma, Ka Lok Man, Tiew On Ting, Hyunshin Lee, Taikyeong Jeong, Jong-Kug Sean, Sheng-Uei Guan, and Prudence W. H. Wong, Insight of Direct Search Methods and Module-Integrated Algorithms for MPPT of Stand-Alone Photovoltaic Systems, *Lecture Notes in Computer Science (LNCS2012)*, vol. 7513, pp. 468-476, 2012.

Abstract

Optimization techniques are widely applied in various engineering areas, such as modeling, identification, optimization, prediction, forecasting and control of complex systems. This thesis presents the novel optimization methods that are used to control Photovoltaic (PV) generation systems.

PV power systems are electrical power systems energized by PV modules or cells. This thesis starts with the introduction of PV modeling methods, on which our research is based. Parameter estimation is used to extract the parameters of the PV models characterizing the utilized PV devices. To improve efficiency and accuracy, we proposed sequential Cuckoo Search (CS) and Parallel Particle Swarm Optimization (PPSO) methods to extract the parameters for different PV electrical models. Simulation results show the CS has a faster convergence rate than the traditional Genetic Algorithm (GA), Pattern Search (PS) and Particle Swarm Optimization (PSO) in sequential processing. The PPSO, with an accurate estimation capability, can reduce at least 50% of the elapsed time for an Intel i7 quad-core processor.

A major challenge in the utilization of PV generation is posed by its non linear Current-Voltage (I-V) relations, which result in the unique Maximum Power Point (MPP) varying with different atmospheric conditions. Maximum Power Point Tracking (MPPT) is a technique employed to gain maximum power available from PV devices. It tracks operating voltage corresponding to the MPP and constrains the operating point at the MPP. A novel model-based two-stage MPPT strategy is proposed in this thesis to combine the offline maximum power point estimation using the Weightless Swarm Algorithm (WSA) with an online Adaptive Perturb & Observe (APO) method. In addition, an Approximate Single Diode Model (ASDM) is developed for the fast evaluations of the output power. The feasibility of the proposed method is verified in an MPPT system implemented with a Single-Ended Primary-Inductor Converter (SEPIC). Simulation results show the proposed MPPT method is capable of locating

the operating point to the MPP under various environmental conditions.

Contents

Declaration i

Acknowledgement ii

Publications iii

Abstract v

Contents xi

List of Figures xv

List of Tables xvii

Nomenclature xxii

1 Introduction 1

1.1 Background 1

1.2 Motivation 2

1.3 Aims and Objectives 4

1.4 Original Contribution 4

1.5 Thesis Organization 6

2 Literature Review **8**

2.1 A Review of Modeling Methods for Photovoltaic (PV) Cells 8

2.1.1 Ideal Single-Diode Model 10

2.1.2 Single-Diode Model 11

2.1.3 Double-Diode Model 11

2.1.4 PV Module Model 13

2.2 Research on Parameter Estimation for PV Electrical Models 14

2.2.1 Analytical Techniques 14

2.2.2 Numerical Techniques 16

2.2.3 Evolutionary Algorithm Techniques 17

2.3 Research on Maximum Power Point Tracking (MPPT) Methods 18

2.3.1 Direct Control 20

2.3.2 Indirect Control 22

2.3.3 Evolutionary Algorithm Techniques 24

2.4 Summary 25

3 Parameter Estimation of PV Model via Cuckoo Search **26**

3.1 Introduction 26

3.2 Related Work 27

3.3 Formulation of Parameter Estimation Problem 28

3.4 Cuckoo Search 30

3.5 Experiments and Results 32

3.5.1 Case Study 1: Parameter Estimation for a PV Cell at The Certain Irradiance Level 33

3.5.2 Case Study 2: Parameter Estimation for a PV Module at The Certain Irradiance Level 34

3.5.3 Case Study 3: Parameter Estimation for a PV Module under Different Environmental Conditions 36

3.6 Summary 39

4 Parameter Estimation of PV Model via Parallel Particle Swarm Optimization Algorithm 42

4.1 Introduction 43

4.2 Related Work 44

4.3 Problem Formulation 45

4.4 Parameter Estimation Algorithm 45

4.4.1 Sequential Particle Swarm Optimization 45

4.4.2 Implementation of Parallel Particle Swarm Optimization 47

4.5 Experiments and Results 50

4.5.1 Parameter Estimation Capability 51

4.5.2 Speedup and Parallel Efficiency 57

4.6 Summary 60

5 Maximum Power Point Tracking Using Model-Based Two-Stage Control Strategy 62

5.1 Introduction 63

5.2 Related Work 64

5.3 Approximate Single-Diode PV Model for Efficient I-V Characteristics Estimation 67

5.3.1 Conventional Single-Diode PV Model 67

5.3.2 Function Approximation 68
5.3.3 Approximate Single-Diode Model (ASDM) 69
5.3.4 Parameter Identification for The ASDM 70
5.3.5 Modeling a PV Array under Partial Shading Conditions 72
5.3.6 The Accuracy and Computational Efficiency of The ASDM . . . 74
5.4 Model-Based Two-Stage MPPT strategy 79
5.4.1 Maximum Power Point Estimation 80
5.4.2 Maximum Power Point Revision 83
5.4.3 The Two-Stage MPPT Strategy 86
5.5 Experimental Setup 88
5.6 Experiments and Results 91
5.6.1 Maximum Power Point Estimation Capability 92
5.6.2 The Performance of The Proposed MPPT Algorithm in a PV System under Steady Environmental Conditions 93
5.6.3 The Performance of The Proposed MPPT Algorithm in a PV System under Rapidly Changing Environmental Conditions . . . 94
5.6.4 The Performance of The Proposed MPPT Algorithm in a PV System under Gradually Changing Environmental Conditions . 94
5.7 Summary 95

6 Conclusions and Future Work **105**

A PV Physical Model Adopted in PSIM **108**

B The Experimental I-V Data of The R.T.C. France PV Cell **109**

C The Experimental I-V Data of The Photowatt-PWP 201 PV Module **110**

D The Experimental I-V Data of The KC200GT PV Module 111

List of Figures

1.1 Evolution of annual PV installations. 2

1.2 Current-voltage-power (I-V-P) curves of a PV array under uniform irradiance and partial shading conditions. 3

1.3 Block diagram of the proposed model-based two-stage PV control system. 5

2.1 Electrical diagram of the ideal single-diode model. 10

2.2 Electrical diagram of the single-diode model. 12

2.3 Electrical diagram of the double-diode model. 12

2.4 Block diagram of the parameter estimation method for PV electrical models. 16

2.5 Electrical characteristic curves of a MSX60 PV module under different atmospheric conditions: (a) I-V curves under various irradiance levels; (b) P-V curves under various irradiance levels; (c) I-V curves under various temperatures; (d) P-V curves under various temperatures. . . . 18

2.6 Operation of a PV array working under partial shading conditions: (a) A PV array with bypass diodes; (b) I-V and P-V curves of the PV array receiving various irradiance levels. 19

2.7 Flowchart depicting the P&O algorithm. 21

3.1 Convergence process of different optimization algorithms during the parameter estimation process of the SDC model. 34

3.2 The simulated I-V characteristic curves of the KC200GT PV module: (a) under different irradiance levels; (b) under different temperature levels. 37

3.3 A comparison of the individual absolute errors among different PV modeling methods: (a) under different irradiance levels; (b) under different temperature levels. 38

3.4 A comparison of the individual absolute errors between CS- and GA-based ISDM: (a) under different irradiance levels; (b) under different temperature levels. 41

4.1 Parallel computing framework utilizing a swarm of particles. 48

4.2 Flow chart of the PPSO algorithm: (a) The main program; (b) Parallel evaluations of RMS error. 49

4.3 Average evolutionary performance of the PPSO with various PV electrical models: (a) SDC; (b) DDC; (c) SDM; (d) DDM. 55

4.4 Distribution of the fitness values obtained by the PPSO with various PV electrical models: (a) SDC; (b) DDC; (c) SDM; (d) DDM. 56

4.5 The execution time and average fitness of the sequential parameter estimation for PV electrical models on Intel i7-4770k: (a) SPSO with the SDC; (b) SPSO with the DDC; (c) SPSO with the SDM; (d) SPSO with the DDM. 57

4.6 The execution time and average fitness of the parallel parameter estimation for PV electrical models on Intel i7-4770k: (a) PPSO with the SDC; (b) PPSO with the DDC; (c) PPSO with the SDM; (d) PPSO with the DDM. 58

5.1 PV array consisting of two series connected modules: (a) circuitry diagram; (b) block diagram. 73

5.2 Electrical characteristics of the PV array shown in Figure 5.1: (a) P-V curves; (b) I-V curve. 73

5.3 I-V curves of a MSX60 PV module at various cell temperatures 75

5.4 I-V curves of a KC200GT PV module at various irradiance levels 76

5.5 I-V curves of a KC200GT PV module at various cell temperatures . . . 76

5.6 Mean absolute errors of the PV models at different atmospheric conditions: (a) SQ150-PC; (b) MSX60; (c) KC200GT; (d) HIT 180 77

5.7 Simulation time of different PV models 79

5.8 Adaptive P&O algorithm. 85

5.9 Flow chart of the proposed model-based two-stage MPPT strategy. . . . 87

5.10 Process at gradual change insolation. 88

5.11 SEPIC converter current flow: (a) SEPIC circuit; (b) circuit with the switch closed and the diode off; (c) circuit with the switch open and the diode on. 89

5.12 Simulation model for PV array with the model-based two-stage MPPT method. 91

5.13 Evolution performance of the MPPE under various testing environment sets: (a) I (b) II (c) III (d) IV (e) V (f) VI (g) VII (h) VIII. 96

5.14 Estimated GMPPs on the P-V curve for various testing environment sets: (a) I (b) II (c) III (d) IV (e) V (f) VI (g) VII (h) VIII. 97

5.15 Time plot of the output power obtained with (a) P&O method under the environment set I (perturbation step = 0.2 V, initial voltage = 52 V); (b) PSO (swarm size = 5 particles, maximum generation = 6, $c_1 = c_2 = 2$, $w = 0.5$); (c) proposed method. 98

5.16 Time plot of the output power obtained with (a) P&O method under the environment set V (perturbation step = 0.2 V, initial voltage = 52 V); (b) PSO (swarm size = 5 particles, maximum generation = 6, $c_1 = c_2 = 2$, $w = 0.5$); (c) proposed method. 99

5.17 Time plot of the output power obtained with (a) P&O method under the environment set VII (perturbation step = 0.2 V, initial voltage = 52 V); (b) PSO (swarm size = 5 particles, maximum generation = 6, $c_1 = c_2 = 2$, $w = 0.5$); (c) proposed method. 100

5.18 Time plot of the output power obtained with the proposed method in different tests: (a) Test 1; (b) Test 2; (c) Test 3; (d) Test 4; (e) Test 5; (f) Test 6. 101

5.18 Time plot of the output power obtained with the proposed method in different tests: (a) Test 1; (b) Test 2; (c) Test 3; (d) Test 4; (e) Test 5; (f) Test 6. 102

5.19 The P-V curve of a PV array receiving gradually changing insolation. . 103

5.20 A PV array receiving gradually changing insolation: (a) irradiance G; (b) output power P_{pva}; (c) reference voltage V_{ref} and operating voltage V_{pva}. 104

List of Tables

2.1 Properties of various PV electrical models. 12

3.1 Estimated parameters of the SDC model using various methods. 33

3.2 Absolute errors of the simulated terminal current for the SDC model. . 35

3.3 Estimated parameters of the SDM using various methods. 35

3.4 Absolute errors of the simulated terminal current for the SDM. 36

3.5 Parameters of the KC200GT PV module obtained by the CS algorithm. 36

4.1 Estimated parameters of SDC and DDC on the R.T. France solar cell using various methods. 50

4.2 PPSO's search ranges for relevant models. 50

4.3 Absolute error e of the simulated terminal current on the R. T. C. France solar cell. 53

4.4 Absolute error e of the simulated terminal current on the Photowatt-PWP 201 PV module. 54

4.5 PPSO's speedup on heterogeneous computing platforms. 59

5.1 Extracted ASDM parameters for different PV modules. 75

5.2 Relative errors of the calculated I_{mp} at various irradiance levels. 78

5.3 Relative errors of the calculated I_{mp} at various temperature levels. . . . 78

5.4 Testing environment sets. 92

5.5 Testing sets for a PV array under rapidly changing environmental conditions. 94

Nomenclature

$\alpha,\ \beta$	Acceleration coefficients towards $pbest_i$ and $gbest$ respectively
$\epsilon_1,\ \epsilon_2$	Independent uniform random numbers within [0, 1]
ε	Root mean square error
d	Number of the measured data
$gbest^t$	The best solution among all participating particles for i^{th} dimension at time t , also known as global best
$pbest_i^t$	The best position for i^{th} dimension at time t of a particle, also known as personal best
$v_{i,j}^t$	Velocity for i^{th} particle in j^{th} dimension at time t
w	Inertia weight
$X_{i,j}^t$	Current position of i^{th} dimension at time t
ΔT	The difference between T and T_n
A_1	Ideality factor of the first diode modeling the diffusion current component
A_2	Ideality factor of the second diode modeling the recombination in the space charge region
E_g	Band gap energy of the semiconductor
E_{gn}	E_g at the STCs ($E_{gn} = 1.12eV$ for silicon cells and $E_{gn} = 1.6\ eV$ for the triple junction amorphous cells)
G	Irradiance
G_n	Irradiance at the STC

I-V	Current-Voltage
I	The terminal current of a PV cell
I'	The terminal current of a PV module
I_{mp}	The current at the maximum power point
I_{o_1}	Reserve saturation current of the first diode modeling the diffusion current component
I_{o_2}	Reverse saturation current of the second diode modeling the recombination in the space charge region
I_{phn}	Photocurrent at the STCs
I_{ph}	The photocurrent
I_{pva}	The terminal current of a PV array
I_{sc}	Short circuit current
k	Boltzmann constant ($1.380650 \times 10^{-23}\ J/K$)
K_i	Short circuit current coefficient
K_v	Open circuit voltage coefficient
N_s	Number of series connected cells in the module
P_{max}	The power at the maximum power point
q	Electron charge ($1.380650 \times 10^{-23}\ J/K$)
R_p	Shunt resistance
R_s	Series resistance
R_{pn}	Shunt resistance at the STCs
R'_p	The shunt resistance of a PV module
R_{sn}	Series resistance at the STCs
R'_s	The series resistance of a PV module
S	Speedup

T Cell temperature

T_n Cell temperature at the STCs

V The terminal voltage of a PV cell

V' The terminal voltage of a PV module

V_t Thermal voltage

V_{D_1} The electrical potential difference between the two ends of the diode

V_{mp} The voltage at the maximum power point

V_{oc} Open circuit voltage

V_{pva} The terminal voltage of a PV array

V_{ref} Reference voltage

V_{step} Perturbation step size

APIs Application Programming Interfaces

APO Adaptive Perturb & Observe

ASDM Approximate Single-Diode Model

BFA Bacterial Foraging Algorithm

C-Si Crystalline Silicon

CF Curve Fitting

CLSA Continuous Least Square Approximation

CPSO Chaos Particle Swarm Optimization

CPV Concentrating Photovoltaics

CS Cuckoo Search

DDC Double-Diode Cell model

DDM Double-Diode Module model

DD Double-Diode model

DE Differential Evolution

DLL Dynamic Link Library

EA Evolutionary Algorithm

FOCV Fractional Open-Circuit Voltage

FSCC Fractional Short-Circuit Current

GA Genetic Algorithm

GMPP Global Maximum Power Point

IEA-PVPS IEA-Photovoltaic Power Systems program

IEA International Energy Agency

ISD Ideal Single-Diode model

LMPP Local Maximum Power Point

LSO Least Square Optimization

LUT Look Up Table

MPPE Maximum Power Point Estimation

MPPR Maximum Power Point Revision

MPPT Maximum Power Point Tracking

PPSO Parallel Particle Swarm Optimization

PSO Particle Swarm Optimization

PS Pattern Search

PWM Pulse Width Modulation

RMS Root Mean Squared

SA Simulated Annealing

SDC Single-Diode Cell model

SDM Single-Diode Module model

SD Single-Diode model

SEPIC Single Ended Primary Inductance Converter

Si Silicon

SPSO Sequential Particle Swarm Optimization

STCs Standard Test Conditions

TD Three-Diode model

TPV Thermo-Photovoltaics

WSA Weightless Swarm Algorithm

Chapter 1

Introduction

This chapter first presents the background and motivation of the thesis work, which is followed by this project's aims and objectives. We highlight the main contributions on the topic of the application of artificial intelligence algorithms to parameter estimation and maximum power point tracking methods. A conclusion and future work of the thesis are provided at the end of the chapter.

1.1 Background

In 1839, a French experimental physicist Edmund Becquerel discovered the creation of a weak electrical current when exposing certain materials to sunlight [1,2]. He named this phenomenon the "Photovoltaic (PV) effect". Owing to the growing worldwide demand for electricity and increasing urgent need to tackle the global challenges of energy security, climate change and sustainable development, significant amount of research effort has been made on developing PV cells, which are basically semiconductors capable of converting the energy of light directly into electricity by the PV effect. Since the output power of PV cells is limited at high voltage levels, PV module, a connected assembly of PV cells, is usually used as an elementary component in large PV systems.

Today's PV technologies are more sophisticated than ever. A variety of silicon (Si) materials have been explored to increase the energy conversion efficiency and reduce production cost. The commercially available PV technologies can be grouped into two categories: wafer-based Crystalline Silicon (C-Si) and Thin-Flim (TF). The conversion efficiency of C-Si made PV modules is around 13-20%, while the conversion efficiency of TF made PV modules is around 6-12 % [3]. TF technologies use small amounts of

active materials and can be manufactured at a lower cost than the C-Si [4]. Recently, many emerging and novel PV technologies, such as Concentrating Photovoltaics (CPV), organic solar cells, advanced inorganic thin-films, Thermo-Photovoltaics (TPV), are already under investigation.

PV markets expand with advances of PV technologies. In light of the IEA-PVPS [1] report, the global PV market grew to at least 36.9 gigawatt (GW) in 2013 [3, 5]. As seen in Figure 1.1, the annual installed capacity has kept increasing over the last decade (from 2003 to 2013).

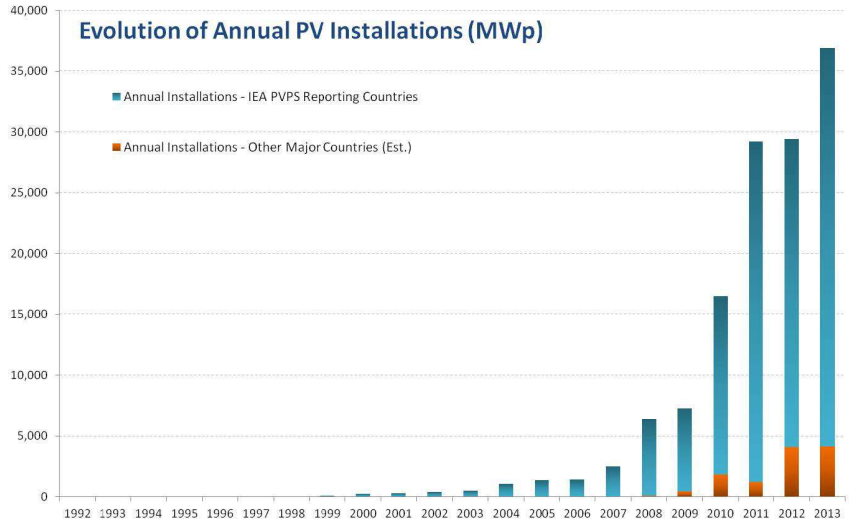

Figure 1.1: Evolution of annual PV installations.

Despite governmental incentives and technological advances, current PV deployment cost cannot compete with the initial installed cost of fossil sources of electrical generation in most cases [2]. This motivates the research for maximizing possible power generation from the PV plants over the entire time of operation as well as developing performance estimation tools.

1.2 Motivation

PV power generation not only can help power producers meet the future energy needs, but also can do so without producing much noise, toxic-gas emissions, or greenhouse gases [6].

[1] The International Energy Agency (IEA) is an autonomous organization working on energy research, forecasts, publications and statistics. Their photovoltaic power systems program is named the IEA-Photovoltaic Power Systems (IEA-PVPS) program.

From the point of view of power electronics, one goal can be addressed by maximizing the energy output of a given PV device. However, due to the varying atmospheric conditions, namely temperature T and irradiance G, the output power of a typical PV cell or module changes as a function of its operating point [7–10]. In addition, the entire or a part of the PV system might be wholly or partly shaded by trees, passing clouds, high building, etc., which are called partial shading conditions. Under these conditions, the power-voltage (P-V) characteristics of the system display multiple peaks (only one of which is the Global Maximum Power Point (GMPP); the rest are Local Maximum Power Points (LMPPs) as shown in Figure 1.2) [9,11]. The GMPP is particularly complicated to track when the insolation changes rapidly. These environmental conditions impose additional challenges for developing parameter estimation and Maximum Power Point Tracking (MPPT) algorithms. The inherent non-linear I-V relationship make the modeling work computationally costly. Typically, the process of parameter estimation takes a long execution time to obtain optimal model parameters from a large-size measured data. The existing MPPT algorithms are capable of tracking the operating point efficiently at the MPP under non-uniform solar irradiance level, but their performance deteriorates under partial shading conditions. Therefore, effective artificial intelligence optimization algorithms are applied in this work.

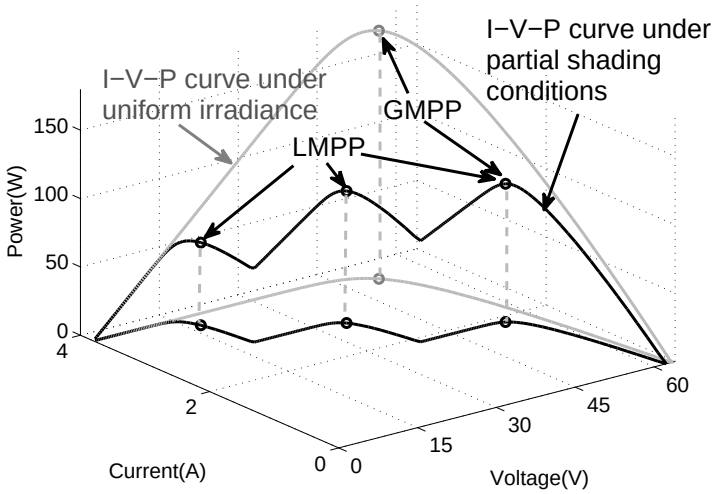

Figure 1.2: Current-voltage-power (I-V-P) curves of a PV array under uniform irradiance and partial shading conditions.

1.3 Aims and Objectives

Modern optimization algorithms such as Cuckoo Search (CS) and Particle Swarm Optimization (PSO) have demonstrated their power in dealing with various engineering optimization problems [12–15]. In this work, these optimization algorithms are applied in simulation and control of PV systems. The overall research objectives are as follows:

i. to study artificial optimization algorithms and to apply them in parameter estimation with serial and parallel programming frameworks,

ii. to estimate an optimization algorithm predicting the approximate GMPP locus with a simplified single-diode model,

iii. to develop a model-based two-stage MPPT strategy that is suitable for various environmental conditions (e.g. steady and rapidly changing environmental conditions).

1.4 Original Contribution

In this thesis, a sequential CS algorithm and a Parallel Particle Swarm Optimization (PPSO) method are designed to extract the parameters of PV models from the experimental data. The optimization concepts are applied in the task of MPPT as well. To deliver a good initial value for a conventional direct MPPT method, the proposed two-stage MPPT strategy combines offline Maximum Power Point Estimation (MPPE) with an online Adaptive Perturb & Observe (APO) method. Figure 1.3 shows a block diagram of the proposed PV control system, which consists of a parameter estimator and a PV-supplied DC-DC converter with the MPPT function block. The parameter estimator is applied to extract optimal parameters for the model. With the simulated terminal current and power (I, V), the MPPE derives an estimated voltage of the GMPP V_{mp}. The online MPPT algorithm further improves the tracking accuracy by small perturbation steps. In the control process, the operating point position is adapted by the input Pulse Width Modulation (PWM) signal. The current control block defines the duty cycle of the PWM according to the output voltage V_o and the reference voltage V_{ref}.

The major contributions of this thesis are summarized as follows:

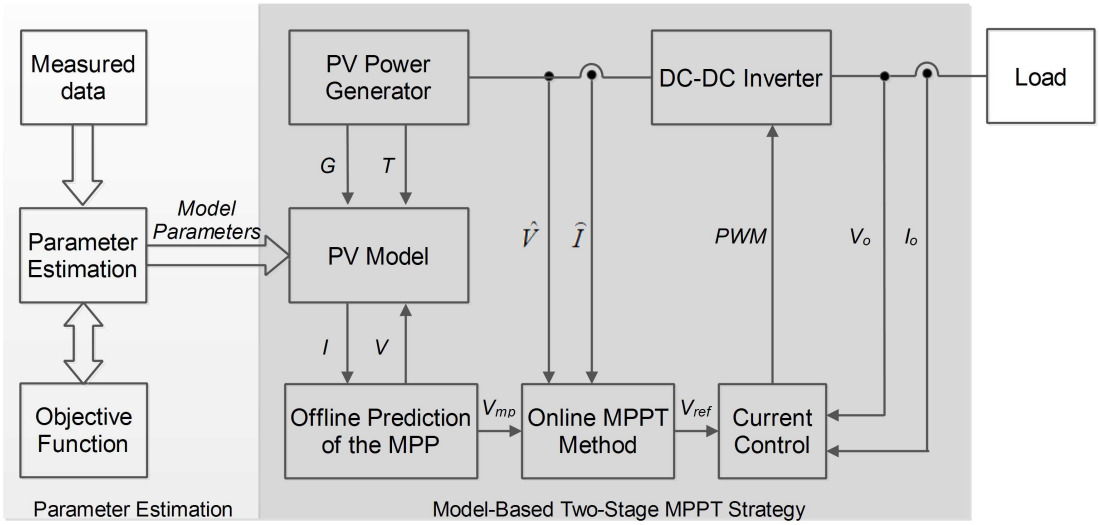

Figure 1.3: Block diagram of the proposed model-based two-stage PV control system.

i. The CS algorithm based parameter estimation method is proposed to obtain accurate PV system parameters. The CS is invented based on the inspiration of brood parasitic behavior of some Cuckoo species in combination with the Lévy flight behavior. With the aim of serving as a thorough evaluation of the CS algorithm in estimating the PV parameters, both single diode model and improved single diode model are considered. Two case studies are designed to estimate the CS algorithm in model parameters estimation: 1) a commercial 57mm diameter solar cell (R.T.C. France [16]) operating at the standard irradiance level; 2) a PV module (KC200GT multicrystal PV module) operating under varied environment conditions. The simulation results and experimental data show that the CS algorithm is capable of obtaining all the parameters with extremely high accuracy, depicted by a low Root Mean Squared (RMS) error. In this study, the proposed method outperforms Chaos Particle Swarm Algorithm (CPSO) [17], Genetic Algorithm (GA) [18], and Pattern Search (PS) [19].

ii. A parallel computing paradigm is considered to speed up the process of parameter estimation for the single-diode and double-diode model. The PSO is a derivative-free method particularly suitable for continuous variable problems and has been successfully applied to many engineering optimization problems. Its fitness evaluation function for a particle is independent of any other particle, and therefore it is performed in parallel in the proposed Parallel Particle Swarm Optimization (PPSO) method. The experimental I-V data of a R.T.C. France PV cell and a Photowatt-PWP 201 PV module comprising of 36 polycrystalline silicon cells

are used as test examples. The experiment and simulation results demonstrate the effectiveness of the proposed algorithm over two most common PV electrical models.

iii. An Approximate Single-Diode Model (ASDM) is developed to simplify the existing single diode model via function approximation approaches. The ASDM enables high speed predictions for the electrical characteristics of commercial PV cells and modules at a variety of atmospheric conditions. The proposed mathematical modeling approach is easy, straightforward and does not depend on iterative procedures to obtain solutions. The simulation results show that the calculated I-V characteristics fit the measured data with high accuracy. Furthermore, compared with existing modeling methods, our proposed model reduces the simulation time by approximately 30%.

iv. A novel model-based two-stage MPPT framework is proposed to combine offline maximum Power Point Estimation (MPPE) using the Weightless Swarm Algorithm (WSA) with an online Maximum Power Point Revision (MPPR) method. The ASDM is used as a fitness evaluation function in WSA algorithm to predict the output power of the applied PV array. The feasibility of the method is verified in an MPPT control system implemented with a Single Ended Primary Inductance Converter (SEPIC). Steady and rapidly changing environmental conditions are considered in this study. The simulation results suggest that the proposed model-based two-stage MPPT framework significantly outperforms the conventional Perturb and Observe (P&O) and the PSO-based MPPT method in terms of both efficiency and capability in tracking the GMPP.

1.5 Thesis Organization

The thesis is organized as follows:

- In Chapter 2, a review of the most widely used PV electrical models is presented. The research on the parameter estimation for PV electrical models and the MPPT methods is introduced in Section 2.2 and 2.3.

- Chapter 3 presents the CS algorithm and its application to parameter estimation for PV electrical models. The proposed approach is evaluated on a PV cell at the certain irradiance level and on a PV module at the different irradiance levels.

- In Chapter 4, a PPSO algorithm is presented. The workload of the parameter estimation algorithm is appropriately distributed to the applied computing devices in parallel mode. The accuracy and computational efficiency of the proposed method are evaluated by identifying the parameters of two most widely applicable PV electrical models.

- Chapter 5 describes a model-based two-stage MPPT strategy for varying environmental conditions. The first stage is MPPE, in which the voltage at GMPP is predicted. The tracking performance is enhanced by the variable-step Adaptive Perturb & Observe (APO) method. The proposed method is further evaluated on a PV-supplied Single Ended Primary Inductance Converter (SEPIC) constructed in the PSIM simulator. The simulation results are shown in the last part of this section.

- Conclusions and future work are outlined in Chapter 6.

Chapter 2

Literature Review

The primary purpose of this chapter is to review the studies on PV parameter estimation and Maximum Power Point Tracking (MPPT) methods with respect to their motivation and strategies. To this end, this chapter first introduces the most widely used electrical models for Photovoltaic (PV) devices which our research is based on. It then proceeds to present the state and progress of the current literature on the related work documented in this thesis.

Part of the content of this chapter has been published in the following review paper:

- Jieming Ma, Ka Lok Man, Tiew On Ting, Hyunshin Lee, Taikyeong Jeong, Jong-Kug Sean, Sheng-Uei Guan, and Prudence W. H. Wong, Insight of Direct Search Methods and Module-Integrated Algorithms for MPPT of Stand-Alone Photovoltaic Systems, *Lecture Notes in Computer Science (LNCS2012)*, vol. 7513, pp. 468-476, 2012.

2.1 A Review of Modeling Methods for Photovoltaic (PV) Cells

Although PV module prices fell by 74% from 1995 to 2011 [20], the initial cost of a PV system is still relatively high. An accurate assessment of the electrical characteristics is therefore indispensable in the system design [21]. PV manufacturers usually provide typical electrical characteristics of their PV modules, such as the current at Maximum Power Point (MPP) I_{mp}, the voltage at the MPP V_{mp}, the power at MPP P_{max}, the open-circuit voltage V_{oc} and short-circuit current I_{sc}. These values are gen-

erally measured at the Standard Test Conditions (STCs) which correspond to a module temperature of 25 ℃ and an irradiance of 1000 W/m^2 at 1.5 air mass spectral distributions. The current and voltage (I-V) characteristic curves under several different test conditions may also be presented by manufactures. Despite this, the data available in manufactures' data sheet are still limited and usually cannot fulfill the engineering requirements because PV modules always operate under environments far from these test conditions.

Any PV device can be modeled using the equivalent circuit models [22]. These electrical models, with the ability to predict I-V characteristics of a PV cell or module under the working environment other than STCs, are predictive performance tools that allow PV system designers to understand, optimize, and develop PV power generation systems. They are broadly applied to estimate whether a PV power generation system is economically feasible. Recently, many MPPT techniques have been proposed to overcome the problems caused by partial shading conditions and rapidly changing environmental conditions [7,10,11,23,24]. For instance, Chen et al. [10] utilized model-based Particle Swam Optimization (PSO) to search the Global Maximum Power Point (GMPP). In [25,26], the PV array was adaptively reconfigured by a control algorithm integrated with emulated PV module models. These methods have high-lighted the need for a reliable PV electrical model with high accuracy but very complex.

Significant research efforts have been made to develop electrical models of PV systems [27]. These models include analytical models based on PV cell physics, empirical models, and a combination of these two approaches [22]. Their mathematical expressions formulate the terminal current I with the most crucial technical characteristics and environment variables, such as terminal voltage V, the ambient temperature T, and the irradiance G. Even though the other environment factors (e.g. dust and wind velocity) may change the electrical characteristics of PV modules, it is quite impossible to obtain a model that accounts for every single effect on the performance of a PV model [28]. Among numerous modeling approaches, the Ideal Single-Diode (ISD) model achieves the lowest computational complexity. The Single-Diode (SD) model is usually considered to offer a good compromise between simplicity and accuracy [29]. In consideration of the recombination loss in the depletion region, Sah [30] introduced a more accurate model known as Double-Diode (DD) model. The Three-Diode (TD) model can be found in [31]. Although it takes into account the influence of grain boundaries and leakage current through the peripheries, the extra diode increases the number of

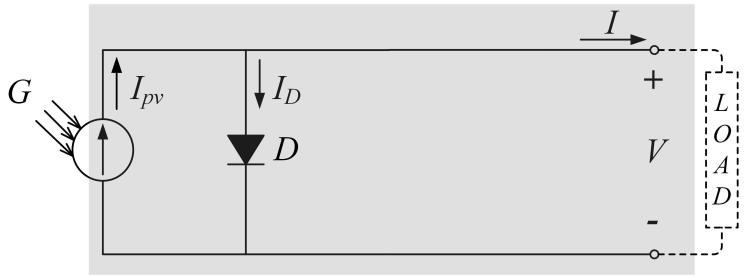

Figure 2.1: Electrical diagram of the ideal single-diode model.

parameters. Accordingly, more computational effort is needed to predict the electrical characteristics via a TD model. In the next three subsections we will present through a variety of PV electrical models, including the ISD model, SD model and DD model. Since the TD model has complex non-linear analytical expressions and not suitable for fast computation, it is not studied in this thesis.

2.1.1 Ideal Single-Diode Model

The elementary PV device is a PV cell, which is basically a semiconductor diode. It generates a reverse current when its p-n junction is exposed to light. The current is termed as photocurrent I_{ph}. In darkness, the PV cell behaves like a diode, and thus its dark I-V characteristics are usually mathematically expressed by the Shockley diode equation [32]:

$$I_{D_1} = I_{o_1}(e^{\frac{V_D}{A_1 V_t}} - 1), \tag{2.1}$$

where V_D represents the electrical potential difference between the two ends of the diode, I_{o_1} denotes the reverse saturation current, and A_1 is the diode ideality factor. V_t is named as thermal voltage, and its value can be estimated as a function of temperature T:

$$V_t = \frac{kT}{q}, \tag{2.2}$$

where k and q represent the Boltzmann constant ($1.602176 \times 10^{-19}\ C$) and the electron charge ($1.602176 \times 10^{-19}\ C$), respectively. Assuming that the superposition principle holds, the full I-V characteristics are simply the sum of the dark and illuminated $I-V$ characteristics:

$$I = I_{ph} - I_{o_1}(e^{\frac{V_D}{A_1 V_t}} - 1). \tag{2.3}$$

In the literature [33, 34], Equation (2.3) is the mathematical expression of the ISD model, in which the I_{ph} is modeled as a current source.

2.1.2 Single-Diode Model

As reported in [32], the output current I is dependent on the contact resistance of the metal base with the p semiconductor layer, the resistances of the p and n bodies, the contact resistance of the n layer with the top metal grid, and the resistance of the grid. These losses are roughly represented by series resistance R_s. In addition, the shunt resistance R_p exists mainly due to the leakage current of the p-n junction and depends on the fabrication method of the PV cell [21]. Taking into account the effects of series resistance, Townsend [35] presented a circuit model assuming that the shunt resistance is infinite. In this thesis, this model is named Simplified Single-Diode (SSD) model and its terminal current value is given by:

$$I = I_{ph} - I_{o_1}(e^{\frac{V+IR_s}{A_1 V_t}} - 1). \tag{2.4}$$

Duffie and Beckman [36] improved the SSD model by including an additional parallel resistance in the equivalent circuit model, so called SD model. Its I-V relation is given by the following equation:

$$I = I_{ph} - I_{o_1}(e^{\frac{V+IR_s}{A_1 V_t}} - 1) - \frac{V + IR_s}{R_p}. \tag{2.5}$$

The corresponding electrical diagram of the SD model is shown in Figure 2.2. In the existing literature, the SD model is frequently used in PV modeling and simulation [21, 37, 38].

More recently, these PV models are frequently used to aid real-time optimization of PV energy [6, 8, 10, 24, 25, 39–43]. The increasing need for high-speed performance estimation has led to renewed interests in the application of SSD model and ISD model. However, their accuracy is not guaranteed [43]. Furthermore, tedious iterative root finding methods (i.e Newton-Raphson method) are still required in the SD model and SSD model to solve the implicit transcendental I-V relations.

2.1.3 Double-Diode Model

The dark characteristics of PV cells have been intensively studied by many authors. In the DD model, the second diode, in parallel with the first, is used to model the recombination in the space charge region [44, 45]. Figure 2.3 shows the electrical diagram of

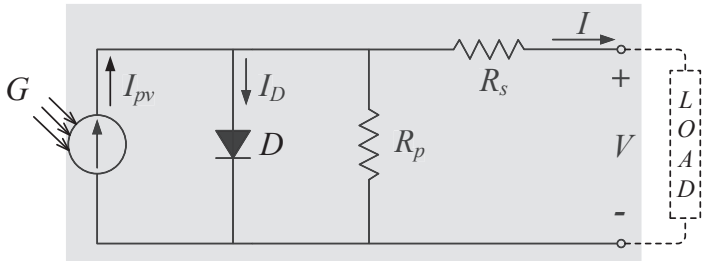

Figure 2.2: Electrical diagram of the single-diode model.

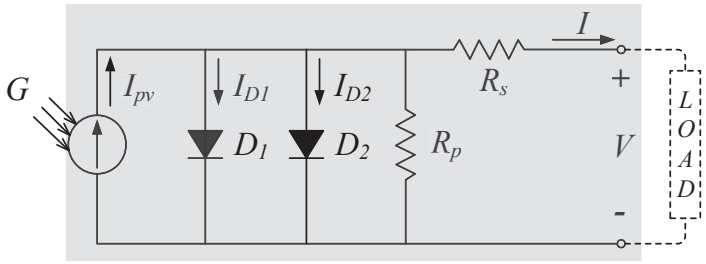

Figure 2.3: Electrical diagram of the double-diode model.

the double-diode model; its electrical model is expressed in equation (2.6):

$$I = I_{ph} - I_{o_1}(e^{\frac{V+IR_s}{A_1V_t}} - 1) - I_{o_2}(e^{\frac{V+IR_s}{A_2V_t}} - 1) - \frac{V + IR_s}{R_p}, \tag{2.6}$$

where I_{o_1} and I_{o_2} are the reverse saturation currents of the first and second diode, respectively. Similarly, the two diodes' ideality constants are denoted by A_1 and A_2. The DD model is considered by many authors being more accurate than the SD model [46, 47], but blamed for being imprecise particularly at low irradiance levels [48].

Table 2.1: Properties of various PV electrical models.

Model Name	Diode Quantity	Parameters	Model Equation
ISD model	1	I_{ph}, I_{o_1}, A_1	$I = I_{ph} - I_{o_1}(e^{\frac{V}{A_1V_t}} - 1)$
SSD model	1	I_{ph}, I_{o_1}, A_1, R_s	$I = I_{ph} - I_{o_1}(e^{\frac{V+IR_s}{A_1V_t}} - 1)$
SD model	1	I_{ph}, I_{o_1}, A_1, R_s, R_p	$I = I_{ph} - I_{o_1}(e^{\frac{V+IR_s}{A_1V_t}} - 1)$ $-\frac{V+IR_s}{R_p}$
DD model	2	I_{ph}, I_{o_1}, A_1, I_{o_2}, A_2, R_s, R_p	$I = I_{ph} - I_{o_1}(e^{\frac{V+IR_s}{A_1V_t}} - 1)$ $-I_{o_2}(e^{\frac{V+IR_s}{A_2V_t}} - 1) - \frac{V+IR_s}{R_p}$

The properties of the aforementioned PV electrical models are specified in Table 2.1. In the literature [49–52], models are also named after the parameter quantity (e.g.

the SSD model, SD model, and DD model are termed four-, five-, and seven-parameter models), since they vary with different quantity of parameters.

2.1.4 PV Module Model

In a large PV generation system, PV modules are used as basic components rather than PV cells, because the output power of PV cells is limited at high voltage levels. Researchers have developed the PV module model so as to predict the I-V characteristics before modeling the whole system.

PV module is a packaged, connected assembly of PV cells. Assuming there are N_s cells connected in a module, the module's output voltage and resistance are scaled in accordance with the following rules [33]:

$$\begin{aligned} V' &= N_s \cdot V, \\ I' &= I, \\ R'_s &= N_s \cdot R_s, \\ R'_p &= N_s \cdot R_p, \end{aligned} \tag{2.7}$$

where V', I', R'_s, and R'_p here represent the terminal voltage, series resistance and shunt resistance of the PV module, respectively. After substituting the scaling rules from Equation (2.7) into (2.3), (2.4), (2.5) and (2.6), we obtain the following equations for a PV module:

$$I'(ISD) = I_{ph} - I_{o_1}(e^{\frac{V'}{A_1 N_s V_t}} - 1), \tag{2.8}$$

$$I'(SSD) = I_{ph} - I_{o_1}(e^{\frac{V'+I'R'_s}{A_1 N_s V_t}} - 1), \tag{2.9}$$

$$I'(SD) = I_{ph} - I_{o_1}(e^{\frac{V'+I'R'_s}{A_1 N_s V_t}} - 1) - \frac{V'+I'R'_s}{R'_p}, \tag{2.10}$$

$$I'(DD) = I_{ph} - I_{o_1}(e^{\frac{V'+I'R'_s}{A_1 N_s V_t}} - 1) - I_{o_2}(e^{\frac{V'+I'R'_s}{A_2 N_s V_t}} - 1) - \frac{V'+I'R'_s}{R'_p}. \tag{2.11}$$

In this thesis, only SD model and DD model are considered since the two models are frequently used in PV modeling and system control. For the convenience of description, the models for predicting the I-V relation of PV cells and modules are abbreviated as follows:

i. SDC : Single Diode Cell model,

ii. DDC : Double Diode Cell model,

iii. SDM : Single Diode Module model,

iv. DDM : Double Diode Module model.

2.2 Research on Parameter Estimation for PV Electrical Models

As discussed in the previews section, PV electrical models involve a series of parameters. These models cannot be directly used because of lack of proper model parameters characterizing the PV cells. Parameter estimation is a discipline that provides tools for estimating constants appearing in the model [53]. With the parameters obtained in such a way, the difference between the simulated and experimental data can be minimized.

In the literature [54, 55], conventional parameter estimation methods are classified into two categories:

i. Analytical techniques [56–60];

ii. Numerical extraction techniques [16, 61–65].

2.2.1 Analytical Techniques

An analytical technique utilizes mathematical equations to describe the parameters of PV electrical models. There is much research on addressing the parameter estimation problem by analytical expressions in terms of the physical parameters, such as the coefficient of diffusion of electrons in the semiconductor, lifetime of minority carriers, the intrinsic carrier density, etc. [31]. However, the values of these physical parameters are normally not provided by manufacturers, which impels researchers to explore an alternative way of formulating the parameters by using the information available in datasheet (e.g. short circuit current coefficient K_i, open circuit voltage coefficient K_v, I_{sc}, V_{oc}, V_{mp}, I_{mp}, etc.). In [21], the I_{ph} is expressed in terms of a linear function as:

$$I_{ph} = (I_{phn} + K_i \Delta T) \frac{G}{G_n}, \tag{2.12}$$

where I_{phn}, G_n, and T_n are used to denote the photocurrent, solar irradiance, and cell temperature measured at the STCs, respectively. ΔT is the difference between T and T_n.

Based on the diode theory, Messenger and Ventre [2] presented an approximate linear expression for the diode saturation current I_{o_1}, which can be expressed as

$$I_{o_1} = I_{on1} \left(\frac{T}{T_n} \right) e^{[(qE_g/A_1k)(1/T_n - 1/T)]}, \tag{2.13}$$

where E_g is the material band gap. Usually, E_g is set at a reasonable level depending on the semiconductor materials ($E_g = 1.12\ eV$ for the polycrystalline Si at 25 ℃) in simulation and design tools [66]. De Soto et al. [58] presented an estimation method for E_g in a wide temperature range:

$$E_g = E_{gn}(1 - 0.0002677\Delta T), \tag{2.14}$$

where E_{gn} is a normal value at the STCs ($E_{gn} = 1.12\ eV$ for silicon cells and $E_{gn} = 1.6\ eV$ for the triple junction amorphous cells).

The value of ideality factor is empirical. Numerous authors discussed the means of estimating the correct value of this constant [29, 67]. For simplicity, the A_1 can be assumed to be independent of temperature and set the value in the range $1 \leq A_1 \leq 2$ [21].

A large number of analytical methods have been applied to determine the values of R_s and R_p over the years. In [28], mathematical formulas are derived to predict R_s and R_p. However, the slopes at the open-circuit and short-circuit points are not usually given in I-V datasheets. Iterative process was proposed in [21] and [50] based on several analytical conditions. This approach may obtain lower absolute error, not at the expense of increased computation complexity. Considering the fact that R_s and R_p vary in almost inverse linear mode with the solar irradiance, Brano [50] demonstrated an improved expression for the series and shunt resistances:

$$\begin{aligned} R_s &= \frac{G_n}{G} R_{sn}, \\ R_p &= \frac{G_n}{G} R_{pn}, \end{aligned} \tag{2.15}$$

where the values of the resistances R_{sn} and R_{pn} are evaluated under the STCs. By using the aforementioned relations, the model is able to analytically describe the I-V characteristics of a PV generator for each generic condition of operative temperature and solar irradiance [58].

The analytical techniques conclude approximate relations with the experimental data. Albeit simple, they are generally dependent on the key points on the I-V curve.

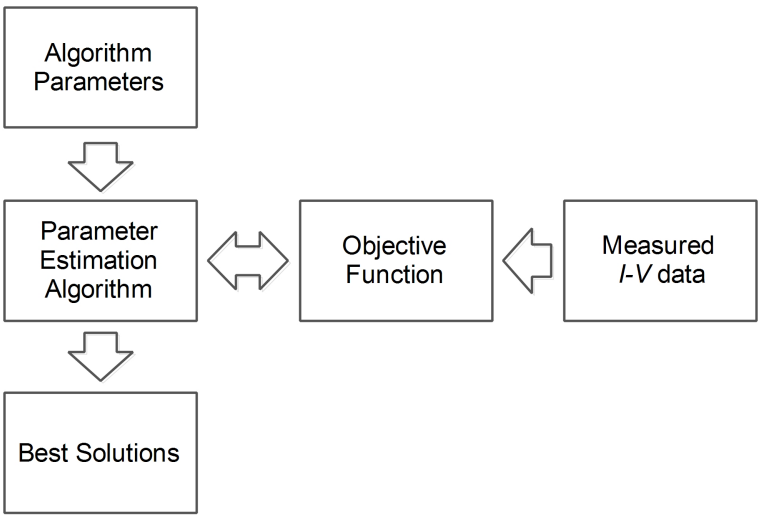

Figure 2.4: Block diagram of the parameter estimation method for PV electrical models.

The errors can be significant and cannot be further improved if these key points are incorrectly specified.

2.2.2 Numerical Techniques

Assisted by a statistical method, numerical extraction techniques fit a great many operating points on the I-V curves to obtain a more accurate solution [61–63, 65]. These curve fitting methods minimize the Root Mean Square (RMS) error ε given in [28] as:

$$\varepsilon = \sqrt{\frac{1}{N}\sum_{d=1}^{N}\left(I_d - \widehat{I}_d\right)^2} \tag{2.16}$$

where d $(d = 1, 2, ..., N)$ is the number of measured I-V data. The simulated and measured data are denoted by I_d and $\widehat{I}_d$, respectively.

The numerical extraction techniques are normally considered as accurate approaches in parameter estimation since all the measured data can be used in calculation. However, it is axiomatic that their performance is also related to the type of fitting algorithm, the cost function as well as the initial values of the parameters to be extracted [61]. The non-linear curve-fitting procedures are quite complicated both mathematically and in terms of computer code [68]. Moreover, the algorithms can be computationally expensive as the size of required data is considerably large.

2.2.3 Evolutionary Algorithm Techniques

Evolutionary Algorithm (EA) techniques are very efficient in optimizing real-valued multi-modal objective functions [12, 13, 69, 70]. To date, Genetic Algorithm (GA) [18], Particle Swarm Optimization (PSO) [17, 71, 72], Bacterial Foraging Algorithm (BFA) [73], Simulated Annealing (SA) [74] , Pattern Search [19], Differential Evolution [75,76] have been employed for estimating parameters of various PV electrical models due to their ability to handle non-linear functions without requiring derivatives information.

PV parameter estimation is basically a process that minimizes the difference between the calculated and measured data by adjusting the normal PV parameters [77]. Figure 2.4 shows the flow diagram of a typical parameter estimation process for PV devices. After importing several constants or parameters, the parameter estimation algorithm starts evaluating possible solutions by using the objective function with the measured I-V data. In general, the objective function is formulated by the RMS error which serves to aggregate absolute differences into a single measure of predictive power. If the number of experimental data is denoted by N, the RMS error can be mathematically formulated as the following equation:

$$\varepsilon = \sqrt{\frac{1}{N}\sum_{d=1}^{N}(f_d(\widehat{V},\widehat{I},\mathbf{X}))^2}, \tag{2.17}$$

where $\widehat{V}$ and $\widehat{I}$ denote the measured voltage and current, respectively. $f_d(x)$ is the objective function for the d^{th} data. $\mathbf{X}$ is a vector representing the model parameters. Take the SDC model for example. $f_d(\widehat{V},\widehat{I},\mathbf{X})$ is a homogeneous form of Equation (2.5), namely:

$$f_d(\widehat{V},\widehat{I},\mathbf{X})_{SDC} = I_{ph} - I_{o_1}(e^{\frac{\widehat{V}+\widehat{I}R_s}{A_1V_t}} - 1) - \frac{\widehat{V}+\widehat{I}R_s}{R_p} - \widehat{I}. \tag{2.18}$$

In the above equation, $\mathbf{X}$ is a vector involving the model parameters I_{ph}, I_{o_1}, A_1, R_s, and R_p.

The EA techniques may obtain the most accurate solution compared with the other methods if their initial points and algorithm parameters are set properly. On the other hand, most of these methods apply multiple agents or particles in random search and do not provide a significant improvement in computational efficiency. Taking into account the fact that extraction is the main component of a PV system simulator, the overall simulation speed would be greatly compromised [75].

2.3 Research on Maximum Power Point Tracking (MPPT) Methods

In a P-V characteristic curve of PV cells or modules, there exists only operating point where the power is maximum. This point is known as the MPP. As shown in Figure 2.5, the MPP locus, denoted by circles, varies with different atmospheric conditions.

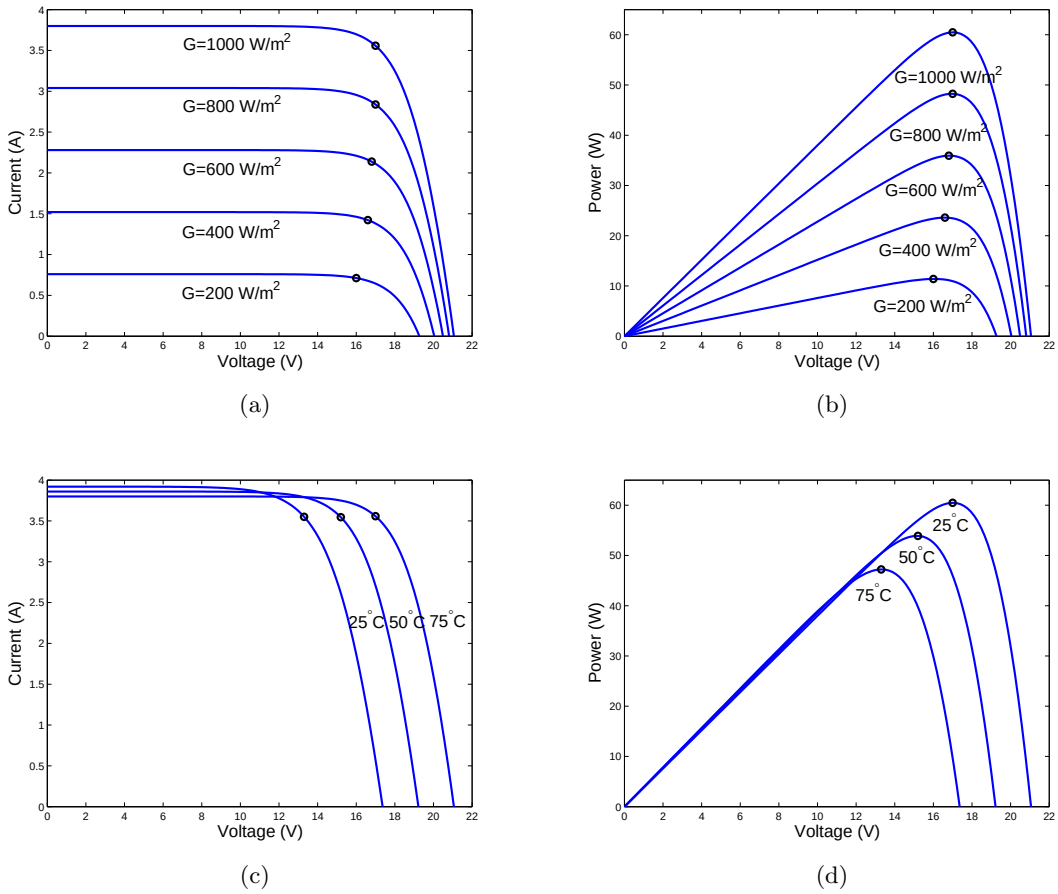

Figure 2.5: Electrical characteristic curves of a MSX60 PV module under different atmospheric conditions: (a) I-V curves under various irradiance levels; (b) P-V curves under various irradiance levels; (c) I-V curves under various temperatures; (d) P-V curves under various temperatures.

PV modules are usually connected in series to scale up the voltage because their open circuit voltage is independent of the module area and is limited by the semiconductor properties [33]. In an outdoor environment, the whole or some parts of the PV array may be under a non-uniform irradiance condition caused by passing clouds, high buildings, trees, etc. In this case, the series connected PV array is in open circuit, which is known as "hot spot" [33]. To avoid this problem, bypass diodes are normally placed

across every PV module as shown in Figure 2.6 (a). Suppose that the three modules receive three different irradiance levels: 1000 W/m^2, 750 W/m^2, and 500 W/m^2. The shape of the P-V curve, shown in Figure 2.6 (b), becomes more complicated - exhibiting multiple peaks. In this thesis, the highest peak is named and other peaks are named GMPP and Local Maximum Power Point (LMPP), respectively.

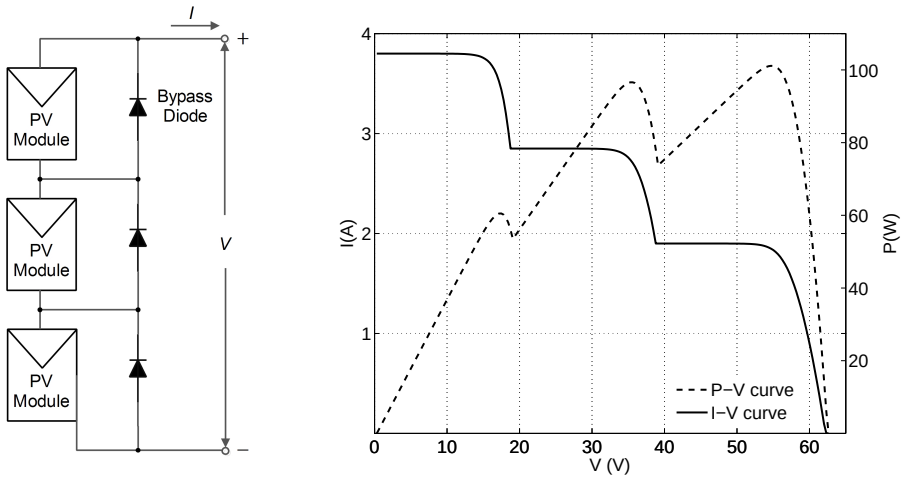

(a) (b)

Figure 2.6: Operation of a PV array working under partial shading conditions: (a) A PV array with bypass diodes; (b) I-V and P-V curves of the PV array receiving various irradiance levels.

Maximum power point tracking (MPPT) is a technique employed to gain maximum power available from PV devices [78, 79]. It varies PV operating voltage corresponding to MPP, constrains the operating point at MPP, and extracts maximum power from the used PV devices [80–82]. A large number of MPPT techniques have been presented in literatures [82]. Based on the function of the methods or control strategies, Salas et al. [83] proposed to group the MPPT methods into two categories:

i. Direct control [84–89];

ii. Indirect control [90–93].

The two approaches will be presented in the following subsections. The recent research on evolutionary algorithms and their applications in MPPT techniques will be discussed at the end of this chapter.

2.3.1 Direct Control

Direct methods search the optimum operating point online by using PV voltage and current measurements. The common advantage of such methods is their environment-independent features. In other words, environmental measurements are unnecessary in the tracking process of direct methods. A small quantity of measurements of not only mean the lower cost that can be attained, but also indicate higher accuracy and reliability that can be achieved [94]. This group of methods include, but not limited to, Perturb and Observe (P&O) [84–86], Incremental Conductance (IncCond) [87], and root-finding methods [88, 89].

Among these direct control MPPT methods, the P&O is a well-known practical MPPT algorithm and is presented in the literature as a reference method. Figure 2.7 shows a flowchart of P&O algorithm for the most basic form. Starting from the measures of the operating voltage and current, the algorithm first obtains the sign of ΔP, which denotes the difference between the current operating power P^t and the power measured in the previous sample P^{t-1}. On the basis of the P-V characteristics curve of a PV module, the P&O method perturbs the operating point and determines the change of search direction as summarized below:

- If $\Delta P = 0$, the voltage for the next sample V^{t+1} will not be changed since the system is working at the MPP;
- If $\Delta P > 0$ and $\Delta V > 0$, the V^t is on the left of the MPP and the V^{t+1} will be located on a point with a higher voltage value so as to reach the MPP.
- If $\Delta P > 0$ and $\Delta V < 0$, the V^t is on the right of the MPP and the V^{t+1} will be located on a point with a lower voltage value so as to reach the MPP.
- If $\Delta P < 0$ and $\Delta V > 0$, the V^t is on the right of the MPP and the V^{t+1} will be located on a point with a lower voltage value so as to reach the MPP.
- If $\Delta P < 0$ and $\Delta V < 0$, the V^t is on the left of the MPP and the V^{t+1} will be located on a point with a higher voltage value so as to reach the MPP.

The P&O algorithm takes effect on steady atmospheric conditions. However, under a rapidly changing environmental condition, the P&O may point out wrong tracking direction toward the MPP due to the changes of P-V characteristics. The IncCond

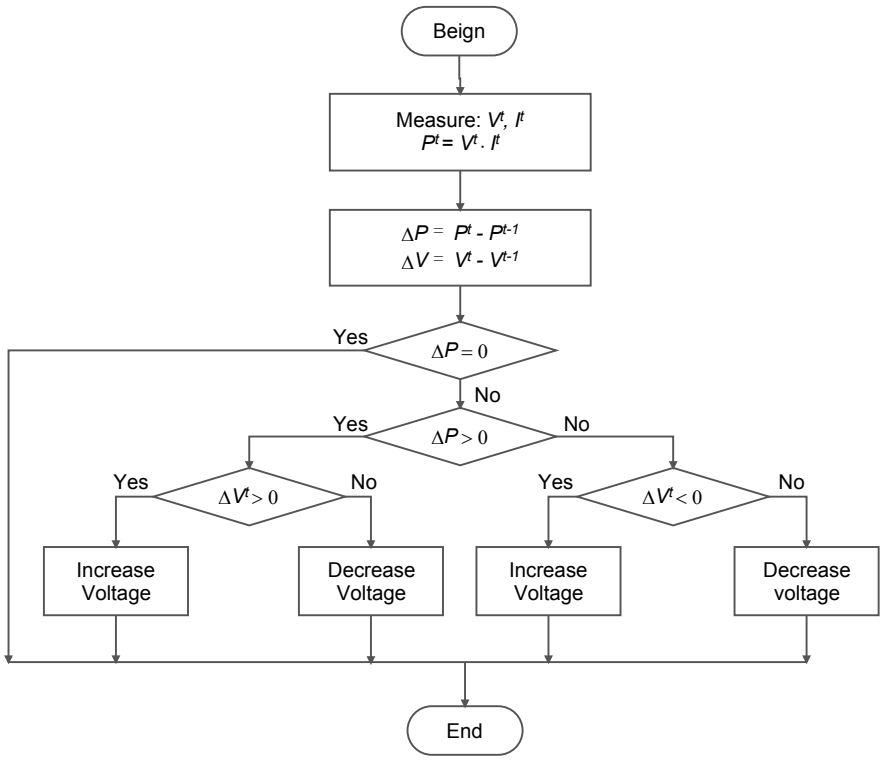

Figure 2.7: Flowchart depicting the P&O algorithm.

method, first introduced by Hussein et al. [87], was implemented to overcome this problem. It determines the search directions by comparing the instantaneous conductance I/V with the incremental conductance dI/dV of the PV device. Although the IncCond method takes into account environment factors, many of the inherent drawbacks, like oscillation and disability of partial shading conditions [9], limit its application.

Since the conventional $P\&O$ and IncCond algorithms vary the operating voltage towards the MPP with fixed step size, they have certain disadvantages: large perturbations result in significant state oscillations while small perturbations result in slow tracking speed [83,95,96]. With the aim of resolving the problems caused by fixed steps, variable step-size MPPT approaches were proposed in the literature [95]. In general, they start with a large perturbation step and end by acknowledging the achievement of tolerance. A case in point is Adaptive Perturb & Observe (APO) method [97], where the perturbation step size is set to a large value when the power changes by a large amount primarily due to environmental variations. The step size may be set as follows:

$$a^t = M\frac{|\Delta P|}{a^{t-1}}; \tag{2.19}$$

where $\Delta P = P^t - P^{t-1}$, representing the change of power, a^{t-1} is the historic value of a^t (always larger than 0), and M is a constant parameter. In this manner, a^t is large

during the transient stage and a^t becomes small in the steady state.

Based on the fact that the derivative of the output power with respect to the output voltage dP/dV approaches zero at MPPs, the MPPT issues can be reduced to a root-finding problem. In digital implementation, dP/dV of an arbitrary operating point O can be approximated by a backward finite divided difference [88]:

$$\left.\frac{dP}{dV}\right|_{V=V_O} \approx \frac{\Delta P}{\Delta V} = \frac{V_O \cdot I_O - V_{O'} \cdot I_{O'}}{V_O - V_{O'}} \tag{2.20}$$

where O' is an operating point sampled immediately after O. The difference between V_O and $V_{O'}$ is ΔV. The V_O and $V_{O'}$ represent the voltage values at O and O' respectively. Similarly, the I_O and $I_{O'}$ are the current values at O and O' respectively.

Chun [88, 89] presented a digital MPPT method by using Bisection Search Method (BSM). The BSM is a numerical method designed to find a root for function $f(x)$. Its search processes are summarized as following steps [98, 99]:

i. given a function $f(x)$ and initial interval $[x_l, x_u]$. The root x^* of $f(x)$ is in this interval. Since $f(x)$ has opposite signs in x_l and x_u , $f(x_l)f(x_u) < 0$;

ii. approximate the root to the midpoint x_m of the interval, given by:

$$x_m = \frac{x_l + x_u}{2}; \tag{2.21}$$

iii. if $f(x_l)f(x_m) < 0$, then set $x_u = x_m$ and repeat the previous step. If $f(x_l)f(x_m) > 0$, then set $x_l = x_m$ and repeat the previous step. If the absolute value of $f(x_m)$ is less or equal to the tolerance ϵ, then take x_m as the root or approximation.

The simulation results show the BSM-based MPPT method converges to the MPP faster and more accurately than the traditional P&O approach at any given environmental condition [88, 89].

2.3.2 Indirect Control

Indirect methods use mathematical functions obtained from empirical data to estimate the MPP, or a database that includes parameters and data, such as I-V curves of the PV generator for different temperatures and irradiance levels [83]. The following methods belong to this category: Look Up Table (LUT) [90], Curve Fitting (CF) [91], Fractional

Open-Circuit Voltage (FOCV) [92], Fractional Short-Circuit Current (FSCC) methods [93], etc.

In the LUT method, the sensed values of the PV generator's terminal current and voltage are compared with the prior stored MPP locations in the control system. The size of these data is usually large and requires a large memory capacity to store [95,100]. Moreover, the system becomes complex for changing environmental conditions [101].

The CF method is used in [91] to characterize a PV device. It is assumed that the P-V relations can be expressed Equation (2.22):

$$P = \alpha V^3 + \beta V^2 + \gamma V + \delta, \tag{2.22}$$

where α, β, γ, and δ are coefficients that are determined by sampled values of the terminal current and voltage. As long as these coefficients are calculated, the approximate voltage at the MPP can be estimated by the following formula:

$$V_{mp} = \frac{-\beta \pm \sqrt{\beta^2 - 3\alpha\gamma}}{3\alpha}. \tag{2.23}$$

In the tracking process, this estimation repeats every few milliseconds since the P-V characteristics may rapidly change. This method is simple to implement; however, its accuracy is dependent on the number of samples. Also, it might require a large memory capacity as the sample size is large.

The FOCV method is based on the empirical fact that a linear dependency between the V_{mp} and open circuit voltage V_{oc}:

$$V_{mp} \cong K_{mv} V_{oc}, \tag{2.24}$$

where K_{mv} is called voltage factor and its value ranges from 0.7 to 0.95 depending upon the characteristics of PV module [92]. Similarly, the FSCC is based on that I_{mp} is approximately linearly proportional to its short-circuit current. Their relations are given in Equation (2.25):

$$I_{mp} \cong I_{mv} I_{sc}. \tag{2.25}$$

The I_{mv} is the current factor whose value is around 0.85 [83].

The FOCV and FSCC methods obtain high-speed tracking performance as their computational complexity is low and the required sensors are less [102]. The main

disadvantage of both methods is its low accuracy. It is difficult to determine proper values of K_{mv} and I_{mv} for PV cells.

2.3.3 Evolutionary Algorithm Techniques

Evolutionary Algorithm (EA) has been attracting more attention. It is a stochastic method that appears to be very efficient in optimizing real-valued non-linear and multimodal objective functions [54, 103]. Recently, GA [104], PSO [10, 23, 24], and CS [105] algorithms have been suggested as solutions to the problem of MPPT.

The GA method, developed by John Holland and colleagues in the 1960s and 1970s, is probably the most popular evolutionary algorithm in terms of the diversity of applications [12]. The GA is based on Charles Darwin's theory of natural selection. The optimization function is encoded as arrays of binary character strings representing the chromosomes. These chromosomes evolve through selection and genetic operators like crossover and mutation, which drive a better solution to the problem concerned in the next population. In the selection process, the best fitted chromosomes in the current population are selected in terms of the elitist strategy. It ensures the offspring chromosomes inherit the best possible combination of the genes of their parents. Crossover recombines the chromosomes chosen by selection while mutation changes some of the genes randomly. The new population of chromosomes is formed by combining the chromosomes from the selection, crossover and mutation. The reason why the GA applies crossover and mutation may lie in their capability to avoid local optimum in the searching process.

The PSO method is one of the most successful numerical optimization algorithms applied in a variety of fields. It is inspired first by general artificial life, the same as bird flocking, fish schooling and social interaction behavior of human and second by random search methods of evolutionary algorithms [106]. The birds and fishes, modeled by particles, travel in a swarm. Each particle adjusts its position and velocity using the swarm information as it reduces individual's effort for search of the best position.

The CS algorithm is invented based on the inspiration of brood parasitic behavior of some cuckoo species in combination with the Lévy flight behavior. In [14, 107], Yang and Deb reported that the CS algorithm outperforms PSO and GA for various standard test functions.

These EA-based MPPT methods have the capability of tracking the PV devices receiving non-uniform irradiance, under which condition the conventional MPPT algorithms like the P&O and FOCV methods may fail [103, 104, 108, 109]. Moreover, these methods do not prescribe an accurate PV electrical model and are robust in MPPT.

2.4 Summary

This chapter has reviewed the ideal, single-diode, and double-diode electrical models for PV cells and modules, and discussed the most widely used parameter estimation methods for these models. Then, the existing MPPT methods, grouped into direct, indirect and evolutionary algorithm based methods, have been presented.

Having presented the review of relevant literature and the theoretical framework established for this study, the following chapter will describe the research methodology including the research methods adopted, the experiments and results.

Chapter 3

Parameter Estimation of PV Model via Cuckoo Search

In this chapter, the evolutionary algorithm based parameter estimation methods are discussed. It is followed by the introduction of the proposed cuckoo search method as well as the formulation of the objective function. The simulation results are analyzed in Section 3.5, and Section 3.6 presents concluding remarks.

The content of this chapter has been published in the following paper:

- Jieming Ma, Tiew On Ting, Ka Lok Man, Nan Zhang, Sheng-Uei Guan, and Prudence W. H. Wong, Parameter Estimation of Photovoltaic Models via Cuckoo Search, *Journal of Applied Mathematics*, vol. 2013, no. 362619, 1-8, 2013.

3.1 Introduction

Photovoltaic (PV) cells, normally assembled into modules or arrays on mounting systems, are capable of producing electrons when photons strike their surfaces. Taking the advantages of many promising features like renewability, less pollution, and ease of installation, PV systems are envisaged to be an important energy source for the future.

Due to the high initial cost of a PV-supplied system, predictive performance tools are used extensively by engineers to optimize the system performance [110, 111]. PV manufacturers normally provide limited tabular data measured under the Standard Test Conditions (STCs), which correspond to a cell temperature of 25℃ and an irradiance of 1000 W/m^2 at 1.5 air mass spectral distributions. As reported in [50], PV generators

always operate under environments far from the STCs. Owing to this reason, the data available in the datasheet usually fail to fulfill the engineering requirements. PV electrical model, with the ability to predict I-V characteristics of PV generators under an operating environment other than the STCs, is a predictive performance tool that allows consumers to maximize the cost effectiveness of the system before installation [111]. They are generally analytical equations based on physical descriptions that formulate PV generated current I with the most crucial technical characteristics and the environmental variables, such as the operating voltage V, the ambient temperature T, and the irradiance G. Over the years, significant research efforts have been contributing to the development of the electrical models [21, 44, 51, 58]. Among numerous modeling approaches, the Single-Diode (SD) model is the most widely utilized PV model in the literature. In order to adapt PV model behavior to different operating conditions, de Blas et al. [60] suggested to apply the procedure described in the International Standard IEC 891 that relates current and voltage of the PV characteristics at given values of T and G with the corresponding values at different operating environments. The improved single-diode model presented by De Soto et al. [58] includes the dependence of the PV parameters on operating conditions.

Both the SD model and the De Soto's model obtain unknown parameters. Parameter estimation is a tool that estimates the values of these parameters by using the measured data. In this chapter, we discuss the Cuckoo Search (CS) algorithm and its application to parameter estimation for the SD model and the De Soto's model. Simulation and experimental results show superior accuracy and feasibility of the proposed parameter estimation method.

3.2 Related Work

Analytical methods [48, 57, 112] are common approaches to estimate the parameters by mathematical expressions in terms of the physical parameters like the electron charge, diffusion coefficient for electrons, lifetime of minority carriers, and intrinsic carrier density, etc [31]. These parameters are normally not provided by the PV manufacturers. To overcome this problem, De Soto et al. [58] proposed an analytical method that uses the tabular data available on the datasheets. Although having the merit of simplicity, it is usually incorrect and the errors are hard to be further reduced.

Recently, PV parameter estimation is considered to be as a multidimensional op-

timization problem. Several computational intelligence methods, such as Genetic Algorithm (GA) [18], Particle Swarm Optimization (PSO) [17, 71, 72], Bacterial Foraging Algorithm (BFA) [73], Simulated Annealing (SA) [74], Pattern Search (PS) [19], Differential Evolution (DE) [75, 76], were proposed in the literature. These algorithms usually extract relevant parameters by minimizing the Root Mean Square (RMS) error as the objective function in the optimization process. Askarzadeh and Rezazadeh [114] suggested that the optimization methods normally produce better results than analytical methods. Reported by [19, 74], the SA and PS show better estimation accuracy than the results in [115]. Ye et al. [72] compared the convergence speed between the PSO and GA methods toward the SD model, as well as Double-Diode (DD) model. The results show that the GA method is not apt to be used in parameter extraction. Slightly better results can be achieved using the PSO, BFA, and DE algorithms.

The CS is one of the latest nature-inspired meta-heuristic algorithms. It is based on the fascinating breeding behavior such as brood parasitism of certain species of cuckoos. The algorithm applies by Lévy flight rather than simple random search. In [14, 107], Yang and Deb demonstrated that the CS algorithm outperforms the PSO and the GA for various standard test functions. In the following sections, we discuss its performance in parameter estimations.

3.3 Formulation of Parameter Estimation Problem

As discussed in Section 2.1, the SDM, predicting the I-V characteristics for a PV device, is considered. In this chapter, the SD model for a PV cell is named Single-Diode Cell (SDC) model while the SD model for a PV module is named Single-Diode Module (SDM) model. Their I-V relations can be mathematically expressed as follows:

$$I(SDC) = I_{ph} - I_{o1}(e^{\frac{V+IR_s}{A_1 V_t}} - 1) - \frac{V + IR_s}{R_p} \tag{3.1}$$

$$I'(SDM) = I_{ph} - I_{o1}(e^{\frac{V'+I'R'_s}{A_1 N_s V_t}} - 1) - \frac{V' + I'R'_s}{R'_p}. \tag{3.2}$$

In the above equations, V', I', R'_s and R'_p represent the voltage, current, series and shunt resistance values for a PV module. The five model parameters involved are photocurrent I_{ph}, saturation current I_{o1}, diode ideality constant A_1, series resistance R_s (or R'_s), and shunt resistance R_p (or R'_p).

The parameter estimation method for PV electrical models can be implemented

by various Evolutionary Algorithms (EAs) with experimentally determined I-V curve. The objective function was the RMS errors ε in the current prediction as calculated by:

$$\varepsilon = \sqrt{\frac{1}{N}\sum_{idata=1}^{N}(f_d(\widehat{V},\widehat{I},\mathbf{X}))^2}, \tag{3.3}$$

where $\widehat{V}$ and $\widehat{I}$ denote the measured voltage and current, respectively. N is the number of measures. $f_d(x)$ is the objective function for the d^{th} data. $\mathbf{X}$ is a vector representing the model parameters. $f_d(\widehat{V},\widehat{I},\mathbf{X})$ is a homogeneous form of the model expression. As for the SDC model, $f_d(\widehat{V},\widehat{I},\mathbf{X})$ is given as:

$$f_d(\widehat{V},\widehat{I},\mathbf{X})_{SDC} = I_{ph} - I_{o1}(e^{\frac{\widehat{V}+\widehat{I}R_s}{A_1V_t}} - 1) - \frac{\widehat{V}+\widehat{I}R_s}{R_p} - \widehat{I}, \tag{3.4}$$

where $\mathbf{X}$ is a vector involving the model parameters I_{pv}, I_{o1}, A_1, R_s, and R_p.

In a similar way, Equation (3.5) is used as the objective function during the parameter estimation process for a PV module.

$$f_{id}(\widehat{V'},\widehat{I'},\mathbf{X})_{SDM} = I_{ph} - I_{o1}(e^{\frac{\widehat{V'}+\widehat{I'}R_s}{A_1N_sV_t}} - 1) - \frac{\widehat{V'}+\widehat{I}R'_s}{R'_p} - \widehat{I'}. \tag{3.5}$$

The original SDM ignores the operating conditions effect on these parameters. However, some studies have demonstrated that the parameters, such as I_{ph} and I_{o1}, vary with different environmental conditions. These are due to the changes of temperature and irradiance. Aiming to evaluate PV behaviors at the environmental conditions other than the normal values T_n and G_n, the relations between the operating parameters and the normal parameters are studied by numerous researchers [2, 21, 58].

The following dependence of all of the parameters in the model on the operating conditions is considered:

$$I_{ph} = (I_{phn} + K_i\Delta T)\frac{G}{G_n}, \tag{3.6}$$

$$I_{o1} = I_{on1}\left(\frac{T}{T_n}\right)e^{[(qE_g/A_1k)(1/T_n - 1/T)]}, \tag{3.7}$$

$$E_g = E_{gn}(1 - 0.0002677\Delta T), \tag{3.8}$$

where I_{phn}, I_{on1}, E_{gn}, G_n, and T_n, denote the photocurrent, diode saturation current, material band gap, solar irradiance, and cell temperature measured at STCs, respectively. ΔT presents the difference between T and T_n. K_i represents the short-circuit current coefficient.

By using these relations, De Soto et al. [58] proposed a PV electrical model that is able to analytically describe the I-V characteristics of a PV device for different temperature and solar irradiance.

3.4 Cuckoo Search

The CS algorithm [12,14,107], proposed by Yang and Deb, is a nature-inspired stochastic global search algorithm that follows three idealized behavior rules:

i. a cuckoo lays an egg and dumps it randomly into other bird species' nests;

ii. the best nests with high quality eggs will be carried forward to the next generation;

iii. there are a fixed number of available host nests. If a host bird discovers that the eggs are not its own, it will either throw these alien eggs away, or it may abandon the nest and build a brand new nest at a nearby location.

Algorithm 1: Cuckoo Search via Lévy Flights

Input: The measured I-V data.
Output: The best solutions in the search space.
Initialization of n host nests (population);
while *Stopping criterion is not satisfied* **do**
  Choose a cuckoo egg by Lévy flights and evaluate its fitness (F_i);
  Choose an egg in others nest randomly and calculate its fitness (F_j);
  if $F_i > F_j$ **then**
    replace j^{th} egg by i^{th} egg;
  end
  A fraction (p_a) of worse nests are demolished and replaced by new ones;
  Preserve good nests (best solutions).
end

Based on the three rules, the basic steps of CS can be briefly summarized by the pseudo code shown in Algorithm 1. In the CS algorithm, a pattern corresponds to a nest while each individual attribute of the pattern corresponds to an egg laid by the cuckoo. On the basis of random-walk algorithms, the general system equation of the CS algorithm is given by:

$$X_{g+1;i} = X_{g;i} + \alpha \otimes levy(\lambda) \tag{3.9}$$

where g and i denote the generation number ($g = 1, 2, 3, ..., MaxGen$) and the pattern number ($i = 1, 2, ..., n$), respectively. The product $\otimes$ means entry-wise multiplications.

Here $\alpha > 0$ is the step size scaling factor which should be related to the scales of the problem of interest [107]. The j^{th} attributes of the i^{th} pattern is initiated by using Equation (3.10):

$$X_{g=0;j,i} = rand \cdot (Ub_i - Lb_i) + Lb_i, \tag{3.10}$$

where Ub_i and Lb_i are the upper and lower bounds of the j^{th} attributes, respectively. In each computation step, the CS algorithm checks whether the value of an attribute exceeds the allowed search range. If this happens, the value of this attribute will be updated with the corresponding boundary value.

Before the searching process, the CS algorithm detects the most successful pattern as X_{best} pattern. Among the existing algorithms for generating Lévy flights in the literature, Yang and Deb [14, 107] reported that Mantegna's algorithm [116] works well in most of the optimization problems. Accordingly the evolution phase of the pattern is initialized with the detection step of φ, which is given by Equation (3.11) [117]:

$$\varphi = \left(\frac{\Gamma(1+\beta) \cdot \sin(\pi \cdot \beta/2)}{\Gamma\left(\left(\frac{1+\beta}{2}\right) \cdot \beta \cdot 2^{\frac{\beta-1}{2}}\right)} \right)^{\frac{1}{\beta}} \tag{3.11}$$

where β is 1.5 in the standard software implementation of the CS algorithm [118]. Γ denotes the gamma function, expressed by:

$$\Gamma(x) = \int_0^\infty e^{-t} t^{x-1} dt. \tag{3.12}$$

After initialization, the evolution phase of the X_i pattern starts by defining the donor vector $\mathbf{V}$, where $\mathbf{V} = [X_1, X_2, ..., X_i]$. The required step size of the j^{th} attributes can be calculated by the following equation:

$$s_j = 0.01 \cdot \left(\frac{u_j}{v_j}\right)^{\frac{1}{\beta}} \cdot (V - X_{best}) \tag{3.13}$$

where $u_j = \varphi \cdot randn[D]$ and $v_j = randn[D]$. The $randn[D]$ function generates a uniform integer between $[1, D]$ [119]. The donor pattern V is then randomly adjusted by

$$V = V + s_j \cdot randn[D] \tag{3.14}$$

The CS algorithm will evaluate the fitness of the random pattern. If a better solution is taken, the X_{best} pattern will be updated. The unfeasible patterns are revised by the crossover operator given in Equation (3.15) as follows:

$$V_i = \begin{cases} X_i + rand \cdot (X_{r1} - X_{r2}), & rand > p_0 \\ X_i & , \quad others \end{cases} \tag{3.15}$$

where p_o is the mutation probability value ($p_o = 0.25$ in the standard software implementation [118]), X_{r1} and X_{r2} are random permutation of the X_1 and X_2 respectively. The final step in a generation is to check if the revised infeasible patterns deliver a better solution.

3.5 Experiments and Results

In order to provide a thorough evaluation of the CS algorithm in estimating the PV parameters, both SD and De Soto's model [58] are considered in this thesis. Three case studies are designed to estimate the CS algorithm in model parameters estimation:

1. a commercial 57mm diameter solar cell (R.T.C. France [16]) operating at the standard irradiance level;
2. a PV module (Photowatt-PWP 201 [16]) comprising 36 polycrystalline silicon cells;
3. a PV module (KC200GT multi-crystal PV module) operating under various environment conditions.

The electrical models for the three PV devices are named as the SDC model, the SDM model and the De Soto's Module model. The measured data of the R.T.C. France silicon PV cell, Photowatt-PWP 201 PV module, and KC200 GT PV module are given in Appendix B, C, and D, respectively. During the parameter extraction process, the objective function $f(V, I, \mathbf{X})$ is minimized with respect to the range of parameters. In theory, the value of I_{pvn} is slightly larger than that of I_{sc}. E_{gn} is in a loose range from 1 eV to 2 eV. K_i is around the value provided by the datasheet (normally less than 0.02%/°C). The I_{on1} is usually less than 50 μA. As stated in [120], the ideality factor A_1 ranges between 1 and 2. PV modules produced by most manufacturers have R_s less than 0.5 Ω and R_p between 5 Ω and 170 Ω [28, 38]. As for PV cell, the ranges of R_s and R_p can be scaled by simply dividing N_s [75].

Statistical analysis is performed to evaluate the quality of the fitted models to the experimental data. Besides RMS error, other two fundamental measures, namely,

Individual Absolute Error (IAE) and the Mean Absolute Error (MAE), are applied to evaluate in this paper. Equations (3.16) and (3.17) represent the IAE and MAE, respectively:

$$IAE = |I - \widehat{I}|, \tag{3.16}$$

$$MAE = \frac{1}{N}\sum_{d=1}^{N} IAE_d. \tag{3.17}$$

where I is the simulated data and $\widehat{I}$ is the measured data.

The optimization algorithms applied in this paper are programmed in MATLAB. Similar simulation conditions, including population size, maximum generation number, and search ranges, are set to ensure a fair evaluation (population size = 25; maximum generation number = 5000).

3.5.1 Case Study 1: Parameter Estimation for a PV Cell at The Certain Irradiance Level

Table 3.1 lists the model parameters of the R.T.C France PV cell at 33 ℃, which are extracted from the experimental data in [16]. The parameters obtained from the CS algorithm is compared with three different parameter estimation approaches: CPSO [17], GA [114], and PS [19]. From the RMS errors of these methods, which are listed in the last row of Table 3.1, the CS algorithm outperforms the other three optimization methods. The CS obtained slightly lower RMS error, recording 9.86E-04 in numerical value.

Table 3.1: Estimated parameters of the SDC model using various methods.

Parameter	CS	CPSO [17]	GA [114]	PS [19]
I_{pv}	0.7608	0.7607	0.7619	0.7617
I_o	3.23E-07	4.00E-07	8.09E-07	9.98E-07
n	1.4812	1.5033	1.5751	1.6000
R_s	0.0364	0.0354	0.0299	0.0313
R_p	53.7185	59.0120	42.3729	61.1026
RMS error	9.86E-04	2.65E-03	1.91E-02	1.49E-02

During the parameter estimation process for the SDC model, the values of the objective function in different optimization algorithms are shown in Figure 3.1. The function "ga" in MATLAB [121], whose crossover rate $P_c = 0.8$ and mutation rate $P_m = 0.2$, is utilized for the convergence process test. As for the CPSO implementation [122],

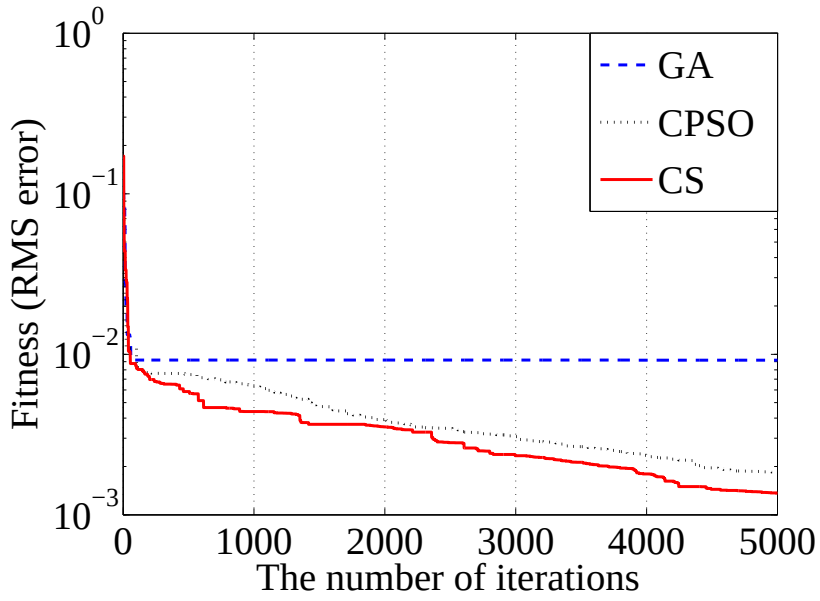

Figure 3.1: Convergence process of different optimization algorithms during the parameter estimation process of the SDC model.

the algorithm parameters are set as learning factors $c_1 = c_2 = 2$, inertia factors w_{max} $= 0.9$, $w_{min} = 0.4$, and velocity clamping factor $V_{max} = 0.5$. In Figure 3.1, no further improvement by GA is observed after 500 iterations. On the contrary, the CS algorithm shows continuous improvement until the maximum generation. The CS algorithm, whose convergence speed is slightly faster than the CPSO, shows the most accurate result in the minimization task after 5000 iterations.

To evaluate the goodness of fit of the obtained solution, these parameters are substituted into the SDC model. The PV terminal current I is solved by the Newton-Raphson method [98], as the I-V relations demonstrate non-linear characteristics. In Table 3.2, the calculated results IAEs are shown. Although the CS show higher error in the 2nd, 3rd, 5th, 6th, 8th, 15th and 23rd measurements, the majority of the simulated results show the most accurate solutions. The MAE of the CS is 20.82 % lower than that of CPSO.

3.5.2 Case Study 2: Parameter Estimation for a PV Module at The Certain Irradiance Level

By using the same parameter setting, the parameters of the SDM are extracted from the measured data of the Photowatt-PWP 201. Table 3.3 lists the estimated parameters of the SDM using diverse methods. The absolute errors of the simulated terminal current

Table 3.2: Absolute errors of the simulated terminal current for the SDC model.

No	AE_{CS}	AE_{CPSO} [17]	AE_{GA} [114]	AE_{PS} [19]
1	8.7644E-05	2.7202E-04	2.2146E-03	6.7575E-04
2	6.6264E-04	4.3069E-04	2.4081E-03	1.4227E-03
3	8.5473E-04	7.3998E-04	2.2499E-03	1.7724E-03
4	3.4577E-04	3.5310E-04	7.2753E-04	7.1577E-04
5	9.4415E-04	8.5370E-04	1.6653E-04	2.4622E-04
6	9.5699E-04	7.7812E-04	4.5523E-04	3.4363E-04
7	9.1588E-05	3.4850E-04	3.2720E-04	1.4730E-03
8	8.5793E-04	5.3601E-04	8.9998E-04	5.5044E-04
9	4.1268E-04	4.6071E-05	7.7422E-04	9.2199E-04
10	3.3553E-04	4.4991E-05	1.1130E-03	7.4835E-04
11	8.8806E-04	1.2371E-03	4.6442E-04	1.4421E-03
12	8.4834E-04	1.1065E-03	1.3052E-03	4.7600E-04
13	1.5969E-03	1.7007E-03	1.6054E-03	1.7571E-04
14	6.0323E-04	6.9924E-04	5.0507E-03	4.2440E-03
15	4.5325E-04	1.6865E-04	5.2366E-03	5.2996E-03
16	2.0514E-04	5.9467E-04	6.9379E-03	8.0583E-03
17	1.1157E-03	1.4518E-03	8.4983E-03	1.0665E-02
18	9.1800E-04	1.0170E-03	8.6153E-03	1.1602E-02
19	4.9155E-04	7.7379E-04	7.4815E-03	1.0825E-02
20	4.9344E-04	1.2195E-03	8.1890E-03	1.1247E-02
21	7.1936E-04	1.8449E-03	9.5808E-03	1.1613E-02
22	1.0301E-04	1.5005E-03	1.3112E-02	1.3352E-02
23	7.7884E-04	7.0380E-04	1.8327E-02	1.6105E-02
24	7.5094E-04	2.1142E-03	2.2553E-02	1.7299E-02
25	1.3816E-03	3.4688E-04	3.1906E-02	2.3090E-02
26	8.0668E-04	1.4752E-03	3.5821E-02	2.4138E-02
MAE	6.8091E-04	8.5990E-04	7.5393E-03	6.8654E-03

for the SDM are shown in Table 3.4. From the simulation results, the proposed CS method shows the best capability of estimating parameters. Its RMS error is up to 2.43E-03 while the MAE is 1.7284E-04. Both the MAE and RMS error show the lowest value in the tests.

Table 3.3: Estimated parameters of the SDM using various methods.

Parameter	CS	CPSO [17]	PS [19]
I_{ph}	1.0305	1.0286	1.0313
I_{o1}	3.48E-06	8.30E-06	3.18E-06
A	1.3512	1.4512	1.3414
Rs	1.2013	1.0755	1.2053
Rp	981.9824	1850.1000	714.2857
RMS error	2.43E-03	6.24E-03	1.18E-02

Table 3.4: Absolute errors of the simulated terminal current for the SDM.

No	AE_{CS}	AE_{CPSO} [17]	AE_{PS} [19]
1	2.3922E-03	3.5763E-03	2.1175E-03
2	2.6299E-03	3.0301E-03	2.9946E-03
3	2.7210E-04	1.4440E-05	1.2192E-03
4	2.0899E-03	2.9404E-03	6.1614E-04
5	4.2697E-03	5.5153E-03	2.3269E-03
6	4.4044E-03	5.8087E-03	2.0562E-03
7	2.3396E-03	3.5866E-03	3.4007E-04
8	4.8357E-04	1.1943E-03	2.4398E-03
9	2.8229E-03	3.0278E-03	5.8902E-03
10	3.3380E-03	4.7214E-03	6.4455E-03
11	3.2778E-03	5.8455E-03	6.3349E-03
12	2.4035E-03	5.8080E-03	5.3532E-03
13	1.6569E-04	3.4060E-03	2.6676E-03
14	7.6688E-05	3.0079E-03	2.8320E-03
15	1.6103E-03	6.0438E-06	1.1359E-03
16	2.1594E-03	2.2452E-03	6.5327E-04
17	1.4291E-03	3.1777E-03	1.5129E-03
18	1.5867E-03	4.6373E-03	1.5264E-03
19	4.7370E-04	4.2541E-03	2.8309E-03
20	3.0675E-04	3.5412E-03	3.8061E-03
21	2.2819E-03	9.7757E-04	5.9677E-03
22	2.1913E-04	2.3020E-03	3.6377E-03
23	4.4178E-04	8.5170E-04	3.5680E-03
24	3.1187E-04	1.3409E-03	3.8318E-03
25	1.4241E-03	2.5758E-03	2.8346E-03
MAE	1.7284E-03	3.0957E-03	2.9976E-03

3.5.3 Case Study 3: Parameter Estimation for a PV Module under Different Environmental Conditions

Table 3.5: Parameters of the KC200GT PV module obtained by the CS algorithm.

I_{ph}	I_{on1}	A_1	R_{sn}	R_{pn}	k_i	E_{gn}
8.1847	5.12E-10	1.017	0.2574	117.9224	0.0028	1.2474

In this section, the validity of the CS algorithm is evaluated using KC200GT PV module operating under different environmental conditions. The estimated parameters of De Soto's model is shown in Table 3.5. As illustrated in Section 3.1, the main application of the parameter extraction is to predict the I-V characteristics for design purpose. It is worth noting that the SDM can be accurate with the parameters extracted from the data at a uniform test condition. Significant errors may occur when the experimental data are measured under different environmental conditions. In the commercial simulation tool like PSIM [66], the parameters of the SDM are firstly es-

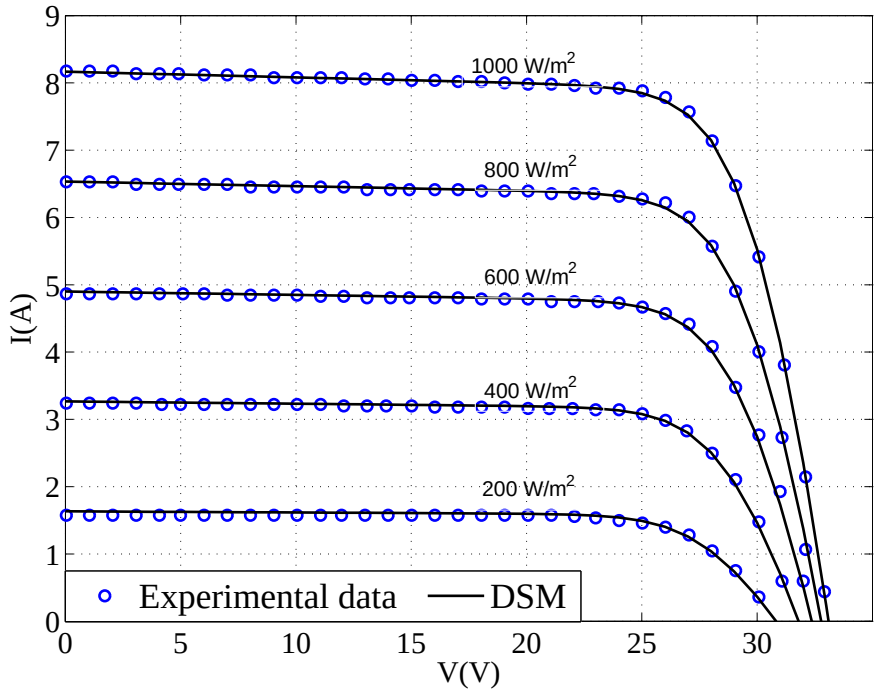

(a)

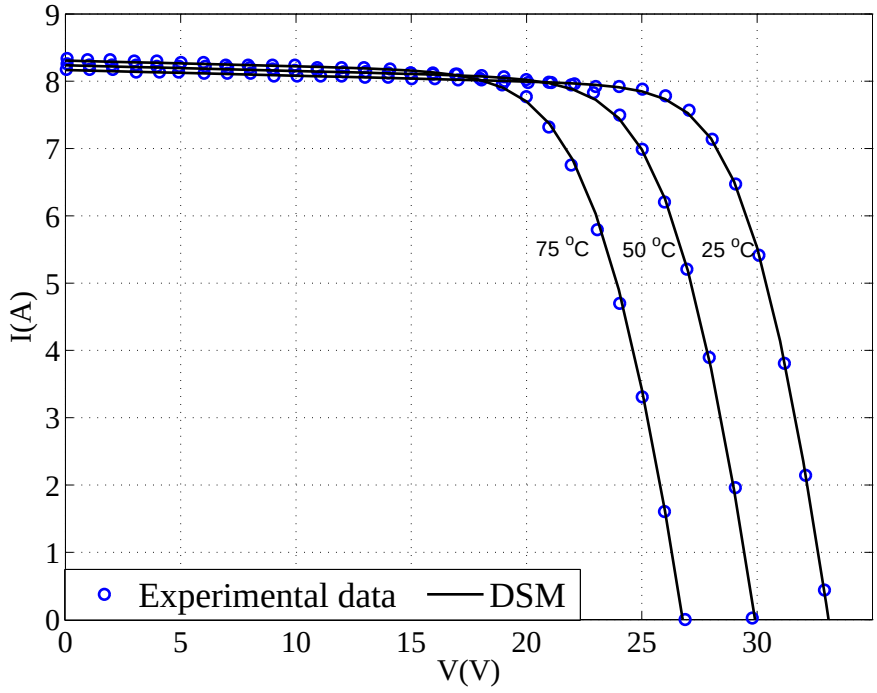

(b)

Figure 3.2: The simulated I-V characteristic curves of the KC200GT PV module: (a) under different irradiance levels; (b) under different temperature levels.

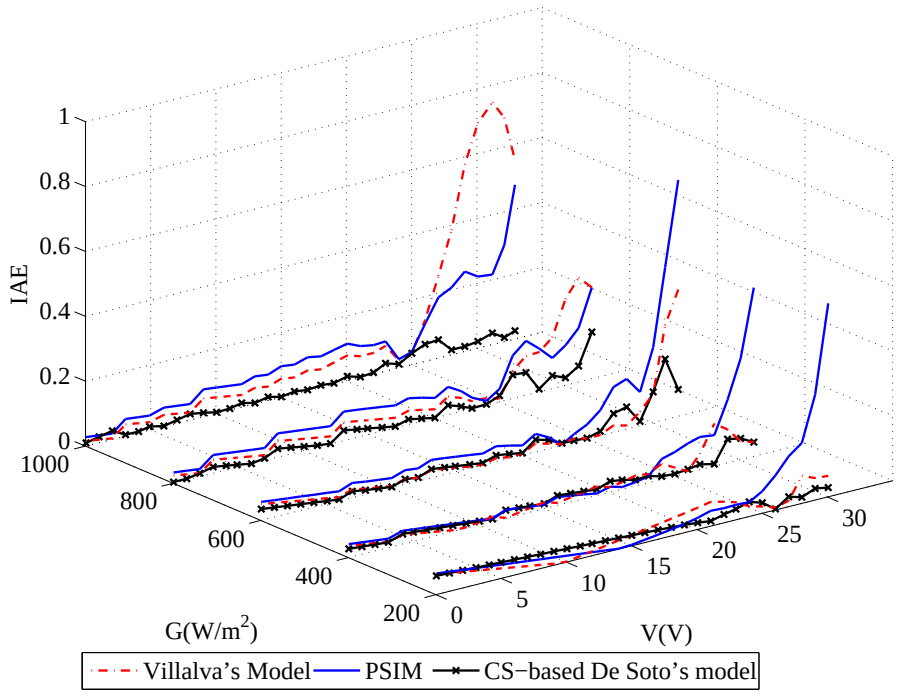

(a)

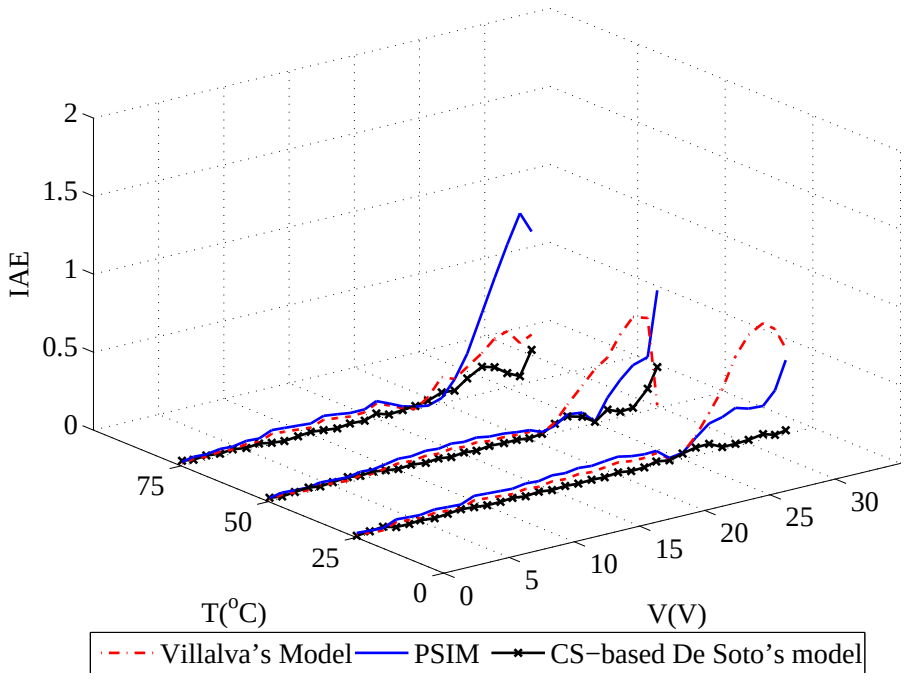

(b)

Figure 3.3: A comparison of the individual absolute errors among different PV modeling methods: (a) under different irradiance levels; (b) under different temperature levels.

timated at the STCs, then the equations (given in the Appendix A) are applied to calculate the electrical characteristics of different operating conditions. In a similar way, the parameter estimation, based on the De Soto's model, can be performed by the data measured under any condition. Figure 3.2 displays the I-V curves generated using the parameters obtained by the CS algorithm. The simulated results are compared with the experimental data, which are collected at five different irradiance levels (1000 W/m^2, 800 W/m^2, 600 W/m^2, 400 W/m^2, and 200 W/m^2) and three different temperature levels (25 ℃, 50 ℃, and 75 ℃). It can be seen that the I-V curves of the De Soto's model fit the whole range of the experimental dataset.

Figure 3.3 shows the absolute current errors of three performance predicting methods under different operating conditions. The three modeling methods are the Villalva's model [21], PSIM model, and De Soto's model with the parameters obtained by the CS algorithm. It is evident the CS-based De Soto's model is more accurate than other analytical models. The PSIM model does not exhibit a good prediction performance under varying environmental conditions. The Villalva's modes show high errors at low temperature or high irradiance levels.

To further validate the accuracy of the CS-based parameter estimation method, the extracted parameters is compared with the ones obtained by the GA in Figure 3.4. In general, the CS algorithm gives the better performance than the GA for all cases. The Maximum Power Point (MPP), usually locating around 74% of the open circuit voltage, is an important technical data in PV modeling. However, a negative point of the GA-based ISDM is that the errors in the high voltage range are relatively high. The maximum absolute error of the GA-based ISDM is up to about 0.8 A, while the absolute error of the CS is kept below 0.2 A.

3.6 Summary

In this work, the Cuckoo Search (CS) algorithm has been implemented to estimate the parameters of two PV models, namely, Single Diode (SD) model and its improved version (De Soto's model). The feasibility of the proposed method has been validated by estimating the parameters of two commercial PV devices. The simulation and experimental results showed that the CS algorithm is capable of not only extracting all the parameters of the SD model under a certain condition but also successfully estimating all the parameters of De Soto's model under different environmental conditions. In

statistical analysis, the CS algorithm recorded the lowest RMS error value compared with the other algorithms such as the GA, CPSO and PS.

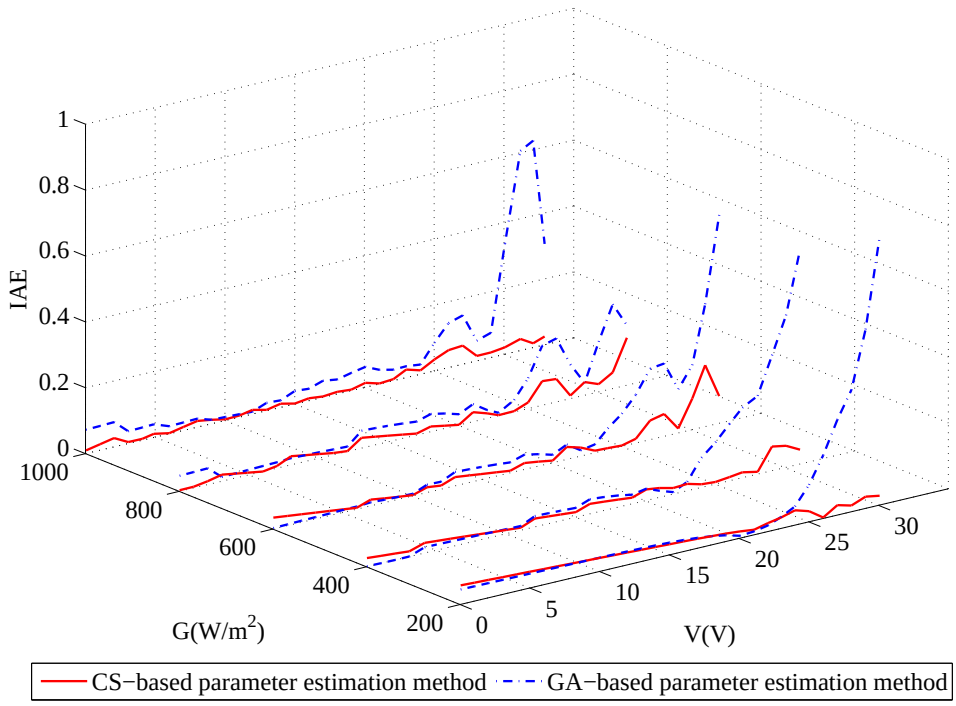

(a)

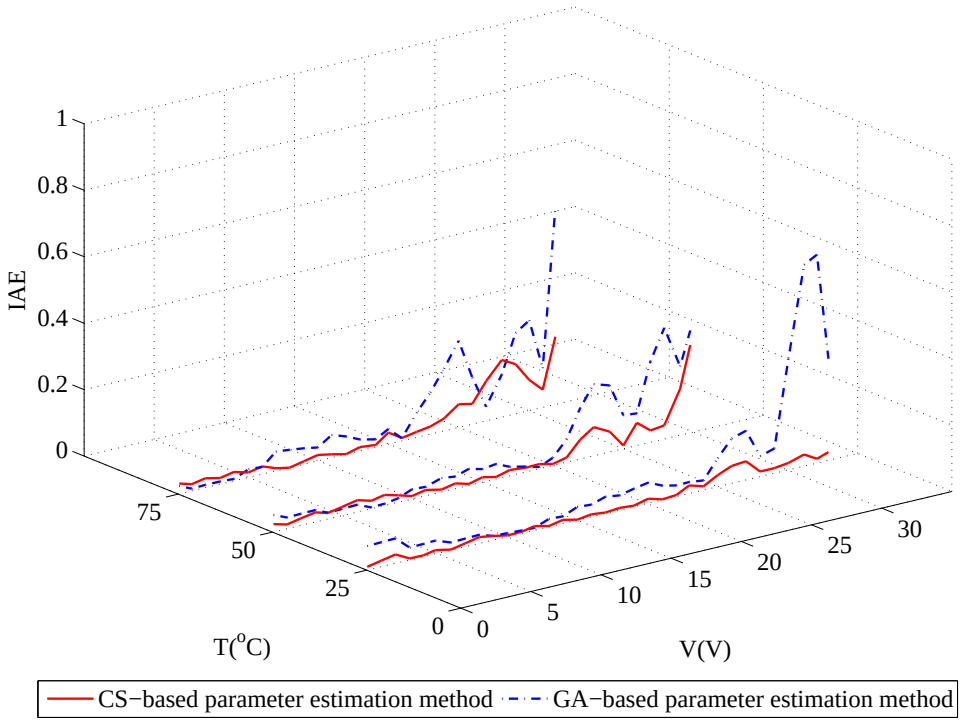

(b)

Figure 3.4: A comparison of the individual absolute errors between CS- and GA- based ISDM: (a) under different irradiance levels; (b) under different temperature levels.

Chapter 4

Parameter Estimation of PV Model via Parallel Particle Swarm Optimization Algorithm

Recently, bio-inspired metaheuristic algorithms have been proven to be powerful optimization tools and are widely utilized to estimate crucial parameters of Photovoltaic (PV) model. However, the computation cost increases as data size or the complexity of the applied PV electrical model increases. To overcome these limitations, this chapter presents Parallel Particle Swarm Optimization (PPSO) algorithm implemented in Open Computing Language (OpenCL) to solve the parameter estimation problem for a wide range of PV electrical models.

This chapter is structured as follows. The first section presents the problem of parameter estimation. Section 4.2 discusses the related works. The parameter estimation problem is formulated in Section 4.3. Section 4.4 sketches the SPSO process, and this is followed by implementation of the proposed PPSO method. Extensive experimental results obtained from the computation on Central Processing Units (CPUs) and Graphic Processing Units (GPUs) are discussed in Section 4.5. Finally, Section 4.6 concludes the work with proposed insights for future work.

The content of this chapter has been published in the following paper:

- Jieming Ma, Ka Lok Man, Tiew On Ting, Nan Zhang, Sheng-Uei Guan, and Prudence W.H. Wong, Accelerating Parameter Estimation for Photovoltaic Models via Parallel Particle Swarm Optimization, *IEEE International Symposium on Computer, Consumer and Control*, pp. 175-178, 2014.

4.1 Introduction

Since the initial silicon PV cell was developed by using the single crystal, varieties of silicon materials have been applied to develop PV cells. For examples, polycrystalline and amorphous silicon cells are designed to be less energy intensive. Thin silicon cells make a compromise between crystalline and amorphous cell. They are reported to achieve better efficiency and stability [2]. With numerous PV cells made of various semiconductor materials using different manufacturing processes, a general performance estimation tool, known as PV electrical model, is crucial to predict the electrical characteristics of these cells before installation. Unfortunately, the PV electrical model cannot be directly utilized because of the lack of proper model parameters characterizing PV cells. The term parameter estimation refers to the process of using sample data to calculate parameters of the selected PV electrical model [53]. With the parameters obtained in such a way, the differences between simulated and experimental data can be minimized considerably.

The bio-inspired metaheuristic algorithms are quite flexible. They do not necessitate the gradient information to guide their search process nor do it impose certain characteristics on the objective function such as convexity or continuity. In the literature [17, 71, 72] and [38], the Particle Swarm Optimization (PSO) was implemented in C-program or MATLAB script to extract the parameters for numerous PV cells and modules. The simulation results show the cohort of methods are capable of extracting the parameters in a high accuracy rate.

Today's programing environments, such as Open Computing Language (OpenCL), are more multifaceted and enable an algorithm to execute in a range of Central Processing Units (CPUs), Digital Signal Processors (DSPs), Field Programmable Gate Arrays (FPGAs), and Graphic Processing Units (GPUs) [123]. These programing environments or Application Programming Interfaces (APIs) exploit the computing capabilities of devices using the languages that only require the highest-level descriptions of parallel process management [124].

With the aim of distributing the workload of a parameter estimation algorithm appropriately to computing devices in parallel mode, a form of computation, in which the PSO-based parameter estimation algorithm is carried out simultaneously, is presented. The parallel program is named Parallel Particle Swarm Optimization (PPSO) in this chapter. It is implemented in OpenCL, which is a heterogeneous programming

framework that supports a wide range of levels of parallelism and efficiently maps to a variety of computing devices [125].

It is desirable that the PPSO outperforms its sequential version, Sequential Particle Swarm Optimization (SPSO), in two aspects:

i. the computational speed tends to be faster than the SPSO with the same amount of work load;

ii. more computational units can be utilized in optimization, and thus it is scalable.

The accuracy and computational efficiency of the proposed method are evaluated by identifying the parameters of two most widely applicable PV electrical models.

4.2 Related Work

As discussed in Chapter 2, the conventional parameter estimation methods are classified into two categories: analytical and numerical techniques. The former represents model parameters mathematically by a series of equations, while the latter extracts parameters utilizing numerical methods to minimize the error of the applied model. Feasible as they are, both of them have inevitable defects. The analytical technique addresses the parameter estimation problem by analytical expressions in terms of the key points on the PV current-voltage (I-V) curve (e.g. the Maximum Power Point (MPP), short-circuit current I_{sc}, and open-circuit voltage V_{oc}, etc). Its errors can be significant and cannot be further reduced if these fundamental elements are incorrectly specified. Numerical parameter extraction is normally considered as an accurate approach in parameter estimation as all the measured data can be used in the calculation. It is axiomatic that its performance depends on the type of fitting algorithm, the cost function as well as the initial values of parameters to be extracted [61]. Moreover, many algorithms can be computationally expensive as the size of the required data is considerably large.

More recently bio-inspired metaheuristic algorithms, such as Genetic Algorithm (GA) [18], Particle Swarm Optimization (PSO) [17,38,71,72], Bacterial Foraging Algorithm (BFA) [73], Pattern Search (PS) [19], Simulated Annealing (SA) [74], Differential Evolution [75, 76], and Cuckoo Search (CS) [77] have been proposed to determine the values of PV model parameters. Albeit accurate, most of these methods apply multiple

agents or particles in random search and do not facilitate a meaningful improvement in computational efficiency.

4.3 Problem Formulation

Based on an optimization algorithm, the parameter estimation method minimizes the differences between calculated current and measured data by adjusting parameters of the PV models [77]. Normally, the parameter estimation process, the fitness value of a trial solution is evaluated by the Root-Mean-Square (RMS) error f_{rms} which serves to aggregate absolute differences into a single measure of predictive power. If the size of experimental data is denoted by N, the RMS error can be mathematically described by the following equation:

$$f_{rms} = \sqrt{\frac{1}{N}\sum_{d=1}^{N}\Big(f_d(\widehat{V},\widehat{I},\mathbf{X})\Big)^2}, \tag{4.1}$$

where $\widehat{V}$ and $\widehat{I}$ denote the measured voltage and current, respectively. The fitness function $f_{rms}(\mathbf{X})$ is the objective function for the d^{th} data, $\mathbf{X}$ is a vector representing the model parameters. Take the SDC for an example, $f_{rms}(\widehat{V},\widehat{I},\mathbf{X})$ is a homogeneous form of (2.5), namely:

$$f_{rms}(\widehat{V},\widehat{I},\mathbf{X}) = I_{ph} - I_{o_1}(e^{\frac{\widehat{V}+\widehat{I}R_s}{A_1V_t}} - 1) - \frac{\widehat{V}+\widehat{I}R_s}{R_p} - \widehat{I}, \tag{4.2}$$

where $\mathbf{X}$ is a vector involving the model parameters I_{ph}, I_{o_1}, A_1, R_s, and R_p.

4.4 Parameter Estimation Algorithm

4.4.1 Sequential Particle Swarm Optimization

By mimicking the swarm behavior of fishes and birds, Kennedy and Eberhart [15] developed a nature-inspired metaheuristic algorithm in 1995. This derivative-free method is particularly suited for continuous variable problems and has been successfully applied to many engineering optimization problems [71, 126]. In [13], Kennedy et al. implemented the algorithm in procedure C-program. We name it the SPSO in this paper.

Algorithm 2: Pseudocode for the SPSO algorithm

```
Input: The measured I-V data
Output: The best solutions in the search-space
Initialize SPSO parameters;
Initialize locations x_{i,j} and velocity v_{i,j} of i^{th} particles in j^{th} dimension;
while Stopping criterion is not satisfied do
    Load the measured I-V data;
    for i = 1 to P (particle) do
        for j = 1 to D (dimension) do
            Evaluate the model error f_d(X);
        end
        Calculate the fitness value RMS via Equation (4.1);
    end
    Update the w via Equation (4.5)
    Update the pbest_i for each particle;
    Update the gbest in the swarm;
    for i = 1 to P (particle) do
        for j = 1 to D (dimension) do
            Update the velocity v_{i,j} via Equation (4.4);
            if v_{i,j} exceeds the bounds then
                Set v_{i,j} to the bounds;
            end
            Update the location x_{i,j} via Equation (4.3);
            if x_{i,j} exceeds the bounds then
                Set x_{i,j} to the bounds;
            end
        end
    end
end
```

The basic idea behind SPSO is to search a space by adjusting the trajectories of particles, which represent possible solutions to the objective function. The pseudocode depicting the SPSO is shown in Algorithm 2. Assume that the swarm size is P and the problem dimension is D. The i^{th} $(i = 1, 2, ...P)$ particle in j^{th} $(j = 1, 2, ...D)$ dimension is denoted by $x_{i,j}$. Similarity, the i^{th} velocity in j^{th} dimension is $v_{i,j}$.

The PSO firstly initializes the algorithm parameters (e.g. inertia weight, learning parameters, etc.) as well as the velocity and position of each particle. In an iteration t $(t = 1, 2, ...t_{max})$, the fitness of particles is evaluated individually by its objective function. When a particle i arrives a location that is better than any positions it arrived, it records the new position as local best position $pbest_i$. In a swarm of particles, there are P local best positions. Among them, the one with the best solution is termed as global best position $gbest$ in the literature. Kennedy and Eberhart proposed that the movements of particles are mainly attracted toward the $pbest_i$ and $gbest$, and the

new position of a particle in the iteration $t+1$ can be mathematically expressed in the following manner:

$$x_{i,j}^{t+1} = x_{i,j}^{t} + v_{i,j}^{t+1}, \tag{4.3}$$

where $v_{i,j}^{t+1}$ is the velocity, expressed as:

$$v_{i,j}^{t+1} = wv_{i,j}^{t} + \alpha\epsilon_1(x_{i,j}^{t} - gbest^{t}) + \beta\epsilon_2(x_{i,j}^{t} - pbest_i^{t}). \tag{4.4}$$

In 4.4, the notations α and β are the learning parameters. Typically, $\alpha \approx \beta \approx 2$. The two random vectors ϵ_1 and ϵ_2 are in the range between 0 and 1. The inertia weight w is utilized to balance the global and local search. It can be taken either as a constant from 0.5 to 0.9 for simplicity, or a linear function in terms of iteration t. In this paper, the value of w is defined as:

$$w^t = w_{max} - (w_{max} - w_{min})\frac{t}{t_{max}}, \tag{4.5}$$

where w_{max} and w_{min} represent the maximum and minimum of the w, respectively.

Normally, lower and upper boundaries are set to ensure the particles are within the predetermined range. If the velocity or position of a particle exceeds the upper bound, it will be reset to the maximum, and vice versa. The algorithm will then continue to evaluate the fitness and a new iteration starts. The PPSO will not stop searching for better solutions until it meets the stopping criterion.

4.4.2 Implementation of Parallel Particle Swarm Optimization

Workload behaviors can be generally classified into two types: data intensive and control intensive. In fact, there is no best architecture that runs optimally on all types of workloads. According to [125], control-intensive applications tend to run faster on super-scalar CPUs, where significant computing efforts have been devoted to branch prediction mechanisms, while data-intensive applications tend to run fast on vector architectures, where the same operation is applied to multiple data items concurrently.

The structure of SPSO has a mix of the workload characteristics. Consider the fitness evaluation function. In a procedure C-program, the RMS errors are computed particle by particle in a for loop. In order to parallelize this function, a separate execution instance is generated to perform fitness evaluation for each particle. Figure 4.1 depicts the concurrent process. With the measured I-V data, the RMS error

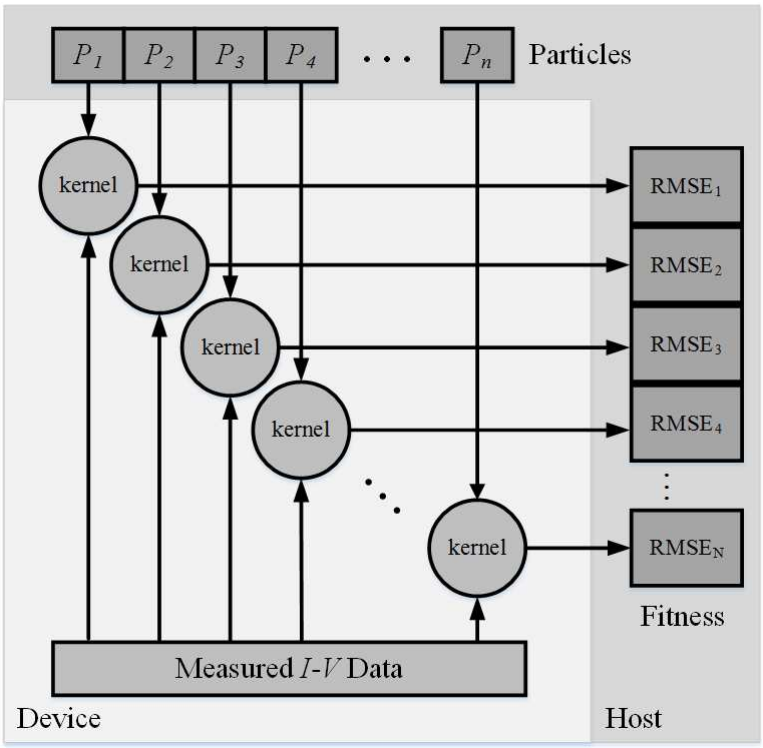

Figure 4.1: Parallel computing framework utilizing a swarm of particles.

can be calculated concurrently in a kernel, which actually is a piece of code executing tasks on a multi-core processor. The fitness evaluation process for a particle does not depend on any other particle, and thereby possesses significant data level parallelism. On the other hand, the function updating the swarm's velocities and positions, especially the process checking whether the values exceed the predefined bounds, can be assigned to the category of control-intensive applications since it involves explicit flow-control constructs such as *if-then-else*. From these considerations, it is desirable that a programming framework with the capability of execution across a wide range of device types so that the workload can be executed most efficiently on a specific style of hardware architecture.

The OpenCL, managed by the nonprofit technology consortium Khronos Group, is such a heterogeneous programming framework that supports a wide range of levels in parallelism and efficiently maps to a variety of computing devices [125]. A host and a device-side language are both defined in the OpenCL. The former offers a management layer that supports efficient plumbing of complicated concurrent programs, while the latter maps the heavy work load into a wide range of memory systems.

In our implementation, the main program was written in OpenCL code. APIs are

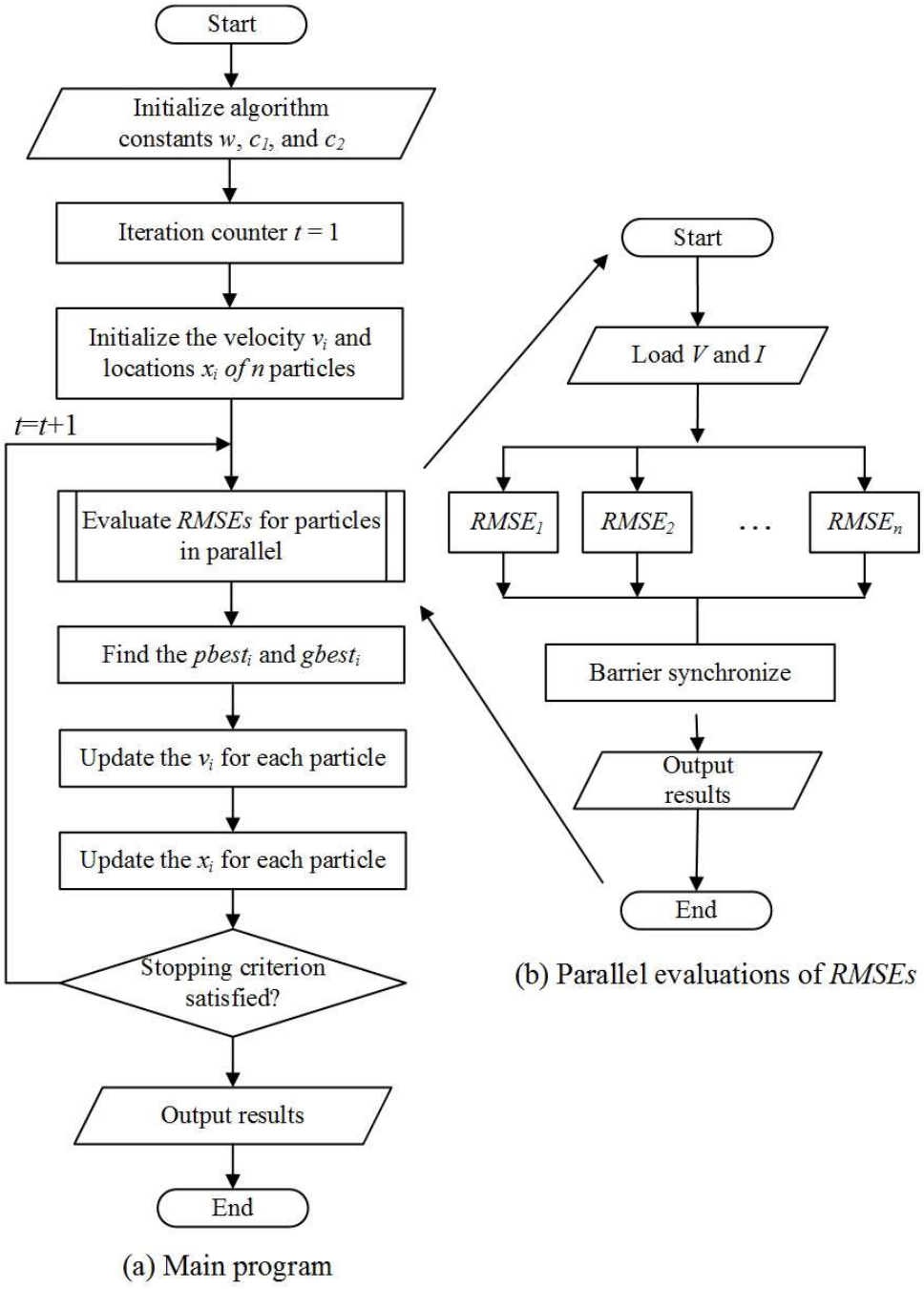

Figure 4.2: Flow chart of the PPSO algorithm: (a) The main program; (b) Parallel evaluations of RMS error.

used to configure a context which allows commands and data passing to the device. Figure (4.2) represents the whole algorithmic flow of the proposed PPSO. After initialization, velocities and positions of particles are transferred from the host to the device. In the OpenCL kernel function, fitness evaluations are decomposed to perform the evaluations concurrently on a multi-processor device. Global synchronization or

barrier function is applied to ensure that all of the fitness evaluations are completed before they are transferred back to the host. The local best and global best positions are aided to determine the new velocities and positions of particles. The algorithm will then return to the parallel process by evaluations through the objective function until the stopping criterion is satisfied.

4.5 Experiments and Results

Table 4.1: Estimated parameters of SDC and DDC on the R.T. France solar cell using various methods.

PV model	Method	$I_p v(A)$	$R_s(\Omega)$	$R_p(\Omega)$	$I_{o_1}(\mu A)$	a_1	$I_{o_2}(\mu A)$	a_2
SDC	PPSO	0.7608	0.0364	53.7185	0.3230	1.4812	-	-
	LSO [16]	0.7608	0.0364	53.7634	0.3223	1.4837	-	-
	PS [19]	0.7617	0.0313	64.1026	0.9980	1.6000	-	-
	SA [74]	0.7620	0.0345	43.1034	0.3130	1.5172	-	-
DDC	PPSO	0.7608	0.0370	56.5710	0.3230	1.4317	1.1793	2
	SA [74]	0.7623	0.0345	43.1034	0.3230	1.5172	1.1793	2
SDM	PPSO	1.0305	1.2013	981.9823	3.4823	1.3512	-	-
	LSO [16]	1.0318	1.2057	549.4505	3.4823	1.3458	-	-
	PS [19]	1.0313	1.2053	714.2857	3.1756	1.3414	-	-
	SA [74]	1.0031	1.1989	833.3333	3.4823	1.3561	-	-
DDM	PPSO	1.0305	1.2013	981.9845	3.4823	1.3512	0.0001	2

Table 4.2: PPSO's search ranges for relevant models.

Model Type	SDC DDC	SDM DDM
I_{ph}	[0.7, 1]	[0.9, 1.2]
R_s	[0.001, 1]	[0.001, 1]
R_p	[20, 200]	[20, 3000]
I_{o1}	[1E-10, 1E-4]	[1E-10, 1E-4]
a_1	[0.8, 2]	[0.8, 2]
I_{o2}	[1E-10, 1E-4]	[1E-10, 1E-4]
a_2	[0.8, 2]	[0.8, 2]

The proposed PPSO is implemented in OpenCL and simulations were performed under Microsoft Windows 7 64-bit operating system. Its algorithm parameters are set as learning factors $c_1 = c_2 = 2$, the maximum inertia factor $w_{max} = 0.9$, the minimum inertia factor $w_{min} = 0.4$.

With the aim of conducting a comprehensive evaluation, both SDM and DDM are

applied in parameter estimation. The experimental I-V data of a 57 mm diameter commercial silicon PV cell (R.T.C. France) and a PV module (Photowatt-PWP 201) comprising 36 polycrystalline silicon PV cells are considered as test examples in this paper. (The measured data of the R.T.C. France silicon PV cell and Photowatt-PWP 201 PV module are given in Appendix B and C, respectively.) Their values were obtained under the controlled conditions of an automated measuring system with a CBM8096 microcomputer demonstrated in [16]. It is assumed that all the silicon cells in a PV module are identical and work under the same temperature (R.T.C. France PV cell at 33°C and Photowatt-PWP 201 PV module at 45°C).

Extensive simulation results and statistical analysis are presented in the next sections. Section 4.5.1 studies the parameter estimation capability by evaluating the evolutionary performance and the distribution of fitness values for the proposed PPSO method. Besides RMS error, the other two fundamental measures, namely, the absolute error e and the mean absolute error $\bar{e}$, are used to evaluate how close simulated current values I are to the measured data $\widehat{I}$. Their mathematical expressions are shown as follows:

$$e = |I - \widehat{I}|, \tag{4.6}$$

$$\bar{e} = \frac{1}{N}\sum_{d=1}^{N} e_d, \tag{4.7}$$

where $\widehat{I}$ is the measured terminal current.

In Section 4.5.2, we demonstrate how the PPSO method outperforms its sequential version in terms of computational speed. Speedup is used to qualify the ratio of sequential execution time to parallel execution time:

$$S = \frac{T_s}{T_p}, \tag{4.8}$$

where T_s is the execution time of the sequential algorithm on the host processor and T_p is the execution time of the parallel algorithm on multi-core devices.

4.5.1 Parameter Estimation Capability

As stated in [127], 'no free lunch theorems for optimization', that is to say there is no universally best algorithm. Among so many optimization algorithms, our purpose is to find a method that performs the best in the parameter estimation for PV electrical models.

Table 4.1 shows the estimated parameters for different PV electrical models obtained from the best of 30 runs of the proposed PPSO method, in which the swarm size and maximum iteration number are set to 2048 and 80000 respectively. It is worth noting that the objective function is minimized with respect to the range of parameters throughout parameter extraction process. In this investigation, the search range for each parameter is tabulated in Table 4.2. In order to make a comprehensive comparison of the accuracy of these parameter estimation methods, the parameters estimated by other methods (e.g. Least Square Optimization (LSO) [16], Pattern Search (PS) [19] and Simulated Annealing (SA) algorithms [74]) are also listed in Table 4.1 for reference. The LSO is a non-linear algorithm based on the Newton model modified with Levenberg parameter. Unlike LSO, PS and SA as well as PPSO, they do not require the gradient information to guide their search process nor do they impose certain characteristics on the objective function such as convexity or continuity, and thus these methods are quite flexible and straightforward to implement. The PS finds a sequence of trial solutions that approach the optimal fitness value. A pattern is a set of vectors used to determine which trial solution to choose. At each iteration, a set of solutions, called a mesh, will be polled by evaluating the fitness. If a solution that yields a better fitness value, it becomes the current point at the next iteration. Otherwise, the poll is unsuccessful and the solution remains the same at the next iteration. The SA, however, obtains the optimal value by mimicking the annealing process in material processing when a metal cools and freezes into a crystalline state with the minimum energy and larger crystal size [12].

With these parameters, the simulated value of the terminal current is available for reconstruction. This can be achieved by substituting back into (2.5), (2.6), (2.10), or (2.11). In this case, terminal voltage V (or V'), temperature T and solar irradiance G are known quantities. The terminal current I (or I') acts as an unknown and its value is obtained numerically by Newton method [74].

In Table 4.3 and 4.4, the absolute errors obtained from the PPSO algorithm are compared with three different parameter estimation approaches: LSO, PS and SA methods. The absolute errors of the PPSO method are in the range [8.7615E-5, 1.5969E-3] for the SDC, [7.2612E-5, 1.4192E-3] for the DDC, [3.2125E-5, 4.4171E-3] for the SDM, and [3.3165E-5, 4.4171E-3] for the DDM. The mean absolute errors $\bar{e}$ are listed in the last row of the two table to show the average performance of these algorithms. For all the applied PV electrical models, the PPSO appears to be the most accurate, followed by

Table 4.3: Absolute error e of the simulated terminal current on the R. T. C. France solar cell.

No.	e (SDC)				e (DDC)	
	PPSO	LSO [16]	PS [19]	SA [74]	PPSO	SA [74]
1	8.7615 E-5	1.09 E-4	5.3700 E-4	9.8000 E-4	7.6234 E-5	2.48 E-3
2	6.6261 E-4	6.8600 E-4	1.3430 E-3	1.71 E-3	5.7046 E-4	2.71 E-3
3	8.5470 E-4	8.7900 E-4	1.7470 E-3	2.04 E-3	8.2803 E-4	2.58 E-3
4	3.4581 E-4	3.2100 E-4	7.3900 E-4	9.70 E-4	3.1332 E-4	1.08 E-3
5	9.4418 E-4	9.1900 E-4	3.1400 E-4	4.90 E-4	8.6004 E-4	2.10 E-4
6	9.5703 E-4	9.3100 E-4	4.5300 E-4	5.80 E-4	8.3090 E-4	5.00 E-5
7	9.1557 E-5	1.2000 E-4	1.6220 E-3	1.72 E-3	2.4571 E-4	7.60 E-4
8	8.5796 E-4	8.2600 E-4	7.3700 E-4	8.40 E-4	6.9610 E-4	4.10 E-4
9	4.1271 E-4	3.6900 E-4	1.1510 E-3	1.32 E-3	2.7078 E-4	2.00 E-4
10	3.3556 E-4	2.6100 E-4	1.0320 E-3	1.38 E-3	2.4619 E-4	3.90 E-4
11	8.8803 E-4	1.0440 E-3	1.8170 E-3	2.50 E-3	8.9503 E-4	5.10 E-4
12	8.4833 E-4	1.1820 E-3	1.0050 E-3	2.25 E-3	7.5708 E-4	6.00 E-5
13	1.5969 E-3	2.3090 E-3	6.2800 E-4	2.66 E-3	1.4192 E-3	3.20 E-4
14	6.0302 E-4	7.7500 E-4	3.0400 E-3	5.00 E-5	8.2221 E-4	2.49 E-3
15	4.5414 E-4	3.0650 E-3	3.4050 E-3	5.50 E-4	2.6122 E-4	1.94 E-3
16	2.0195 E-4	4.3300 E-3	5.2200 E-3	5.60 E-4	3.0525 E-4	3.01 E-3
17	1.1069 E-3	6.1680 E-3	6.5810 E-3	1.77 E-3	1.0954 E-3	4.08 E-3
18	8.9946 E-4	1.0241 E-2	5.7470 E-3	1.48 E-3	7.9575 E-4	3.58 E-3
19	5.1961 E-4	1.6846 E-2	2.4770 E-3	5.50 E-4	6.5768 E-4	1.22 E-3
20	5.2319 E-4	2.2874 E-2	1.1200 E-4	1.11 E-3	6.3240 E-4	2.60 E-4
21	7.3999 E-4	3.0060 E-2	2.6910 E-3	1.91 E-3	7.7866 E-4	1.03 E-3
22	1.1132 E-4	3.6806 E-2	3.9100 E-3	1.23 E-3	7.2612 E-5	8.80 E-4
23	7.7634 E-4	4.3444 E-2	3.5900 E-3	5.00 E-4	8.6343 E-4	2.50 E-4
24	7.5309 E-4	5.4194 E-2	5.4230 E-3	9.40 E-4	6.6895 E-4	1.80 E-3
25	1.3770 E-3	5.9145 E-2	3.3400 E-4	4.53 E-3	1.3931 E-3	3.03 E-3
26	8.3088 E-4	6.9445 E-2	3.3900 E-4	2.50 E-3	9.1210 E-4	5.30 E-4
$\bar{e}$	6.8384 E-4	1.4129 E-2	2.1536 E-3	1.43 E-3	6.6415 E-4	1.38 E-3

SA and PS, and finally LSO. Among these test results, the $\bar{e}$ obtained by PPSO with the DDC achieves the lowest value, recording 6.6415E-4, which is 51.85% lower than the SA with the same PV electrical model, and is approximately 3 % lower than the PPSO with the SDC. It is observable that the accuracy can be improved if we apply the DDC instead of SDC. However, in the simulation results for Photowatt-PWP 201 PV module, the $\bar{e}$ cannot be decreased by using the DDM. That indicates the complicated model DDM does not always gives an accurate simulation results in parameter estimation, and the proposed method behaves more stable on the SDC and SDM.

Figure 4.3 shows the qualitative representation of the average evolutionary performance of the PPSO method for different electrical PV models. The fitness value,

Table 4.4: Absolute error e of the simulated terminal current on the Photowatt-PWP 201 PV module.

No.	e (SDM)				e (DDM)
	PPSO	LSO [16]	PS [19]	SA [74]	PPSO
1	2.3782 E-3	2.1970 E-3	2.1350 E-3	6.00 E-5	2.3782 E-3
2	2.6159 E-3	3.7830 E-3	3.0300 E-3	6.40 E-4	2.6159 E-3
3	2.5816 E-4	2.6510 E-3	1.2670 E-3	1.41 E-3	2.5815 E-4
4	2.1037 E-3	1.4060 E-3	5.5800 E-4	3.49 E-3	2.1037 E-3
5	4.2831 E-3	2.3600 E-4	2.2620 E-3	5.41 E-3	4.2831 E-3
6	4.4171 E-3	1.0090 E-3	1.9860 E-3	5.29 E-3	4.4171 E-3
7	2.3505 E-3	3.8790 E-3	4.1900 E-4	2.96 E-3	2.3505 E-3
8	4.9114 E-4	6.4210 E-3	2.5280 E-3	8.30 E-4	4.9117 E-4
9	2.8215 E-3	1.0319 E-2	6.0230 E-3	2.82 E-3	2.8215 E-3
10	3.3469 E-3	1.1258 E-2	6.6030 E-3	3.70 E-3	3.3469 E-3
11	3.3028 E-3	1.1449 E-2	6.4990 E-3	4.03 E-3	3.3027 E-3
12	2.4514 E-3	1.0586 E-2	5.4370 E-3	3.50 E-3	2.4513 E-3
13	8.8036 E-5	7.5650 E-3	2.3500 E-3	1.00 E-3	8.8240 E-5
14	1.8993 E-4	7.4220 E-3	2.3080 E-3	1.52 E-3	1.8964 E-4
15	1.4578 E-3	4.7070 E-3	1.1900 E-4	4.40 E-4	1.4582 E-3
16	1.9663 E-3	3.0930 E-3	1.2550 E-3	1.22 E-3	1.9668 E-3
17	1.1963 E-3	3.0740 E-3	6.1700 E-4	3.60 E-4	1.1969 E-3
18	1.3164 E-3	1.7300 E-3	1.1540 E-3	8.00 E-4	1.3171 E-3
19	1.6901 E-4	2.3410 E-3	3.9000 E-4	7.40 E-4	1.6978 E-4
20	6.4246 E-4	2.5470 E-3	1.6150 E-3	1.89 E-3	6.4161 E-4
21	2.6453 E-3	5.0520 E-3	5.2050 E-3	5.34 E-3	2.6444 E-3
22	1.6880 E-4	6.6900 E-4	5.6100 E-4	5.90 E-4	1.6782 E-4
23	3.2125 E-5	2.2830 E-3	5.1000 E-5	6.00 E-5	3.3165 E-5
24	1.1699 E-4	3.1850 E-3	2.4400 E-4	5.23 E-4	1.1590 E-4
25	9.7829 E-4	6.7500 E-3	2.2670 E-3	2.62 E-3	9.7942 E-4
$\bar{e}$	1.6715 E-3	4.6245 E-3	2.2753 E-3	2.0288 E-3	1.6716 E-3

namely the RMS error, is averaged over 30 runs of the applied parameter estimation methods. In general, the average fitness of PPSO drops dramatically in the convergence traces, especially before the first 2000 iterations. The average fitness of the SDM reaches the lowest value after 10000 iterations by using the PPSO with 2048 particles as seen in the plots. Whichever model we use, the algorithm with larger swarm size tends to be faster in terms of convergence speed.

Based on the above analysis, the PPSO shows its consistent performance of extracting the parameters from the experimental data with a relatively high accuracy. Figure 4.4 further demonstrates the distribution of the fitness values obtained from the PPSO method after 20000 iterations. The swarm size is respectively set to 16, 64, 256,

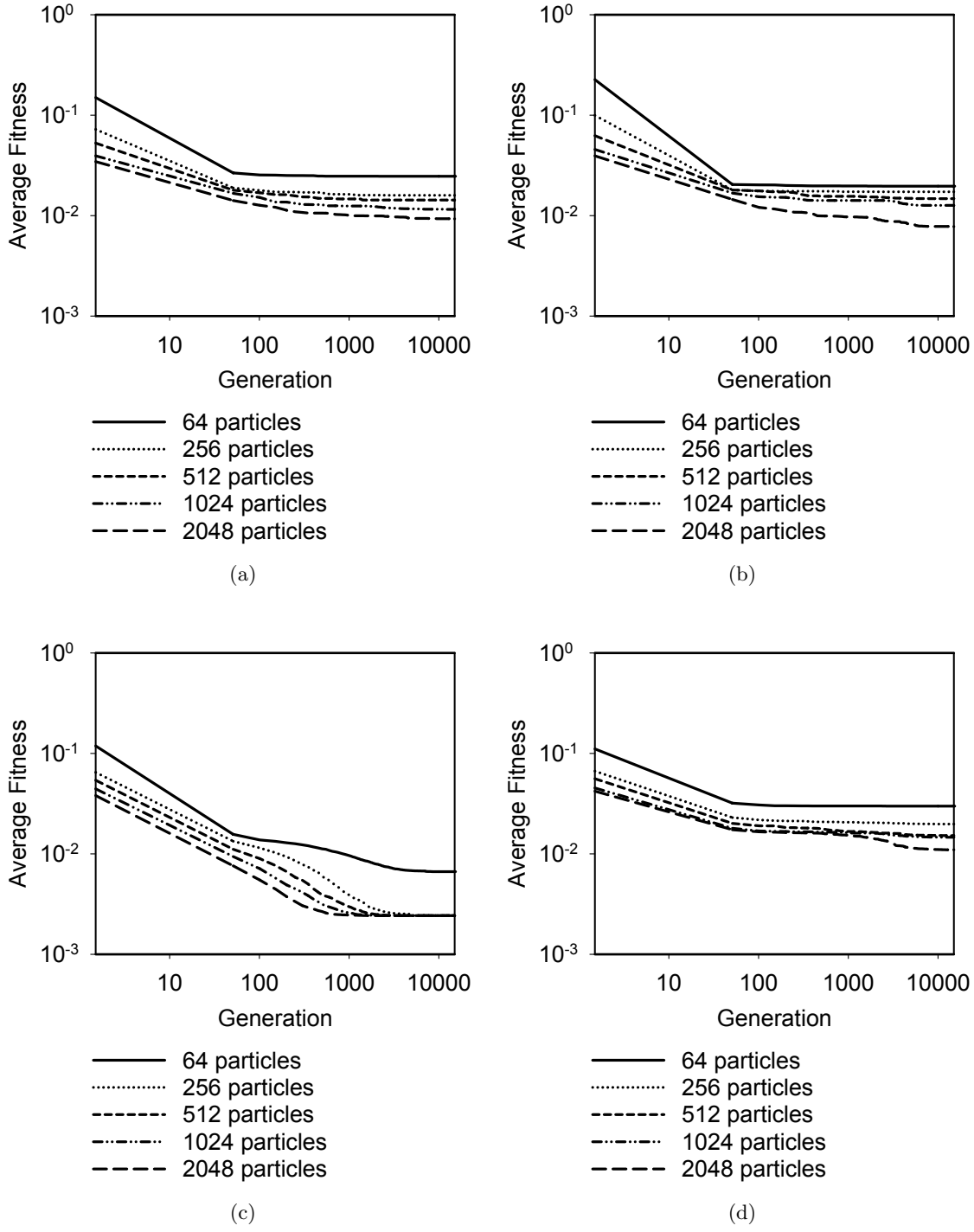

Figure 4.3: Average evolutionary performance of the PPSO with various PV electrical models: (a) SDC; (b) DDC; (c) SDM; (d) DDM.

512, 1024 and 2048. It is observed that the intermediate values tend to decrease with the increasing of the particle number, which agrees well with the simulation results in Figure 4.3. The decreasing trend implies that the PPSO with a large swarm size

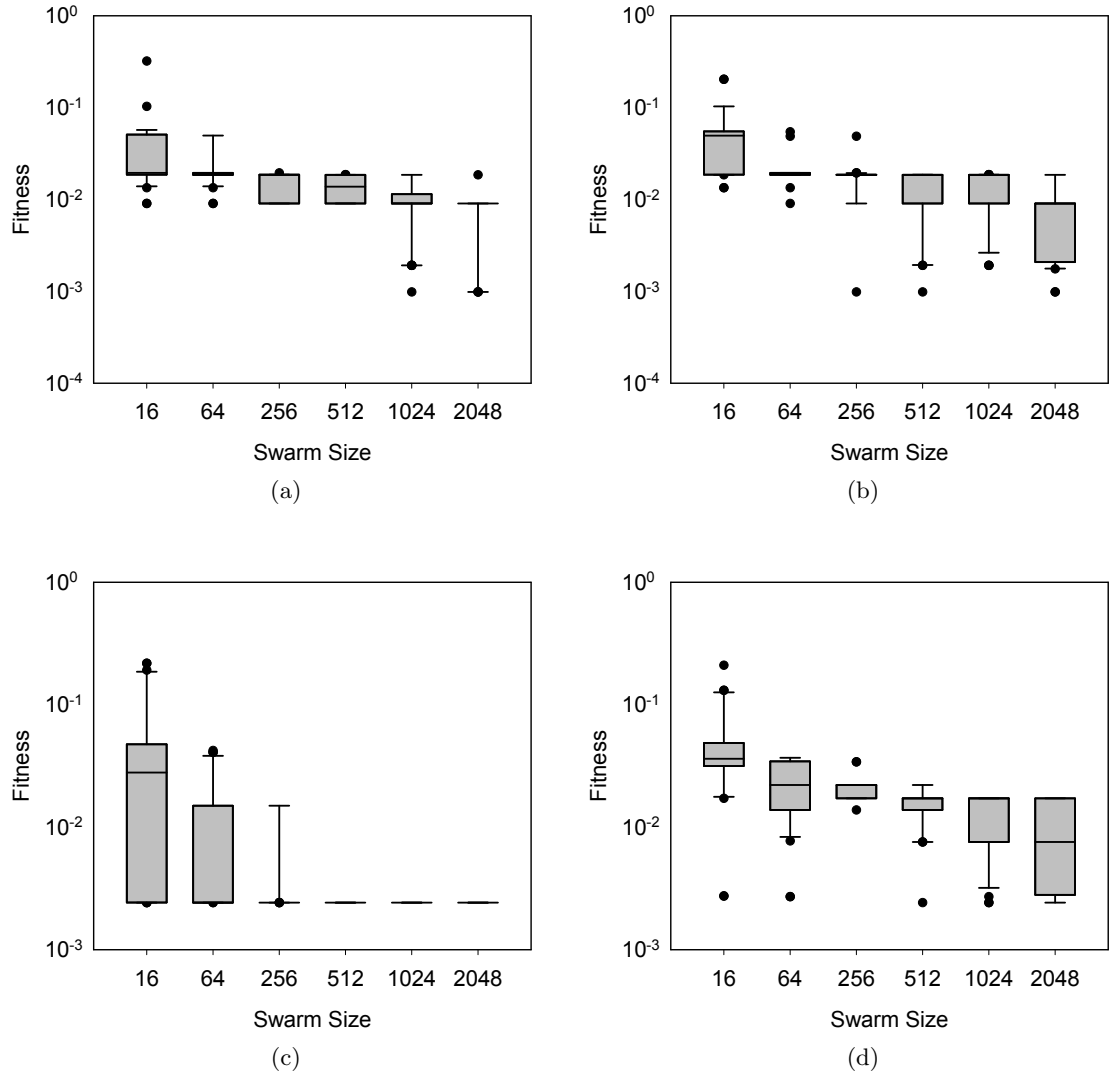

Figure 4.4: Distribution of the fitness values obtained by the PPSO with various PV electrical models: (a) SDC; (b) DDC; (c) SDM; (d) DDM.

has a higher possibility of achieving good fitness value without changing the iteration number. In this sense, the PPSO can improve the accuracy in an unit time on a specified device. From another perspective, the PPSO executes particle evolution processes concurrently with the applied computing device, and in such a way, the efficiency of parameter estimation can be improved. The speedup, as well as the parallel efficiency of the proposed PPSO method, will be discussed in the subsequent subsection.

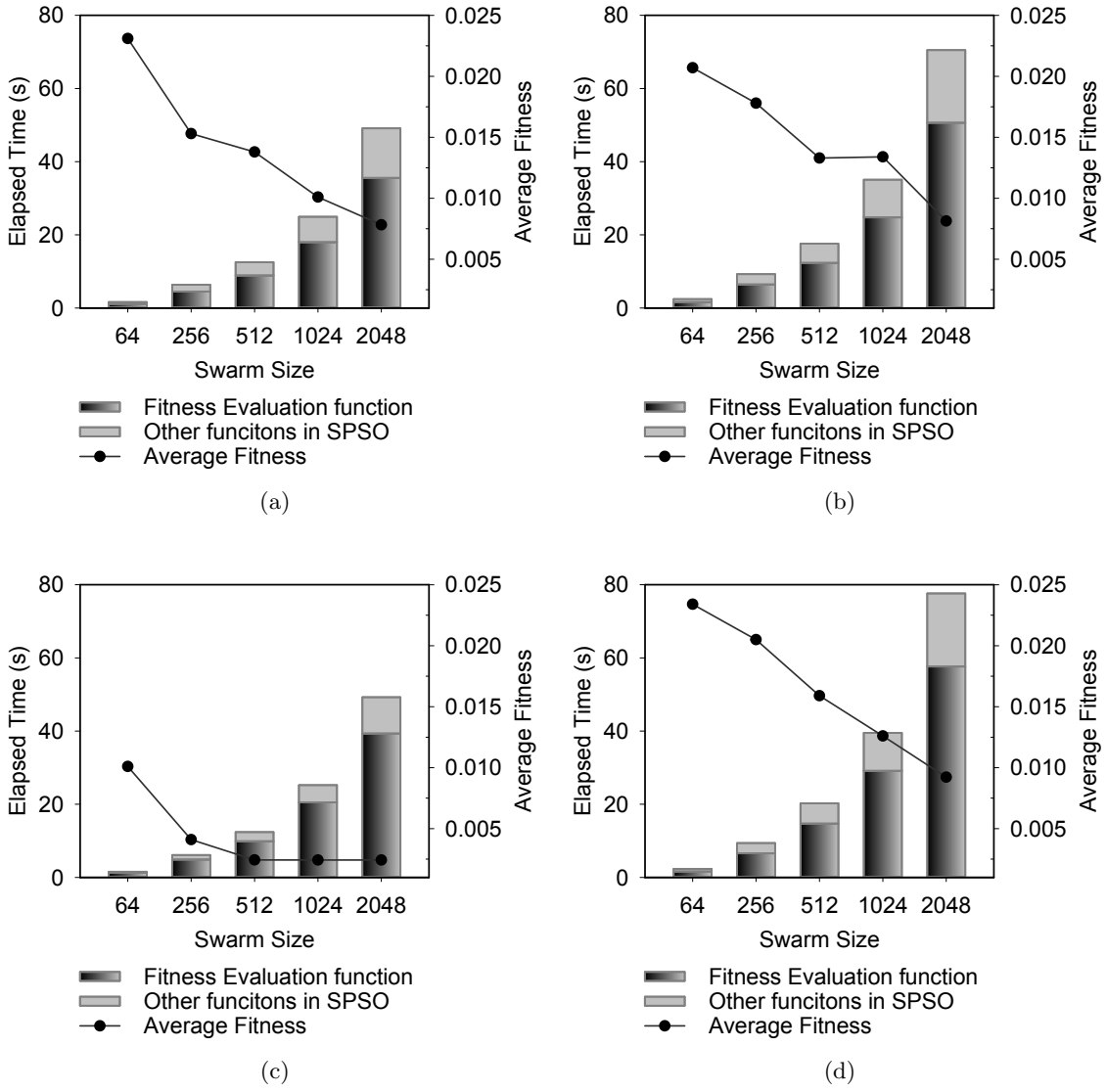

Figure 4.5: The execution time and average fitness of the sequential parameter estimation for PV electrical models on Intel i7-4770k: (a) SPSO with the SDC; (b) SPSO with the DDC; (c) SPSO with the SDM; (d) SPSO with the DDM.

4.5.2 Speedup and Parallel Efficiency

Parameter estimation is an optimization problem for a multi-variable objective function with a huge amount of measured data, and its computational speed are becoming more crucial.

In the implementation of PPSO, we follow a hybrid approach whereby the fitness is evaluated in the kernel and the other processes (e.g. position updating and velocity updating) are performed in the host device. The results averaged over 30 trials of the

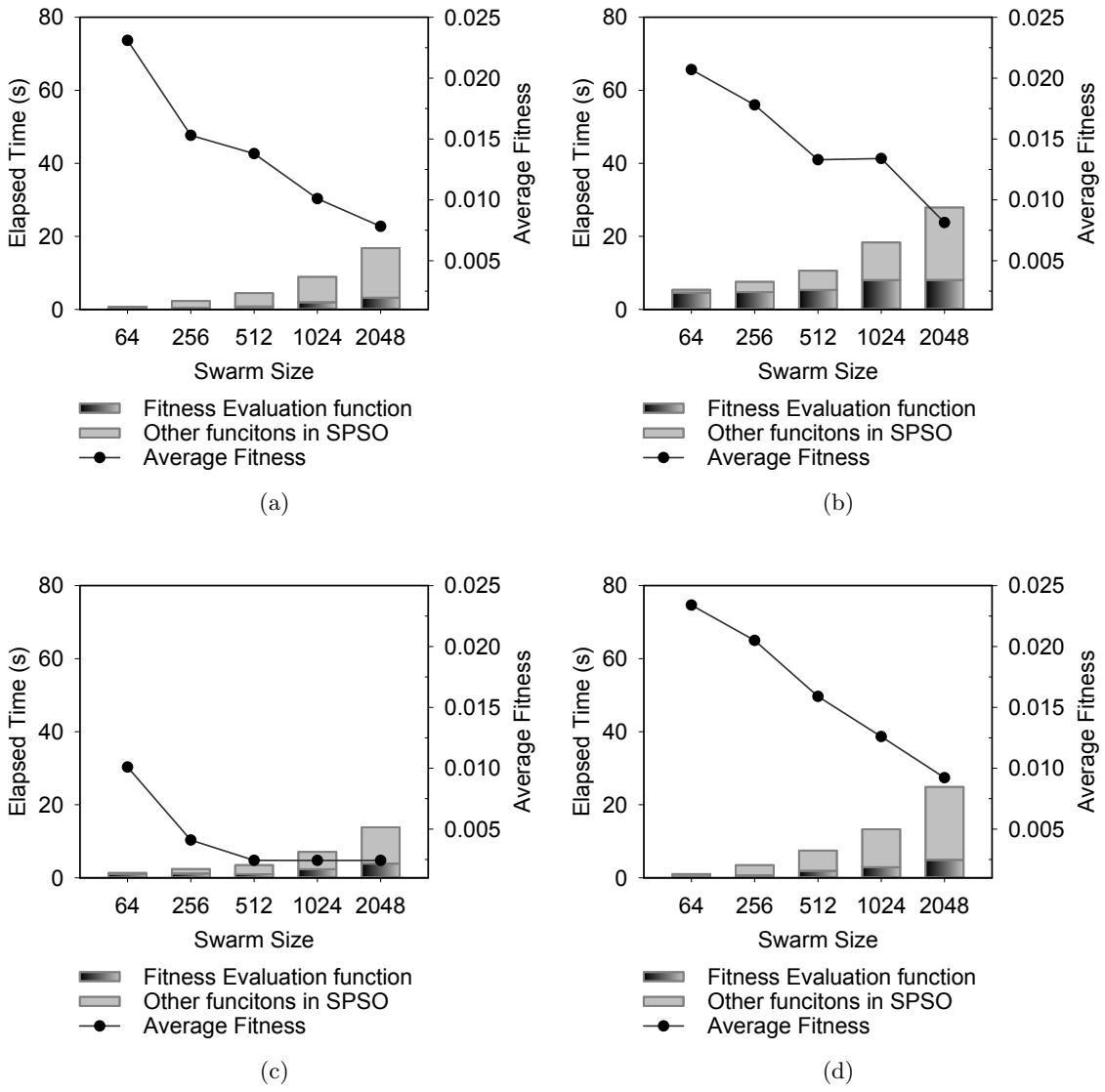

Figure 4.6: The execution time and average fitness of the parallel parameter estimation for PV electrical models on Intel i7-4770k: (a) PPSO with the SDC; (b) PPSO with the DDC; (c) PPSO with the SDM; (d) PPSO with the DDM.

PPSO with 20000 iterations. To show how much the parallel processing speed up the fitness evaluation function, the execution time on the host and the device are denoted by bars with light and dark colors separately. A comparison of the total execution time and fitness values, both measured in the proposed parallel based parameter estimation and its sequential counterpart for PV electrical models, is made in Figure 4.5. From Figure 4.5 (a), (b), (c) and (d), we observe that the execution time on the fitness evaluation makes up much larger percentage than that on the other functions in sequential processing. Except for the fitness evaluation, the codes of the PPSO and SPSO are

Table 4.5: PPSO's speedup on heterogeneous computing platforms.

Model	Host	Device	Swarm Size				
			64	256	512	1024	2048
SDC	Intel i3-3220	Intel i3-3220	1.5096	1.6758	1.7496	1.8583	2.0677
	Intel i5-3470	Intel i5-3470	2.0728	2.4171	2.5966	2.7715	2.9036
	Intel i7-4770k	Intel i7-4770k	2.1304	2.7308	2.7962	2.8049	2.9263
	Intel i7-4770k	Nvidia GT620	0.8506	1.8118	1.9429	1.9841	2.0632
	Intel i7-4770k	Nvidia GTX760	0.5653	1.5336	1.9491	2.1169	2.6899
	Intel i7-4770k	AMD R9 200	1.3445	1.8870	2.6606	3.2312	3.7191
DDC	Intel i3-3220	Intel i3-3220	1.4597	1.7764	2.1751	2.1785	2.8261
	Intel i5-3470	Intel i5-3470	2.2487	2.5149	2.7594	2.8424	2.8292
	Intel i7-4770k	Intel i7-4770k	2.2467	2.6223	2.6979	2.8540	2.9135
	Intel i7-4770k	Nvidia GT620	0.7211	1.6203	1.7543	1.7729	1.8523
	Intel i7-4770k	Nvidia GTX760	0.4404	1.2430	1.7674	1.9659	2.6038
	Intel i7-4770k	AMD R9 200	1.4033	2.0470	2.6382	2.9913	3.4426
SDM	Intel i3-3220	Intel i3-3220	1.5789	1.7464	1.7713	1.8096	2.1682
	Intel i5-3470	Intel i5-3470	2.6659	2.8683	3.0358	3.3117	3.4434
	Intel i7-4770k	Intel i7-4770k	1.1599	2.5349	3.5339	3.5531	3.5648
	Intel i7-4770k	Nvidia GT620	0.8162	1.7427	1.9607	1.9665	2.0687
	Intel i7-4770k	Nvidia GTX760	0.5962	1.7892	2.3770	2.8178	3.5182
	Intel i7-4770k	AMD R9 200	1.3656	2.0887	3.1276	4.0524	4.6062
SDM	Intel i3-3220	Intel i3-3220	1.7309	1.7893	1.9980	2.2967	2.5823
	Intel i5-3470	Intel i5-3470	2.3141	2.5749	2.7770	2.8632	3.0007
	Intel i7-4770k	Intel i7-4770k	2.2467	2.6979	2.7100	2.9685	3.1185
	Intel i7-4770k	Nvidia GT620	0.7483	1.6447	1.7981	1.9169	1.9219
	Intel i7-4770k	Nvidia GTX760	0.4585	1.2852	1.8869	2.1498	2.7097
	Intel i7-4770k	AMD R9 200	1.3460	1.9324	2.8139	3.3412	3.6521

exactly the same, and therefore their execution time on the host is similar. As seen in Figure 4.5 (e), (f), (g) and (h), the computation time takes in fitness evaluation function can be significantly reduced by the PPSO. In addition, the total execution time for the DDC is longer to the one for SDC. This happens because the computational complexity of the DDM is higher than that of the SDM as seen in (2.10) and (2.11).

To further evaluate the parallel performance of the proposed PPSO algorithm, We evaluate the speedup of PPSO on a number of multi-core computing devices, which includes:

i. **Intel (R) Core (TM)** i3-3220 CPU
   (2 cores, 2 threads, 3.3 GHz)

ii. **Intel (R) Core (TM)** i5-3470 CPU

(4 cores, 4 threads, 3.2 GHz)

iii. **Intel (R) Core (TM)** i7-4770K CPU
(4 cores, 8 threads, 3.5 GHz)

iv. **NVIDIA (R) GeForce (TM)** GTX 760 GPU
(1152 CUDA cores, 980 MHz)

v. **NVIDIA (R) GeForce (TM)** GT 620 GPU
(96 CUDA cores, 700 MHz)

vi. **AMD (R) Radeon (TM)** R9 200 GPU
(2048 stream processors, 1150 MHz)

Table 4.5 lists the average speedup of the PPSO with different swarm size on these devices. From simulation results, some conclusions can be drawn. In most tests, the speedup of the PPSO is above 1. In other words, the execution time of the PPSO is normally shorter than that of the SPSO. Moreover, the parallel program with larger swarm size tends to perform at a faster speed. The exception is made by the PPSO with a swarm size of 64 particles. Its speed is even lower than the corresponding sequential version on GT 620 and GTX 760, which implies the overheads on data communication and kernel scheduling are more significant on the two GPUs. With more applied particles, the speedup appears to be a larger ratio. This is because the speedup on the applied multi-core devices over the host processor is large enough to compensate for the initial data transfer cost. From Figure 4.5 (a) and (e), we can conclude that the PPSO can achieve better fitness values if taking the same amount of execution time as the SPSO. Similar trends are observable in the speedup for the DDC, SDM, and DDM. Among these tests, the parallel program with Intel i7-4770k and AMD R9 200 series exhibits the minimum execution time, recording an average speedup ratio from 3.4426 to 4.6062 for a swarm size set of 2048 particles.

4.6 Summary

In this work, a parallel computing paradigm has been shown to speed up the parameter estimation process for four PV models, which are SDM, DDC, SDM, and DDM respectively. The proposed Parallel Particle Swarm Optimization (PPSO) implemented in OpenCL can be executed with a wide range of multi-core computing devices. The

PPSO implemented here does not only show improvement in terms of speed, but also records lower error values in comparison with three other methods (LSO, PS and SA). Hence, it is evident that the PPSO possesses exceptional capability in the parameter estimation. In addition, fitness evaluations are performed concurrently on multi-processor devices, and the simulation results show that the PPSO with 2048 particles is capable of accelerating the computational speed by at least 64% on the used computing platforms.

Chapter 5

Maximum Power Point Tracking Using Model-Based Two-Stage Control Strategy

This chapter deals with Maximum Power Point Tracking (MPPT) control of a Photovoltaic (PV) array, focusing on changing environmental conditions. In the first section, the problem of MPPT is introduced, and this is followed by an overview of the most popular MPPT methods. In Section 5.3, the approximate model used for the proposed MPPT strategy is addressed. Section 5.4 demonstrates a model-based two-stage MPPT framework, including the Maximum Power Power Estimation (MPPE) and Maximum Power Point Revision (MPPR). The experimental setup is introduced in Section 5.5, and the simulation results are presented in Section 5.6. Finally, the concluding remarks are presented in Section 5.7.

The content of this chapter has been published in the following papers:

- Jieming Ma, Ka Lok Man, Tiew On Ting, Nan Zhang, Sheng-Uei Guan, and Prudence W. H. Wong, Approximate Single-Diode Photovoltaic Model for Efficient I-V Characteristics Estimation, *The Scientific World Journal*, vol. 2013, no. 230471, pp. 1-7, 2013.
- Jieming Ma, Ka Lok Man, Tiew On Ting, Nan Zhang, Sheng-Uei Guan, Prudence W. H. Wong, Eng Gee Lim, T. Krilaviius, J. Kapoit-Dzikien, and Chi-Un Lei, Improving Power-Conversion Efficiency via a Hybrid MPPT Approach for Photovoltaic Systems, *Electronics and Electrical Engineering*, vol. 19, no. 7, pp. 57-60, 2013.

- Jieming Ma, Ka Lok Man, Tiew On Ting, Nan Zhang, Sheng-Uei Guan, and Prudence W.H. Wong, Estimation and Revision: A Framework for Maximum Power Point Tracking on Partially Shaded Photovoltaic Arrays, *IEEE International Symposium on Computer, Consumer and Control*, pp. 162-165, 2014.

- Jieming Ma, Ka Lok Man, Tiew On Ting, Nan Zhang, Chi-Un Lei, and Ngai Wong, A Hybrid MPPT Method for Photovoltaic Systems via Estimation and Revision, in *Proceedings of IEEE International Symposium on Circuits and Systems*, pp. 241-244, 2013.

5.1 Introduction

Since the availability of fossil fuels is declining, efforts have been made to explore solar energy. Photovoltaic (PV) generating systems, providing extra electrical power from solar energy, are becoming more common and necessary components in daily life. In these applications, the typical goal is to obtain the maximum possible power from the PV plant over the entire time of operation.

Today a commercial PV inverter has an efficiency of about 99% over a wide range of irradiation conditions [128]. A major challenge in the utilization of PV generation is posed by its non-linear Current-Voltage (I-V) characteristics, which results in an unique Maximum Power Point (MPP) varying with different atmospheric conditions in its Power-Voltage (P-V) curve (e.g. temperature, insolation) [11]. As these quantities vary with time, it is essential to develop an Maximum Power Point Tracking (MPPT) algorithm to extract maximum power from the PV array in real time. However, until recently, tracking under rapidly changing environmental conditions received little attention from manufacturers. In the locations with varying cloud conditions, fast dynamic MPPT can contribute a few additional percentage points to the energy yield [129]. The issue becomes more complicated when the entire PV array receives nonuniform irradiance level - a condition known as partial shading. When a PV array is subjected to partial shading conditions, its P-V curves exhibit multiple peaks with several Local Maximum Power Point (LMPP) and one Global Maximum Power Point (GMPP) [130]. The main drawback of the conventional MPPT method is that for most of the cases, the algorithm is likely to trap at the LMPP since it could not differentiate the LMPP with the GMPP. Consequently, it oscillates around the local peak and remains at that location afterwards. The output power is therefore reduced. More

recently, evolutionary algorithms have been proposed to track the PV devices under partial shading conditions [103, 104, 108, 109]. These methods do not need an accurate mathematical model and are robust in MPPT. Although they prevent the operating point from concentrating at LMPPs, it requires much more computational effort since a large number of random solutions have to be evaluated in every iteration.

Because of recent advances in the PV modeling, the electrical characteristics of various sizes of PV generators, from a single PV module to a multidimensional PV array, can be estimated to aid the task of MPPT. By using the PV electrical model illustrated in [131], this chapter proposes a novel framework for MPPT capitalized on a model-based two-stage search strategy for partially shaded PV arrays. It intends to combine the offline random search using bio-inspired algorithms with the online Adaptive Perturb & Observe (APO) algorithm as an iterative manner. The advantages of the proposed method are threefold:

- The number of online searching iterations can be decreased dramatically by the initial voltage value delivered by a simple yet accurate Maximum Power Point Estimation (MPPE) method.
- The variable-step size APO accelerates the tracking speed.
- Power oscillation, which is considered as an inherent drawback of the conventional direct MPPT methods, can be eliminated by the proposed two-stage method.

5.2 Related Work

In recent years, a number of MPPT methods have been developed and implemented to improve the power-conversion efficiency of PV systems. These methods vary in complexity, sensors requirements, convergence speed and cost [10, 23, 24, 54, 84–93, 103–105]. In the literature [82], MPPT methods are classified into online and offline approaches, depending on the function of tracking methods or control strategies. The former normally uses measured operating power, voltage or current along with an online algorithm to search MPPs of PV generators. The methods in this group include Perturb and Observe (P&O) [84–86] and Incremental Conductance (IncCond) [87]. These approaches, although robust, usually produce slow response to the sudden changes of environmental conditions (e.g. T and G). In addition, fixed perturbation size causes inevitable oscillations of output power, resulting in extra energy loss. Classical Root-Finding (RF)

algorithms are considered as iterative numerical methods with variable-size perturbations. One advantage of the RF based algorithms over the P&O and IncCond methods is that root-finding techniques avoid issues with oscillations [88, 89]. However, the RF algorithms, such as Newton Raphson Method, Secant Method, and Bisection Method, may fail to track the GMPP of a PV array under partial shading conditions.

The offline methods typically predict the MPP based on equations with the mathematical expressions of the electrical characteristics of a PV array, or the algorithms obtained from empirical data. Curve Fitting (CF) [91], Fractional Open-Circuit Voltage (FOCV) and Fractional Short-Circuit Current (FSCC) [132] methods all fall into this category. The CF method is based on the assumptions that the P-V relations can be expressed by a cubic equation (5.1):

$$P_{pva} = \alpha V_{pva}^3 + \beta V_{pva}^2 + \gamma V_{pva} + \delta, \tag{5.1}$$

where α, β, γ, and δ are coefficients that are determined by sampled values of the terminal current and voltage of the PV array (I_{pva} and V_{pva}). As long as these coefficients are calculated, the approximate voltage at the MPP can be estimated by the following formula:

$$V_{mp} = \frac{-\beta \pm \sqrt{\beta^2 - 3\alpha\gamma}}{3\alpha}. \tag{5.2}$$

In the tracking process, this estimation should be repeated every few milliseconds since the P-V characteristics may rapidly change. This method is easy to implement, however, its accuracy is dependent on the number of samples. Also, it might require a large memory capacity as the sample size is large.

The FOCV method is based on the empirical fact that a linear dependency between the V_{mp} and open circuit voltage V_{oc}:

$$V_{mp} \cong K_{mv} V_{oc}, \tag{5.3}$$

where K_{mv} is called voltage factor and its value ranges from 0.7 to 0.95 depending upon the characteristics of PV module [92]. Similarly, the FSCC method is based on the fact that I_{mp} is approximately linearly proportional to its short-circuit current. Their relations are given in Equation (5.4):

$$I_{mp} \cong I_{mv} I_{sc}. \tag{5.4}$$

The I_{mv} is the current factor whose value is around 0.85 [83].

Their performance is directly affected by the precision of the sensors used for measuring T and G, as well as the open voltage V_{oc} and the short current I_{sc}. As reported by Salas [100], few offline MPPT methods are able to obtain the MPP exactly and thus they are known as "quasi seeks".

In recent years, Evolutionary Algorithms (EAs) have been applied to address the global MPPT issues. The standard Particle Swarm Optimization (PSO) was modified to meet the practical consideration of PV generation systems operating under partial shading conditions. According to the experimental results, the PSO-based MPPT method [23, 24] can obtain the GMPP in all the test cases no matter where the GMPP locates. Ahmed [105] implemented a global MPPT method with Cuckoo Search (CS) algorithm, highlighting the significance of the Lévy flight in influencing the algorithm's convergence. The tracking performance of the CS-based MPPT method was compared with the P&O and PSO-based MPPT methods. The results demonstrated that the CS performs better than the P&O and PSO in terms of convergence speed, transient fluctuations and steady state performance. Although most of the EA-based MPPT approaches prevent the operating point from concentrating at LMPPs, it takes time and computational effort for these methods to measure the output power of every trial solution.

A method that overcomes most of the previously explained problems is the model-based MPPT. If an accurate model of the PV panel is available, it will be possible to locate the MPP for each module [133]. The main advantage lies in its quick response to sudden variations of T and G with respect to the conventional P&O MPPT technique.

The model-based approaches have already been investigated in [133–135]. They impel researchers to develop a PV electrical tool with low computational complexity. Ignoring the effect of the resistance is a typical approach to reduce the complexity of PV models. In [34], Mahmoud proposes the Simplified Single-Diode (SSD) model which removes the R_p from the general SD model. The further simplified single-diode model, also known as the Ideal Single-Diode Model , neglects the R_s and R_p as well. Despite their simplicity, accurate estimation of the electrical characteristics is not guaranteed [43]. Furthermore, tedious iterative root finding methods (e.g. Newton-Raphson method) are still needed in the SD model and SSD model to solve the implicit transcendental equations. In [136, 137], Jain et al. proposed Lambert-W function based SD model which enables the solutions to be exact, explicit, straightforward, and does not need to ignore resistance effects. However, that model does not intrinsically reduce the

complexity because the root of the Lambert W-function can only be calculated using iterative approximations [138].

Another problem in the existing model-based MPPT methods is the fact that they normally require an accurate (and very expensive) pyranometer whose accuracy significantly affected the tracking performance of the model-based MPPT method. Moreover, for a large scale PV array, the GMPP cannot be estimated by using the SDM model alone.

5.3 Approximate Single-Diode PV Model for Efficient I-V Characteristics Estimation

5.3.1 Conventional Single-Diode PV Model

As discussed in Section 5.2, a reliable and flexible PV model that enables an accurate estimation of the PV generated electricity towards various operating conditions is of significance in the design phase.

The Single-Diode (SD) model compromises the accuracy and computational efficiency, and thus it has been widely used to estimate the I-V characteristics. Figure 2.2 shows the circuitry diagram of the SD model. When a PV cell, connecting an external circuit, is exposed to incident light, a reverse current is generated across the p-n junction. This current is known as photocurrent (I_{pv}). By eliminating the effect of photocurrent, a PV cell behaves like a normal diode. Its I-V characteristics can be simply modeled as a linear independent current source in parallel with a diode. The SD model improves the simple model by recognizing the series resistance R_s and shunt resistance R_p. Its equivalent Thevenin circuit equation is mathematically expressed by the following equation:

$$I = I_{ph} - I_{o_1}(e^{\frac{V+IR_s}{A_1 V_t}} - 1) - \frac{V + IR_s}{R_p}. \tag{5.5}$$

In a large PV generation system, PV modules are used as basic components rather than PV cells since the output power of PV cells is limited at high voltage levels. Owing to the fact that the PV module is a packaged, connected assembly of N_s PV cells, its output voltage and resistance are scaled in accordance with the following rules [33]:

$$V' = N_s \cdot V,$$

$$
\begin{aligned}
I' &= I, \\
R'_s &= N_s \cdot R_s, \\
R'_p &= N_s \cdot R_p,
\end{aligned} \tag{5.6}
$$

where V', R'_s, and R'_p here represent the terminal voltage, series resistance and shunt resistance of the PV module, respectively. After substituting the scaling rules from Equation (5.6) into (5.5), we obtain the expression for a Single-Diode Module (SDM) model:

$$
I' = I_{ph} - I_{o1}(e^{\frac{V'+I'R'_s}{A_1 N_s V_t}} - 1) - \frac{V' + I'R'_s}{R'_p}. \tag{5.7}
$$

Equation (5.7) is transcendental, and requires tedious iterative root finding methods (e.g. Newton-Raphson method) to obtain the I'. Aiming to overcome this problem, a simple yet accurate Approximate Single-Diode Model (ASDM) is proposed in the following subsection. The exponential diode behavior is approximated via function approximation, which permits designers or engineers to predict the current I' by solving a closed-form expression.

5.3.2 Function Approximation

Function approximation provides an approach to represent a complicated function $f(x)$ ($f(x) \in C[a, b]$) by an easier form $\phi(x; a_0, a_1, ..., a_n)$, where a_0, a_1 ..., a_n are parameters to be determined so as to achieve the best approximation of $f(x)$. The term least squares describe a frequently used means to solve over-determined or inexactly specified equations (e.g. transcendental functions, integrals and solutions of differential or algebraic equations) in an approximate sense [139]. Normally, Least Squares Approximation (LSA) can be viewed as finding proper coefficients a_0, a_1, ..., a_n to:

$$
\text{minimize } ||f(x) - \phi(x; a_0, a_1, ..., a_n)||_2, \tag{5.8}
$$

where $\phi(x; a_0, a_1, ..., a_n)$ is usually a polynomial $P_n(x)$ of degree at most n:

$$
P_n = a_0 + a_1 x + ... + a_n x^n = \sum_{k=0}^{n} a_k x^k. \tag{5.9}
$$

The approximation problem might be regarded as a process of minimizing the error E, which is given in Equation (5.10):

$$
E \equiv E(a_0, a_1, ..., a_n) = \int_b^a (f(x) - P_n(x))^2 dx. \tag{5.10}
$$

By applying derivative to Equation (5.10), we get:

$$\frac{\partial E}{\partial a_j} = -2\int_a^b x^j f(x)dx + 2\sum_{k=0}^{n} a_k \int_a^b x^{j+k}dx. \tag{5.11}$$

With the aim of finding real coefficients a_0, a_1 ..., a_n, a necessary condition that should be considered is:

$$\frac{\partial E}{\partial a_j} = 0,\ j = 0, 1, ..., n \tag{5.12}$$

After substituting Equation (5.12) into Equation (5.10), the linear normal equations, expressed by Equation (5.13), can be derived to solve the unknown coefficients a_0, a_1 ..., a_n. It has been proven that the normal equations always have a unique solution provided $f(x) \in C[a, b]$ [98].

$$\int_a^b x^j f(x)dx = \sum_{k=0}^{n} a_k \int_a^b x^{j+k}dx,\ \text{for each } j = 0, 1, ..., n \tag{5.13}$$

The above approximation process is called Continuous Least Square Approximation (CLSA) in the field of applied mathematics.

5.3.3 Approximate Single-Diode Model (ASDM)

In a typical SD model, the analytical expression of the forward I-V characteristics contains a transcendental function for predicting the value of I_{D_1}, which is formulated as:

$$I_{D_1} = I_{o_1}(e^{\frac{V+IR_s}{A_1 V_t}} - 1). \tag{5.14}$$

Assuming that the parameters are constant at a certain test condition, the value of I' varies directly with the reference V'. Let $m = R'_s/A_1 N_s V_t$, and then I_{D_1} can be rewritten as a function of I':

$$I_{D_1} = I_{o_1} e^{\frac{mV'}{R'_s}} \cdot e^{mI'} - I_{o_1}. \tag{5.15}$$

The CLSA provides a paradigm that simplifies the transcendental part of Equation (5.15) into a polynomial of degree 1:

$$e^{mI'} \cong a_0 + a_1 I', \tag{5.16}$$

By using the linear normal equations, namely Equation (5.13), the values of a_0 and a_1 can be solved.

According to Equation (5.13), the linear normal equation for $e^{mI'}$ can be rewritten as:

$$\begin{aligned} a_0 \int_0^{I'_{max}} dI' + a_1 \int_0^{I'_{max}} I' dI' &= \int_0^{I'_{max}} e^{mI'} dI', \\ a_0 \int_0^{I'_{max}} I dI' + a_1 \int_0^{I'_{max}} I'^2 dI' &= \int_0^{I'_{max}} I e^{mI'} dI'. \end{aligned} \tag{5.17}$$

where I'_{max} is the upper limit of the PV terminal current that is available at the I-V curves of the manufacturer's datasheet. After performing the integration, it yields:

$$\begin{aligned} I'_{max} a_0 + \frac{I'^2_{max}}{2} a_1 &= \frac{e^{mI'_{max}}}{m} - \frac{1}{m}, \\ \frac{I'^2_{max}}{2} a_0 + \frac{I'^3_{max}}{3} a_1 &= \frac{I'_{max}}{m} e^{mI'_{max}} - \frac{e^{mI'_{max}}}{m^2} + \frac{1}{m^2}. \end{aligned} \tag{5.18}$$

Equation (5.18) can be solved to obtain the exact mathematical expressions of a_0 and a_1, given in Equation (5.19) and (5.20) respectively.

$$a_0 = -\frac{2}{mI'^2_{max}} \left[\left(I'_{max} - \frac{3}{m} \right) e^{mI'_{max}} + \left(2I'_{max} + \frac{3}{m} \right) \right], \tag{5.19}$$

$$a_1 = \frac{12}{mI'^3_{max}} \left[\left(\frac{I'_{max}}{2} - \frac{1}{m} \right) e^{mI'_{max}} + \left(\frac{I'_{max}}{2} + \frac{1}{m} \right) \right]. \tag{5.20}$$

The least squares polynomial approximation of degree 1 for I_{D_1} is:

$$I_{D_1}(I) \cong I_{o_1} \left[e^{\frac{mV}{R_s}} \cdot (a_0 + a_1 I) - 1 \right]. \tag{5.21}$$

Finally, the ASDM can be formulated as a rational function:

$$I' \cong \frac{I_{ph} - \left(I_{o_1} e^{\frac{V'}{A_1 N_s V_t}} \right) \cdot a_0 - V'/R'_p}{1 + \left(I_{o_1} e^{\frac{\dot{V}}{A_1 N_s V_t}} \right) \cdot a_1 + R'_s/R'_p}. \tag{5.22}$$

In the next subsection, the methods of determining the parameters I_{ph}, I_{o_1}, A_1, R'_s and R'_p are presented.

5.3.4 Parameter Identification for The ASDM

As a result of the PV effect, the photo current I_{ph} flows in a direction opposite to the forward dark current. Even when the PV module operates at short circuit, this current

continues flowing and is measured as the short-circuit current I_{sc}. From Equation (2.3), it can be seen that the value of I_{ph} is approximately equal to the I_{sc} in a high-quality PV module, and thus the assumption $I_{sc} \cong I_{ph}$ is often used in PV modeling. Although the short current density can be determined by analytical equations in [33], the required parameters are usually not given in manufacturer's tabular data. In view of the fact that the I_{sc} depends linearly on the G and is also slightly influenced by the T, the I_{ph} can be given by Equation (5.23) [44, 58, 140]:

$$I_{ph} \cong I_{sc} = (I_{scn} + K_i \Delta T)\frac{G}{G_n}, \tag{5.23}$$

where I_{scn} and G_n are the short current and irradiance at STCs, respectively. K_i, named short-circuit current coefficient, is a constant available in the datasheet. The difference between T and the standard test temperature T_n is denoted by ΔT .

The saturation current I_{o_1} is the small current that flows when the p-n junction is reverse biased. The dependence of I_{o_1} on the temperature was studied by Villalva et al. [140], in which the authors introduced Equation (5.24) to predict the value of I_{o_1}. In the expression, K_v is the open-circuit voltage coefficient and V_{ocn} represents the open circuit voltage measured at the STCs.

$$I_{o_1} = \frac{(I_{scn} + K_i \Delta T)}{e^{\frac{(V_{ocn} + K_v \Delta T)}{A_1 N_s V_t}} - 1}. \tag{5.24}$$

The ideality factor A_1 is an important parameter used to describe whether the P-N junction behaves close to or apart from the ideal case. As reported in [141], A_1 and R'_s significantly affect the shape of I-V curves around the MPP, whereas the R'_p influences the slope of the I-V curve near the point arriving I_{sc} lower. With the aim of delivering a simplified calculation approach, the parameters of the ASDM are assumed to be constant and the variables $\mathbf{x} = (R'_s, n)$ are solved by the equation system $f(\mathbf{x})$ formed by:

- The terminal current at the MPP:

$$I'_{mp} \cong \frac{I_{ph} - \left(I_{o_1} e^{\frac{V'_{mp}}{A_1 N_s V_t}}\right) \cdot a_0 - V'_{mp}/{R_p}'}{1 + \left(I_{o_1} e^{\frac{V'_{mp}}{A_1 N_s V_t}}\right) \cdot a_1 + {R_s}'/{R_p}'}. \tag{5.25}$$

- The derivative of the terminal current with respect to the voltage at the MPP:

$$\left.\frac{\partial I}{\partial V}\right|_{V=V'_{mp},\, I=I'_{mp}} = -\frac{(a_0 + a_1 I'_{mp}) I_{o_1} e^{\frac{V'_{mp}}{A_1 N_s V_t}}/A_1 N_s V_t + 1/R'_p}{1 + a_1 I_{o_1} e^{\frac{V'_{mp}}{A_1 N_s V_t}} + R'_s/R'_p}$$

$$= \quad -\frac{I'_{mp}}{V'_{mp}}. \tag{5.26}$$

In the above equation system, a_0, a_1, I_{ph} and I_{o_1} are represented by Equations (5.19), (5.20), (5.23) and (5.24) under the STCs. I'_{mp} and V'_{mp} are the current and voltage at MPP under the STCs, and usually can be found in the datasheet. By substituting the known operating points $(0, V_{oc})$ and $(I_{sc}, 0)$ into Equation (5.22), $1/R'_p$ and R'_s/R'_p are expressed as:

$$R'_p = \frac{V_{oc}}{I_{ph} - a_0 I_{o_1} e^{\frac{V_{oc}}{A_1 N_s V_t}} + I_{o_1}}, \tag{5.27}$$

$$\frac{R'_s}{R'_p} = (1 - a_0 - a_1 I_{sc}) \frac{I_{o_1}}{I_{sc}}. \tag{5.28}$$

Finally, the Newton method illustrated in [142] is capable of solving the unknowns n and R_s. In the numerical computing process, the k^{th} generation of variable vector x gets the updated vector estimate:

$$x_{k+1} = x_k - J_k^{-1} f(x_k). \tag{5.29}$$

where J_k is the Jacobian matrix of $f(x_k)$. Other parameters as well as I can be recovered by using Equation (5.19)-(5.27).

5.3.5 Modeling a PV Array under Partial Shading Conditions

In an outdoor environment, the whole or some parts of the PV array may be under a non-uniform insolation conditions caused by passing clouds, high buildings, and trees. All the cells in a series array are forced to carry the same current even though a few cells under shade produce less photon current. In this case, the power delivered by the less illuminated solar cells may be negative, which indicates that some of the power produced by the other cells in the PV array is dissipated by the less illuminated PV cell, acting as loads, draining power from the fully illuminated cells. If the system is not appropriately protected, "hot-spot" problem will arise, and the system can be irreversibly damaged in several cases [33]. Bypass diodes are a standard addition to PV modules, which are placed across every PV cell or across part of the series string to eliminate the 'hot-spot' effect.

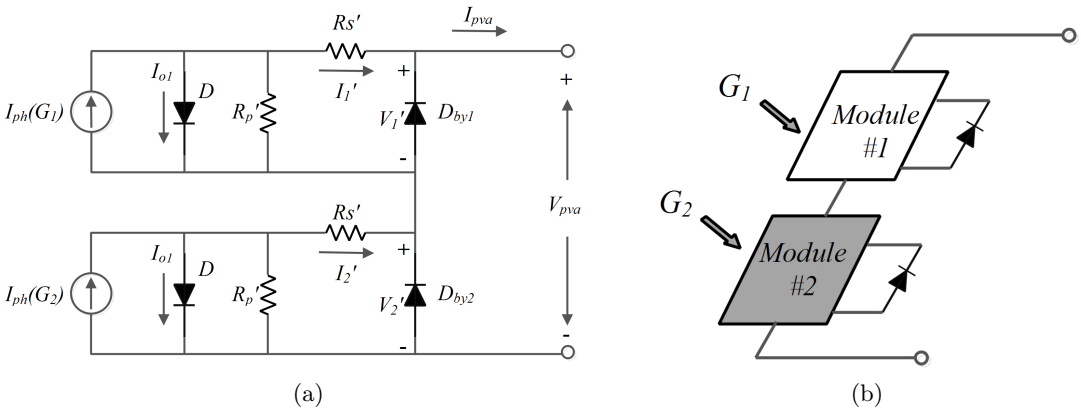

(a) (b)

Figure 5.1: PV array consisting of two series connected modules: (a) circuitry diagram; (b) block diagram.

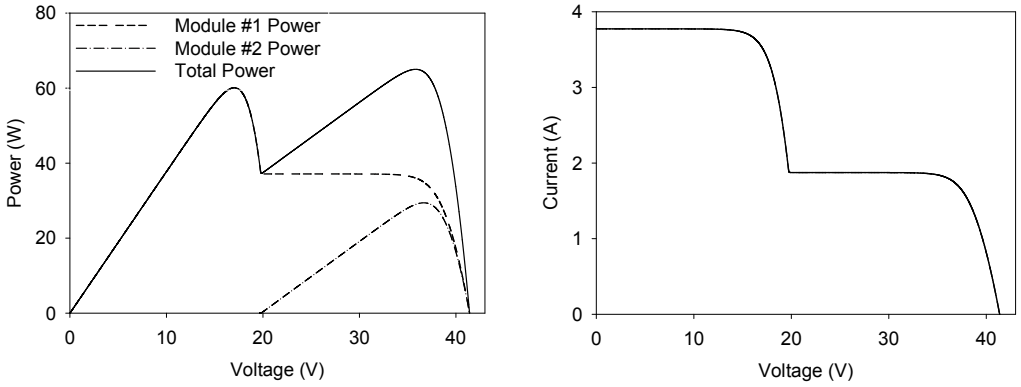

(a) (b)

Figure 5.2: Electrical characteristics of the PV array shown in Figure 5.1: (a) P-V curves; (b) I-V curve.

Figure 5.1 shows a PV array consisting of two series connected modules receiving two irradiance level (G_1=1000 W/m^2 and G_2=500 W/m^2). The PV module composed of N_{s_1} cells receives G_1 while the PV module composed of N_{s_2} cells receives G_2. Assuming that the bypass diodes are ideal components, the terminal current I_{pva} and the terminal voltage V_{pva} of the PV array satisfy the following relations [9]:

$$I_{pva} = \begin{cases} I_{ph}(G_1) - I_{o_1} \mathrm{e}^{\frac{V_1{}' + I_{pva} R_s{}'}{A_1 N_{s_1} V_t}} - \frac{V_1{}' + I_{pva} R_s{}'}{R_p{}'}, & I_{pva} \geq I_{ph}(G_2) \\ I_{ph}(G_2) - I_{o_1} \mathrm{e}^{\frac{V_2{}' + I_{pva} R_s{}'}{A_1 N_{s_2} V_t}} - \frac{V_2{}' + I_{pva} R_s{}'}{R_p{}'}, & I_{pva} < I_{ph}(G_2) \end{cases} \tag{5.30}$$

$$V_{pva} = \begin{cases} V_1{}', & I_{pva} \geq I_{ph}(G_2) \\ V_2{}' + V_1{}', & I_{pva} < I_{ph}(G_2) \end{cases} \tag{5.31}$$

The P-V characteristics of a partially shaded array exhibit multiple peaks as shown in Figure 5.2 (a). The corresponding I-V curve is depicted in Figure 5.2 (b). The I_{pva}

is equivalent to the current generated by the module under full irradiance 1000 W/m^2 until its value reaches the same value as the photo current of the shaded module $I_{ph}(G_2)$. Then I_1' sinks in the current generated by Module #2. The output power P_1' becomes flatten and Module #2 starts to generate power.

Based on the above analysis, Sayedmahmoudian [9] concluded a simple modeling method for the PV array working under the partial shading conditions. The calculation process can be described as follows:

i. Measure the solar irradiance received by each PV modules.

ii. Compute the I_{ph} and N_s of each PV module and define the I_{ph} and N_s matrix respective of the solar irradiance.

iii. Rearrange I_{ph} matrix from the highest to the lowest value.

iv. Calculate the output current of array (I_{pva}) using Equation (5.32).

$$\begin{aligned} I_{pva} &= I'_{(i)}, \quad I_{pva} \geq I_{ph(i+1)} \\ V_{pva} &= \Sigma V'_{(i)} \end{aligned} \tag{5.32}$$

5.3.6 The Accuracy and Computational Efficiency of The ASDM

The ASDM described in this chapter is compared with the physical PV models in the commercial simulation tools, such as PSIM and PVsyst. The Villalva's model [140], a famous comprehensive approach to modeling and simulation of PV arrays in the literature, is also used for comparison. These models are programmed in MATLAB, and their capability of predicting the electrical characteristics of the PV modules is validated by the experimental I-V data extracted from the manufacturer's datasheet. Four different PV modules produced with three diverse manufacturing techniques, namely MSX60 (mutli-crystalline), KC200 GT (multi-crystalline), SQ150-PC (mono-crystalline) and HIT Power 180 (HIT) PV modules, are utilized for verification.

Aiming to evaluate the ASDM's capability of fitting the characteristics of PV panels, statistical analysis is performed. In this work, the accuracy of the PV models is described by the Root Mean Square (RMS) error ε and the Mean Absolute Error (MAE) as well as the Relative Error (RE). They are mathematically expressed by the

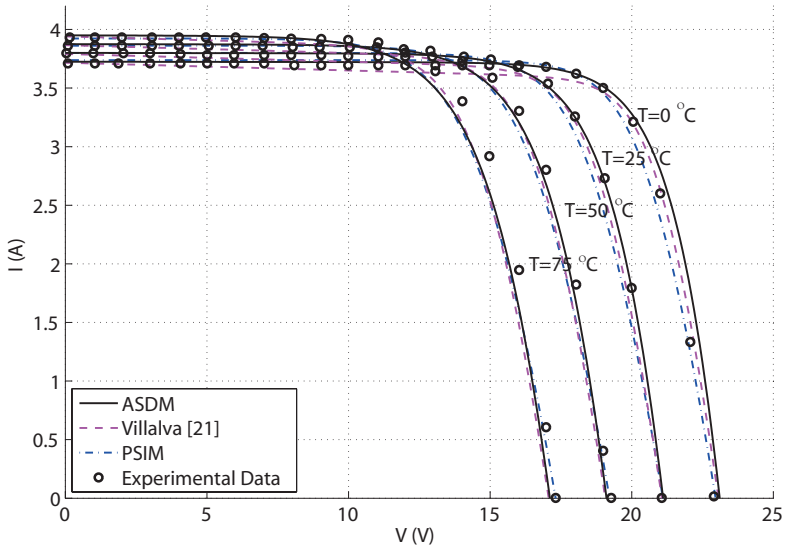

Figure 5.3: I-V curves of a MSX60 PV module at various cell temperatures

following equations:

$$\varepsilon = \sqrt{\frac{1}{n}\sum_{i=1}^{n}(I_i - \widehat{I}_i)^2} \tag{5.33}$$

$$\bar{e} = \frac{1}{n}\sum_{i=1}^{n}|I_i - \widehat{I}_i| \tag{5.34}$$

$$\tilde{e} = \left|1 - \frac{I_i}{\widehat{I}_i}\right| \times 100\% \tag{5.35}$$

where I_i and $\widehat{I}_i$ present the simulated and measured current at the i^{th} operating point among n measured I-V pairs, respectively. Table 5.1 lists the parameters of PV panels by using the methods described in Section 5.3.4, which deliver a convenient parameter estimation method that only requires the tabular information available in the datasheet. The obtained results are extracted under a set of STCs and are assumed to be constant in other operating conditions. The obtained RMS errors for the modules working under the STCs show a good agreement between the simulation results and experimental data.

Table 5.1: Extracted ASDM parameters for different PV modules.

Module	n	$R_s(\Omega)$	$R_p(\Omega)$	a_0	a_1	ε
SQ150	1.6031	0.5334	808	0.9018	0.2877	2.1E-3
KC200GT	1.1266	0.2764	206	0.6939	0.3771	5.29E-2
MSX60	1.5390	0.1035	3140	0.9921	0.0843	6.23E-04
HIT180	1.6240	0.4929	781	0.9753	0.1583	2.24E-2

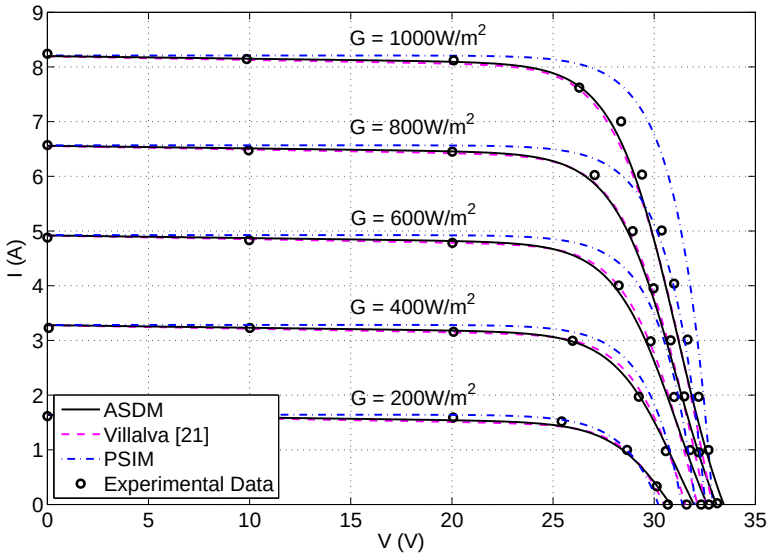

Figure 5.4: I-V curves of a KC200GT PV module at various irradiance levels

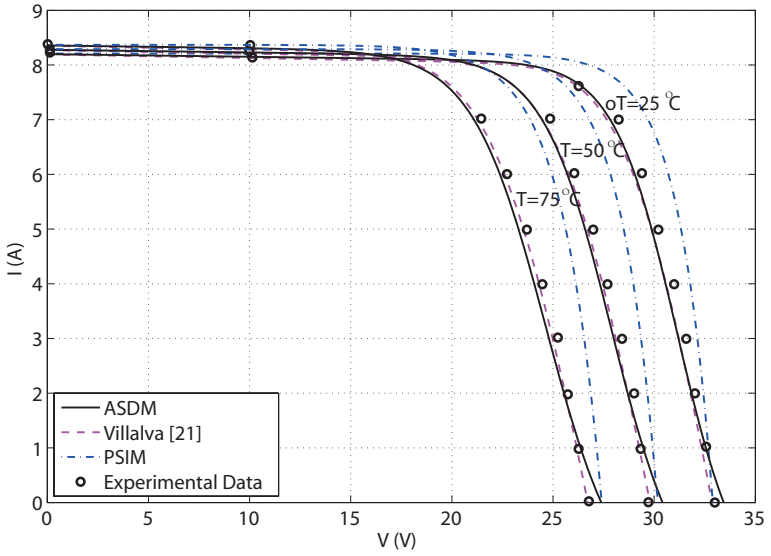

Figure 5.5: I-V curves of a KC200GT PV module at various cell temperatures

Once the model parameters are determined, the ASDM is able to predict the electrical characteristics of PV modules under varied atmospheric conditions. Figure 5.3, 5.4 and 5.5 show the I-V characteristics of MSX60 and KC200GT modules varying with different levels of irradiance and temperature. The simulation results of the PSIM and Villalva's models are also plotted for reference. It is interesting to see that the ASDM obtains more accurate (I, V) above the 25 °C, whereas the operating points of the Villalva's model are closer to the measured data below the 25 °C. Since the

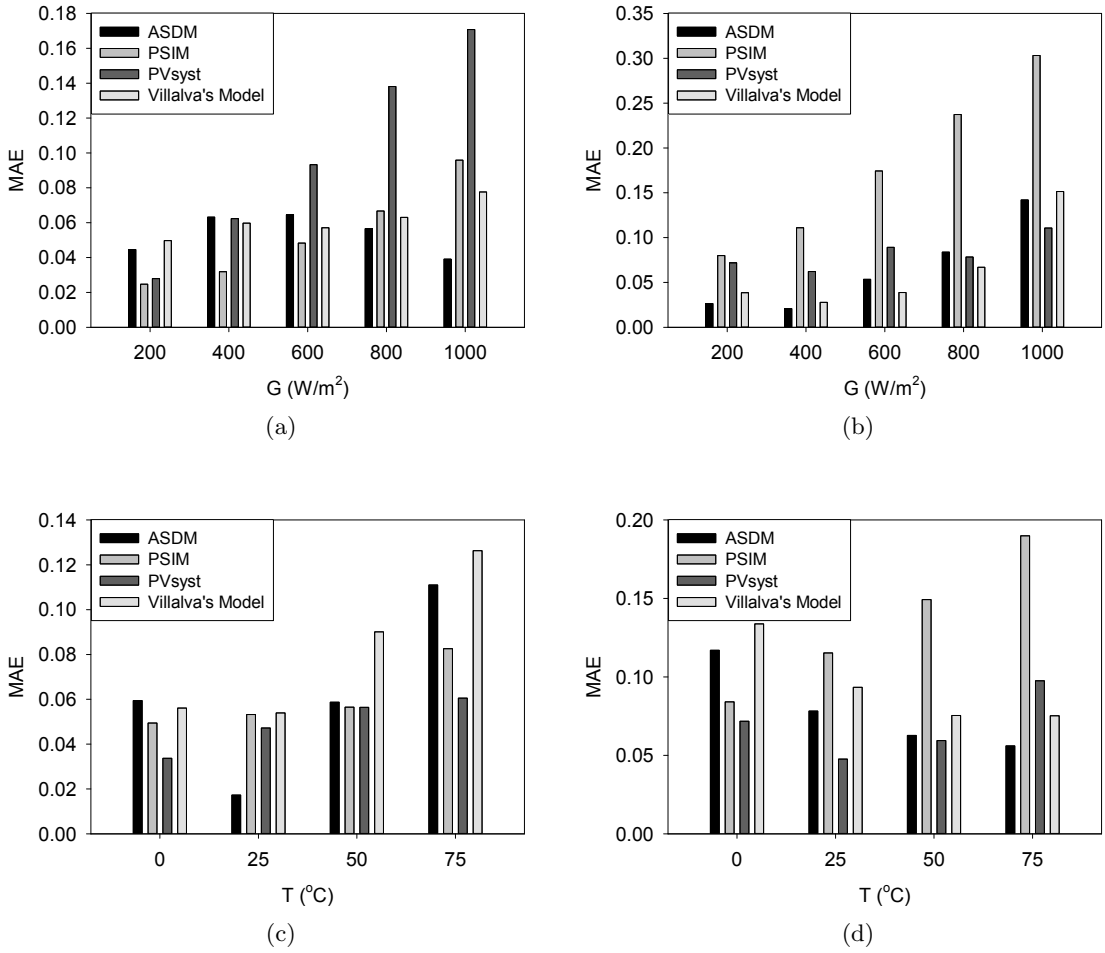

Figure 5.6: Mean absolute errors of the PV models at different atmospheric conditions: (a) SQ150-PC; (b) MSX60; (c) KC200GT; (d) HIT 180

I-V curves of MSX60 at different irradiance levels are not issued in the datasheet, the related tests are not conducted in this work.

In order to further evaluate the estimation performance of the ASDM, more exhaustive tests have been conducted on the tested modules. Figure 5.6(a) and 5.6(b) show the MAEs of the simulated results subjected to irradiance variation, and all measurements are performed at a temperature of 25 °C. On the other hand, Figures 5.6(c) and 5.6(d) demonstrate the MAEs of the ASDM model for MSX60 and HIT Power 180 Modules working at the same irradiance of 1000 W/m^2 but different temperatures. In Figure 5.6, it is evident that the ASDM model outperforms the commercial tools (PSIM and PVsyst) in most cases and obtains better fitness quality than Villalva's model at high irradiance and temperature levels.

Table 5.2: Relative errors of the calculated I_{mp} at various irradiance levels.

Module	G(W/m^2)	T (°C)	$\tilde{e}$			
			ASDM	PSIM	PVsyst	Villalva [140]
SQ150-PC	200	25	6.34%	0.51%	2.11%	1.51%
	400	25	3.29%	2.81%	0.30%	2.99%
	600	25	1.79%	3.60%	0.89%	2.68%
	800	25	1.18%	3.33%	0.29%	1.18%
	1000	25	0.59%	3.32%	0.00%	0.00%
KC200GT	200	25	1.93%	1.31%	0.39%	0.39%
	400	25	0.39%	2.90%	1.93%	1.93%
	600	25	0.00%	4.16%	1.15%	1.15%
	800	25	0.00%	5.48%	0.38%	0.38%
	1000	25	0.38%	6.81%	0.00%	0.00%

Table 5.3: Relative errors of the calculated I_{mp} at various temperature levels.

Module	G(W/m^2)	T (°C)	$\tilde{e}$			
			ASDM	PSIM	PVsyst	Villalva [140]
MSX60	1000	0	1.59%	1.32%	1.59%	1.59%
	1000	25	0.00%	2.16%	0.00%	0.00%
	1000	50	1.31%	3.07%	1.31%	1.31%
	1000	75	3.70%	4.00%	3.70%	3.70%
HIT180	1000	0	2.11%	0.33%	0.35%	2.11%
	1000	25	0.00%	2.57%	2.59%	0.19%
	1000	50	0.82%	1.51%	0.41%	0.82%
	1000	75	0.22%	1.68%	1.12%	0.67%

Similar trend is observed in Tables 5.2 and 5.3, which show the REs of the calculated MPP locus at different operating conditions. In practical, predicting the locus of MPP is of importance in the improvement of power efficiency. For this reason, statistical analysis is conducted. Except the tests on SQ150-PC module under high irradiance test condition, most REs of the ASDM are similar or even lower than that of others.

The simulation results described so far verify the accuracy of the proposed ASDM. Besides its low-error estimation performance, the ASDM has the advantage of deriving the I-V characteristics in closed form, and thus it supports high-speed computing. Figure 5.7 makes a comparison among the computational efficiency of different PV models. In the tests, 10,000 operating points varied within the operating voltage range [0, V_{oc}] are calculated in a general PC with a 2.40GHZ Intel(R) Core(TM) 2 Duo CPU. It shows that the ASDM is able to reduce the simulation time by 30% compared with

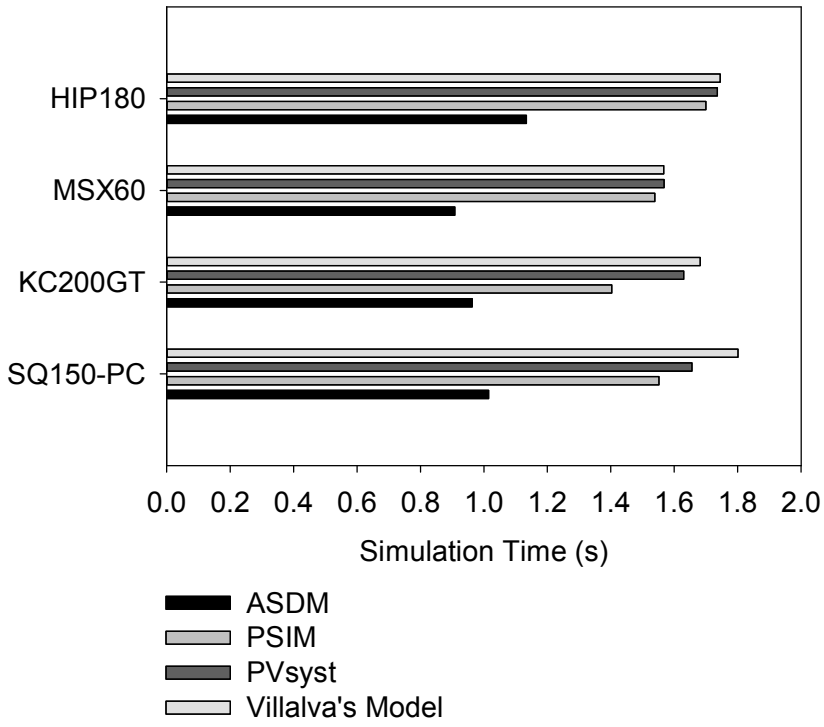

Figure 5.7: Simulation time of different PV models

other tested models.

In conclusion, this section has presented a simple approximate PV model which is capable of predicting the electrical characteristics of PV modules operating at a variety of atmospheric conditions. The CLSA approach is applied to fit PV behaviors in a simple manner. The proposed mathematical modeling approach is easy, straightforward, and does not depend on iterative procedures to obtain solutions. The accuracy of the proposed model is assessed through simulations. The results show that the obtained current values agree well with the experimental data. The application of the ASDM in the MPPT method, discussed in the following section, highlights the value of the approximate model.

5.4 Model-Based Two-Stage MPPT strategy

As discussed in Section 5.2, the traditional MPPT methods can be classified into online and offline approaches depending on the function of tracking methods or control strategies. The former normally uses measured data (e.g. V_{pva}, I_{pva}, P_{pva}, etc.) along

with an online algorithm to search MPPs of PV generators. The most popular online methods are P&O and IncCond. These approaches, although robust, usually produce a slow response to the sudden changes of environmental conditions. The fixed-size perturbation causes inevitable oscillations of output power, resulting in extra energy loss. Moreover, when a PV array is under partial shading conditions, these traditional MPPT control methods can obtain the LMPP, but may not be able to extract GMPP and cause power loss [143]. The offline methods typically predict the MPP based on equations with the mathematical expression of the electrical characteristics of a PV panel, or the algorithms obtained from empirical data. The CF, FOCV, FSCC methods all fall into this category. Their performances are directly affected by the precision of the sensors used for measuring T and G, as well as the V_{oc} and the I_{sc}. As reported by Salas [100], few offline MPPT methods are able to obtain the MPP exactly.

In order to overcome the inherent shortages of online and offline methods, a two-stage MPPT approach, which combines the variable step APO with the Maximum Power Point Estimation (MPPE), is proposed.

5.4.1 Maximum Power Point Estimation

Particle Swarm Optimization (PSO) [15] is one of the prominent algorithms in the category of nature-inspired algorithms and has been one of the most successful numerical optimization algorithms applied in many fields. Compared with many evolutionary algorithms such as Genetic Algorithm (GA) [144], Evolutionary Programming (EP) [145] and Differential Evolution (DE) [146], the PSO normally obtains faster convergence speed. As an original stochastic optimizer with fast speed and simple way of realization, the PSO has been effectively applied to solve large range of problems of renewable energy systems [147]. MPPT is such a successful application, which is used to search the MPP. The PSO based tracking systems do not require any derivatives calculation, therefore it is vigorous and noise-resistive [147].

The basic idea behind the PSO is to search a space by adjusting the trajectories of particles (or commonly known as trial solutions), whose fitness values are evaluated by a similar cost function during the searching process. The PSO works as follows. First, a swarm of particles are seeded onto the search space in a random manner. These particles then move through the problem space. At time t, the historical best solution of the i^{th} particle is recorded as local best $pbest^i$. Among the swarm of particles, the

best *pbest* with the maximum fitness value is termed global best *gbest*. The movement is guided by the essentially important ingredient formulas:

$$x_{i,j}^{t+1} = x_{i,j}^{t} + v_{i,j}^{t+1}, \tag{5.36}$$

where $v_{i,j}^{t+1}$ is the velocity, expressed as:

$$v_{i,j}^{t+1} = wv_{i,j}^{t} + \alpha\epsilon_1(x_{i,j}^{t} - gbest^{t}) + \beta\epsilon_2(x_{i,j}^{t} - pbest_i^{t}). \tag{5.37}$$

whereby:

$v_{i,j}^{t}$ Velocity for i^{th} particle in j^{th} dimension at time t.

w Inertia weight, usually set to 0.5.

$X_{i,j}^{t}$ Current position of i^{th} dimension at time t.

$gbest^{t}$ The best solution among all participating particles for i^{th} dimension at time t, also known as global best.

$pbest_i^{t}$ The best position for i^{th} dimension at time t of a particle, also known as personal best.

$\epsilon_1,\ \epsilon_2$ Independent uniform random numbers within [0, 1].

$\alpha,\ \beta$ Acceleration coefficients towards $pbest^{t}$ and *gbest* respectively.

Particle's velocity in each dimension is clamped to the maximum value V_{max}, so that particles will not move beyond the search space. Large V_{max} may make the particle fly past the good solution while small V_{max} value will cause particles to be trapped in local minima, not allowing them to travel far places in search of a good solution in the search space [69]. In early experiments, particles velocity is usually set within 10%, 50% or 100% of search space [148]. Also, after the updating through Equation (5.36), bounds checking is done to ensure that particles only explore the predefined search space. As the number of generation increases, particles accelerate towards those with better fitness until maximum iteration is reached.

By careful inspection of Equation (5.36) and (5.37), Ting [148] concluded the following interpretations are valid in regard to the PSO:

i. the velocity somehow acts as short-term memory retention and plays a crucial role in the update process;

ii. the update of a dimensional value is guided by the $pbest_i$ and $gbest$. Simply, this means that a particle moves between the $pbest_i$ and $gbest$;

iii. the independent random numbers ϵ_1 and ϵ_2 control the ratio of movement towards the $pbest_i$ and $gbest$.

Although the conventional PSO algorithm has high capability of finding global minima and maxima, it is still computational expensive for real-time systems. To reduce the algorithm complexity, Ting [148] proposed Weightless Swarm Algorithm (WSA), which excludes inertia weight from the canonical PSO. The equation guiding the particles' movements, namely Equation (5.36) and (5.37), is simplified to a single line:

$$x_{i,j}^{t+1} = x_{i,j}^{t} + \alpha\epsilon_1(x_{i,j}^{t} - gbest^{t}) + \beta\epsilon_2(x_{i,j}^{t} - pbest_i^{t}). \tag{5.38}$$

From the results on static numerical problems, Equation (5.38) can be further simplified as:

$$x_{i,j}^{t+1} = x_{i,j}^{t} + \alpha\epsilon_1(x_{i,j}^{t} - pbest_i^{t}). \tag{5.39}$$

which implies that the movements of particles are only guide by the $pbest$. As Equation (5.39) are simple enough, the concept of velocity is not introduced in the WSA. Without $v_{i,j}$, a user also discards the concern of the bound for this parameter, namely V_{max} and V_{min}. Consequently, the complexity of the algorithm is reduced and the tuning of the algorithm is much easier.

In this work, the locus of MPP will be predicted offline by the WSA. The estimation process is so called Maximum Power Point Estimation (MPPE). To illustrate the application of the WSA algorithm in MPPE, a solution vector of operating voltage with N particles at generation t is determined as follows:

$$x_i^t = [x_1^t,\ x_2^t,\ ..., x_N^t]. \tag{5.40}$$

The objective function is defined as:

$$f(x_i^t) = P_{pva,i}^t = V_{pva,i}^t \cdot I_{pva,i}^t, \tag{5.41}$$

where I_i^t can be estimated via the ASDM.

The Pseudocode of the WSA is shown in Algorithm (3). In the first generation, the particles are released randomly within the valid range. They serve as the $pbest_i$ in the

first iteration. The new position of these particles are determined by Equation (5.39). Bounds checking is then carried out to accelerate the search process. The optimization process will not end until it satisfies the stopping criterion. Obviously, implementation of WSA is pretty simple and can be implemented into any existing PSO algorithm with the following steps [149]:

i. set inertia weight $w = 0$;

ii. discard the *gbest* term by setting ϵ_2 in equation 5.37 to zero;

iii. swapping is done during $pbest_i$ update. The swapping for *gbest* will not be performed.

Algorithm 3: Pseudocode for the WSA

```
Initialize WSA parameters;
Initialize locations x_i of the i^th particle;
while Stopping criterion is not satisfied do
    for i = 1 to P (particle) do
        Evaluate the power for each trial via Equation (5.41);
    end
    Update the pbest_i for each particle;
    Update the location x_i via Equation (5.39);
    if x_i exceeds the bounds then
        Set x_i to the bounds;
    end
end
```

5.4.2 Maximum Power Point Revision

The MPPE is developed on the basis of the PV modeling techniques and an artificial optimization algorithm. Implementing the MPPE in an MPPT control system not only needs a thermometer but also light meters. The precision of these instruments, as well as the accuracy of the applied PV electrical model, significantly affects the estimated MPP locus. Thus, Maximum Power Point Revision (MPPR) process is necessary to further improve the tracking performance within a narrow range if the ambient atmospheric conditions are not changed much. Due to the simplicity and robust performance of the P&O, it is potentially an ideal choice for the MPPR.

In a conventional P&O algorithm, the terminal voltage V_{pva} and current I_{pva} are measured. A small perturbation of voltage is then addressed in one direction. The

change of terminal power ΔP is calculated as:

$$\Delta P = P_{pva}^{t+1} - P_{pva}^{t}. \tag{5.42}$$

It is used to guide the search direction as follows:

- If $|\Delta P| < \xi$, the voltage for the next sample V_{pva}^{t+1} will not be changed since the system is working at the MPP;
- If $|\Delta P| > \xi$, $\Delta P > 0$ and $V_{pva}^{t+1} > V_{pva}^{t}$, the V_{pva}^{t} is on the left of the MPP and the V_{pva}^{t+1} will be located on a point with a higher voltage value so as to reach the MPP.
- If $|\Delta P| > \xi$, $\Delta P > 0$ and $V_{pva}^{t+1} < V_{pva}^{t}$, the V^{t} is on the right of the MPP and the V^{t+1} will be located on a point with a lower voltage value so as to reach the MPP.
- If $|\Delta P| > \xi$, $\Delta P < 0$ and $V_{pva}^{t+1} > V_{pva}^{t}$, the V^{t} is on the right of the MPP and the V^{t+1} will be located on a point with a lower voltage value so as to reach the MPP.
- If $|\Delta P| > \xi$, $\Delta P < 0$ and $V_{pva}^{t+1} < V_{pva}^{t}$, the V^{t} is on the left of the MPP and the V^{t+1} will be located on a point with a higher voltage value so as to reach the MPP.

The ϵ is a preset tolerance for ΔP. The process is repeated until the MPP is reached. After that, the system will be oscillated around the MPP.

The major drawback of P&O is that it may deviate from the MPP in case of rapidly changing atmospheric conditions (e.g. passing clouds). There is a trade-off between dynamic response and steady state performance due to the selection of perturbation step size V_{step}. That is, large perturbations result in quick responses during large transients, while they produce large current ripple causing oscillations around the current at the MPP in the steady-state. Through the above analyses, it is ideal to make V_{step} large during the transient stage and to make V_{step} small in the steady state. To achieve that, Adaptive Perturb & Observe (APO) method [97] is used at the MPPE stage, where the perturbation step size is set to a large value when the power changes in a large range primarily due to environmental variation. The step size is set as follows:

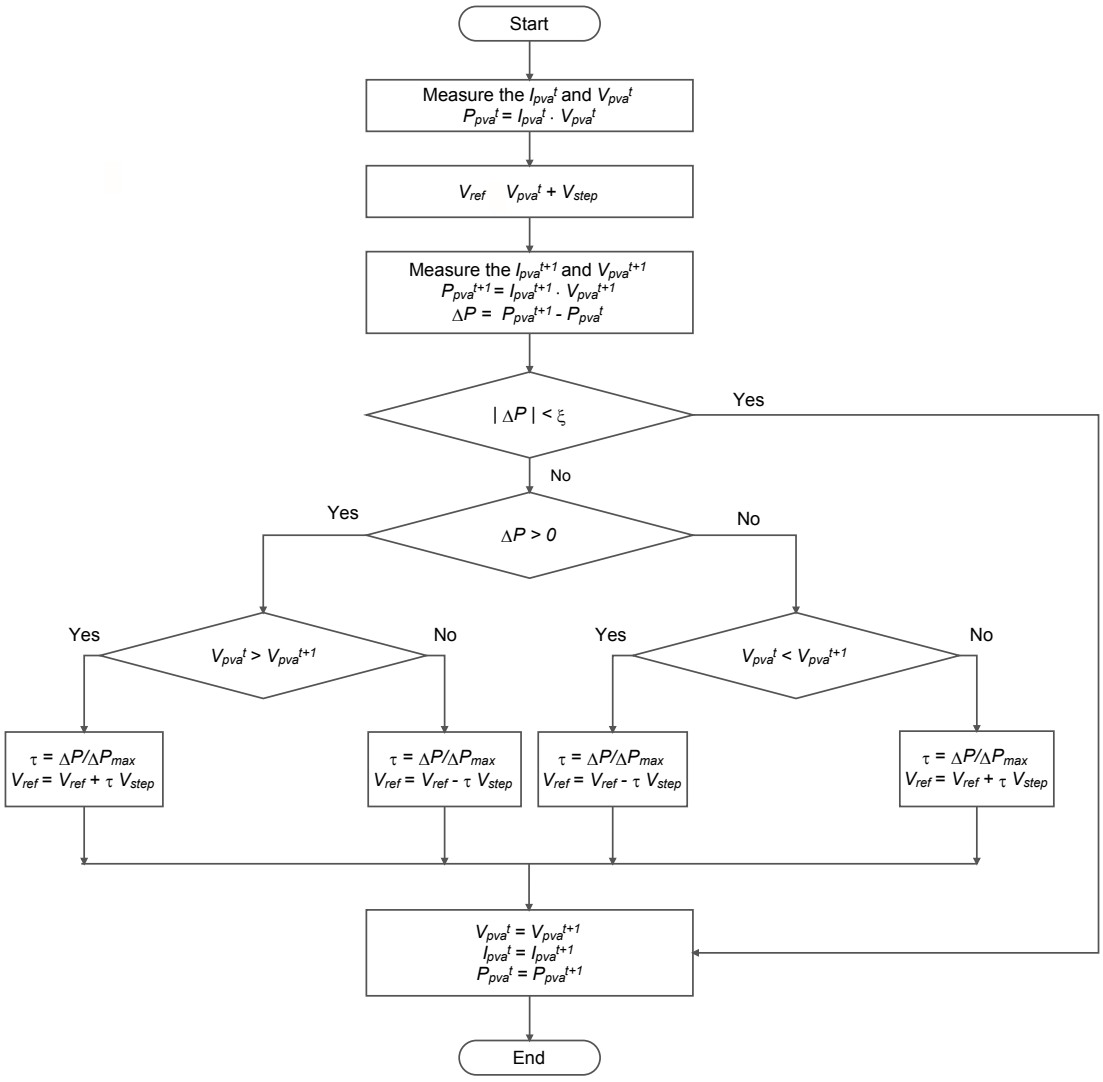

Figure 5.8: Adaptive P&O algorithm.

$$\begin{aligned} \tau &= \Delta P/\Delta P_{max}; \\ V_{ref} &= V_{ref} + \tau V_{step}, \end{aligned} \tag{5.43}$$

where ΔP_{max} denotes the preset upper limit for the ΔP, τ is a coefficient defining the variable step size, and V_{ref} is the reference voltage for the next iteration. The controller is formulated in such a manner that the perturbation can be small when the power change is less than or equal to the ΔP_{max}. The flowchart is illustrated in Figure 5.8.

5.4.3 The Two-Stage MPPT Strategy

The proposed two-stage MPPT strategy has two distinct main offline and online stages: MPPE and MPPR. Since a PV array under different environmental conditions exhibits various P-V characteristics, the algorithm considers two different steady environmental conditions that a PV array may encounter.

- Uniform insolation conditions

  All the PV modules in the array receive the irradiance at the same level. The P-V characteristics exhibit hill-like curve, displaying a single peak.

- Partial shading conditions

  When some parts of the PV system might be shaded, the bypass diodes cause the P-V characteristics of the PV array get complex - displaying multiple peaks (only one of which is the GMPP; the rest are LMPPs).

In the real world, the insolation conditions change continuously, all the time, which makes the task of MPPT even more difficult. In [7], the changing conditions are divided into sudden and gradual insolation changes. It is worth noting that the voltage at MPP also changes with the temperature variations. However, the shape of the P-V curve will not change significantly and the GMPP can be tracked by the APO effectively, and thus only the insolation changes are considered.

In the implementation of our two-stage algorithm, ΔG is used to distinguish the environment changes, and it is defined as:

$$\Delta G = \sum_{i=1}^{N} |G_i^{t+1} - G_i^t|. \tag{5.44}$$

where G_i^t is the i^{th} module at time T in the PV array. The irradiance is divided into two levels ϵ_u and ϵ_l. According to the value of ΔG, the tunning process is expressed as follows:

i. $\Delta G > \xi_u$ (rapidly changing insolation). The voltage at GMPP varies with the ambient atmospheric conditions. Using P&O or APO alone may make the operating point approach a LMPP but not the GMPP, and therefore the algorithm first calls the WSA-based MPPE function so that the reference voltage V_{ref} can

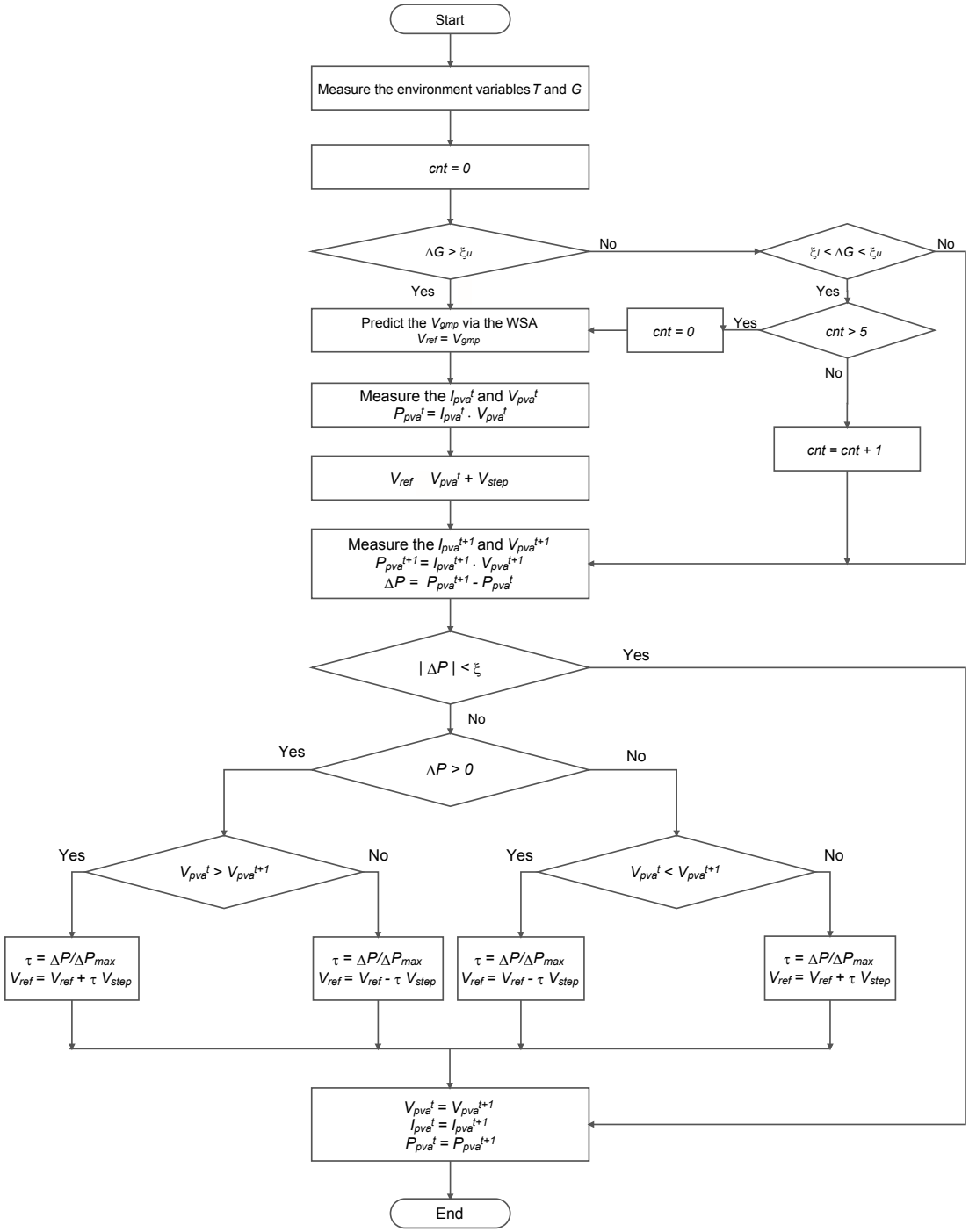

Figure 5.9: Flow chart of the proposed model-based two-stage MPPT strategy.

approach the GMPP immediately. The MPPR function, namely APO algorithm, then continues to track the MPP online by variable-step perturbations. At every sampling point, the power difference between the current and the previous sample points ΔP will be calculated. Equation (5.43) indicates that the V_{ref} will not be changed if $\Delta P = 0$. It essentially avoids the oscillations that happen in the

conventional P&O at steady state.

ii. $\Delta G < \xi_l$ (steady insolation). A slight change in the level of irradiance also implies a small deviation of the MPP locus. In this case, the MPPE is not necessary since the APO is capable of tracking the GMPP according the ΔP. The algorithm applies variable-step perturbations until the ΔP drops to 0.

iii. $\xi_l < \Delta G < \xi_u$ (gradually changing insolation). The entire or a part of PV array may receive the gradually changing of insolation at the intermediate state. During each control cycle, the output power is calculated. Between the consecutive measurements, the environment may change from uniform insolation conditions to partial shading conditions or, conversely, from partial shading conditions to uniform insolation conditions. The changes of the irradiance level are not large enough, yet the shapes of P-V curves can be different, which may cause miss tracking of the position of GMPP. To settle the problem, a loop is set as shown in Figure 5.10. The MPPE, followed by five MPPR steps, performs every six sampling times. Consequently, the algorithm's complexity and accuracy are balanced.

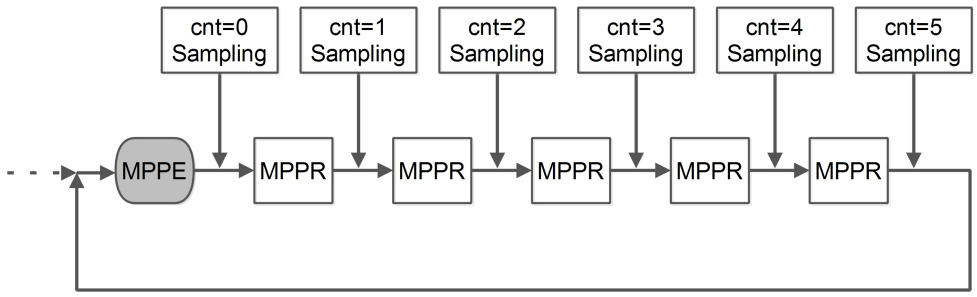

Figure 5.10: Process at gradual change insolation.

Based on the above analysis, the flow chart of the proposed two-stage MPPT strategy is shown in Figure 5.9.

5.5 Experimental Setup

With the aim of verifying the proposed method, a PV-supplied Single Ended Primary Inductance Converter (SEPIC) with the MPPT function is constructed in the PSIM [66] simulator.

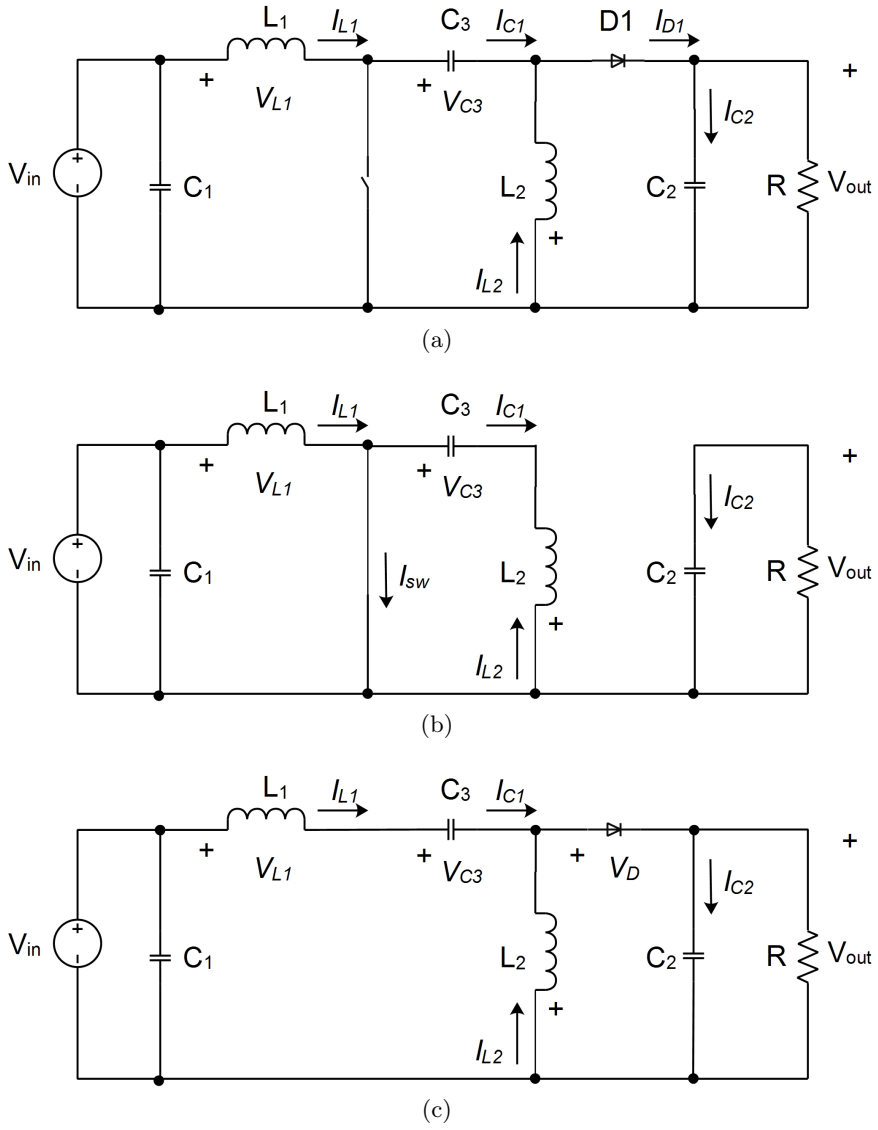

Figure 5.11: SEPIC converter current flow: (a) SEPIC circuit; (b) circuit with the switch closed and the diode off; (c) circuit with the switch open and the diode on.

The SEPIC is a DC-DC converter topology that provides a positive regulated output voltage. It can be higher or lower than the input voltage. Unlike the traditional buck-boost converter, it deliveries non-inverted output.

Figure 5.11 (a) shows a simple circuit diagram of a SEPIC, consisting of an input capacitor C_1, an output capacitor C_2, an AC coupling capacitor C_3, a coupled inductors L_1 and L_2, and a diode D_1. The output voltage V_{out} is controlled by the duty cycle D of the switch (or control transistor).

To understand the basic operation of the SEPIC, it is important to analyze the circuit at DC. Figure 5.11 (b) shows the situation whereby the switch is closed. In this

case, the diode D_1 is off. The voltage across L_1 for interval DT can be calculated by:

$$V_{L1} = V_{in}. \tag{5.45}$$

When the switch is open, the diode is on as shown in Figure 5.11 (c). According to Kirchhoff's voltage law around the path containing V_{in}, V_{L1}, V_{c3}, V_D and V_{out} gives:

$$-V_{in} + V_{L1} + V_{C3} + V_{D1} + V_{out} = 0. \tag{5.46}$$

Assuming that the voltage across C_3 remains the value at the average value. Recall Figure 5.11 (a), Kirchoff's voltage law around the path containing V_{in}, V_{L1}, V_{c3}, V_{L2} gives:

$$-V_{in} + V_{L1} + V_{C3} - V_{L2} = 0, \tag{5.47}$$

where the V_{L1} and the V_{L2} are equal to 0 at the average value. Equation (5.47) can be rewritten as :

$$V_{C3} = V_{in}. \tag{5.48}$$

By substituting Equation (5.48) to Equation (5.46), we get:

$$-V_{in} + V_{L1} + V_{in} + V_{D1} + V_{out} = 0. \tag{5.49}$$

or

$$V_{L1} = -V_{D1} - V_{out}, \tag{5.50}$$

for the interval $(1 - D)T$. Since the average voltage across an inductor is zero for periodic operating, Equation (5.50) and (5.45) can be combined to get the D [150]:

$$\begin{aligned} (V_{L1,swclosed})(DT) + (V_{L1,swopen})(1 - D)T &= 0 \\ V_{in}(DT) - (V_{D1} + V_{out})T &= 0, \end{aligned} \tag{5.51}$$

The value of D can be delivered by:

$$D = \frac{V_{out} + V_{D1}}{V_{in} + V_{out} + V_{D1}}. \tag{5.52}$$

In the simulation model, the SEPIC is supplied by the Renewable Energy Package of PSIM as shown in Figure 5.12. The array is consisted of three series connected MSX60 PV modules, and its terminal voltage V_{pva} is the V_{in} of the SEPIC, which is set between the range of 10 V to 60 V. To keep a stable output voltage of SEPIC V_{out}, a 30V-battery is connected. If the diode D_1 is assumed to be ideal, Equation (5.52) then can be written as:

$$D = \frac{V_{out}}{V_{pva} + V_{out}}. \tag{5.53}$$

Equation (5.53) implies that the operating points of the adopted PV modules are controlled by the duty cycle delivered by MPPT block. For the reason that Proportional plus Integral (PI) controllers do not work efficiently in non-linear applications [108], this work eliminates them and uses the topology stated in [151]. The duty cycle is computed directly by MPPT algorithms. The PSIM provides an interface linking the function model to its schematic program, and the MPPT algorithm is written in C using "Dynamic Link Library (DLL)". By comparing the reference duty cycle with a triangular signal, the switching signal can be generated.

The switching frequency and sampling rate are chosen to be 10 KHz and 20 Hz respectively. The peak-to-peak ripple is set to be 2% of the 30 V output voltage. According to the design guidelines in [152], the parameters of SEPIC are specified as follows: $L_1 = L_2 = 0.66$ mH, $C_1 = C_2 = 660\ uF$, $C_3 = 100$ uF. Figure 5.12 shows the V_{pva} and the V_{ref} are closely matched with each other, which indicates the SEPIC is able to move the operating point with the value computed by the MPPT block.

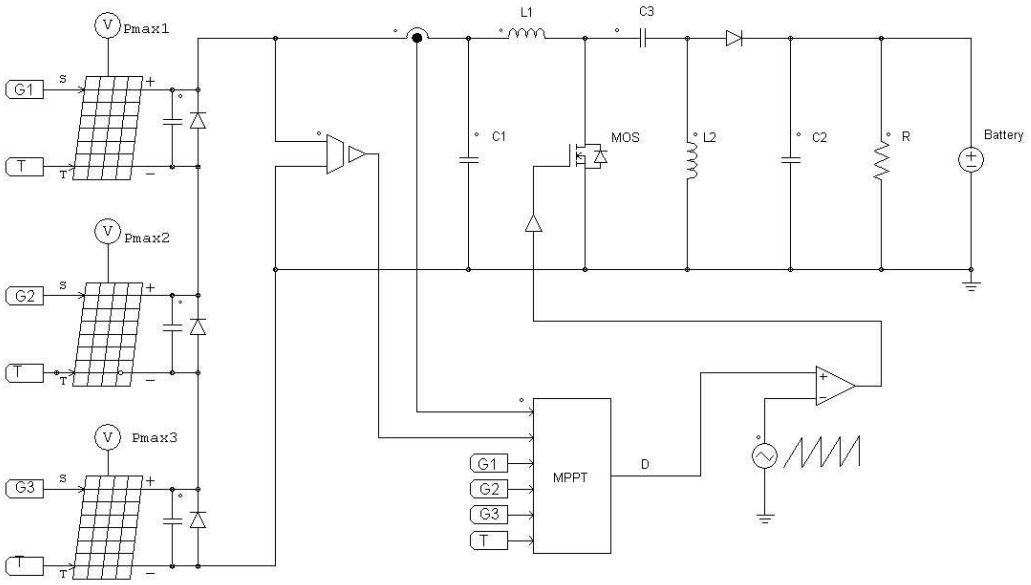

Figure 5.12: Simulation model for PV array with the model-based two-stage MPPT method.

5.6 Experiments and Results

The proposed model-based two-stage MPPE method presented in Section 5.4 is simulated to evaluate its effectiveness. Eight environmental sets are considered, as shown in Table 5.4.

Table 5.4: Testing environment sets.

Environment Set	I	II	III	IV	V	VI	VII	VIII
G1	1000	500	1000	500	1000	500	1000	750
G2	1000	500	1000	500	1000	500	750	500
G3	1000	500	1000	500	500	250	500	250
T	25	25	12	12	25	25	25	25

The rest of the section is structured as follows. First, the MPPE's capability of estimating the GMPP is evaluated. The tracking performance of the proposed MPPT method is studied using three environmental conditions: (a) steady environment (b) rapidly changing insolation (c) gradually changing insolation. The results for the three environmental sets are discussed in section 5.6.2, 5.6.3, and 5.6.4, respectively.

5.6.1 Maximum Power Point Estimation Capability

In the MPPE, the following parameters were used in our experiments:

- learning factor $c_1 = 2$;
- inertia factor $w_{max} = 0$;
- swarm size = 20 particles;
- maximum generation number = 200.

Figure 5.13 shows the qualitative representation of the evolutionary performance of the MPPE method under the environment sets shown in Table 5.4, where the output power represents the fitness value of every particle (or trial solution). In Figure 5.14, the predicted GMPPs for different environment sets are marked by heavy dots on the P-V curve simulated with the PSIM's Renewable Energy Package.

As seen in Figures 5.14 (a)-(d), the P-V characteristics exhibit a single peak for the environment sets I-IV. For these curves, the convergence traces of the WSA are plotted in Figures 5.13 (a)-(d). The best particle first moves to a value closed to the voltage at GMPP V_{gmp}, and then it oscillates around the V_{gmp} to find better solutions. The shapes of P-V curves become more complicated in Figures 5.14 (e)-(f), displaying double peaks for the environment sets V-VI and triple peaks for the environment sets VII-VIII. In Figures 5.14 (e) and (f), the particles are moved around the GMPP directly and the

convergence traces are similar to the ones in Figures 5.14 (a)-(d). On the other hand, the particles may be trapped in a local optimum solution in early search. Figures 5.14 (g) and (h) present the convergence traces in such situation. Before the first 50 iterations, the WSA evaluates the fitness values among the peaks, the best particle delivering more power will be deemed as the GMPP, and then the particles move around the GMPP to achieve a better accuracy. It is observed that the approximate GMPP can be successfully predicted by using the model-based MPPE method. Although the accuracy still needs to improve, the MPPE is capable of preventing the particles from staying stuck in the local best.

5.6.2 The Performance of The Proposed MPPT Algorithm in a PV System under Steady Environmental Conditions

Figures 5.15, 5.16, and 5.17 show the time plot of the output power obtained with different MPPT methods under the environment sets I, V, and VII, respectively. The parameters of P&O and PSO are set as follows:

P&O perturbation step = 0.2 V, initial voltage = 52 V

PSO swarm size = 5 particles, maximum generation = 6, $c_1 = c_2 = 2$, $w = 0.5$

From these figures, the weakness of the P&O as an MPPT method is apparent: (1) the search time can be considerably long if the initial point is far from a peak on the P-V curve; (2) the operating point oscillates as soon as it finds a local best point; and (3) it stops tracking and stay at a local best point closed to its initial point.

The PSO method releases trial solutions randomly in the first generation. The fitness values, namely the P_{pva}, are measured online. The movements of particles are then guided by the positions of the local best and the global best. It is worth pointing out that the accuracy depends on the number of generations and the applied particles. For an unimodal P-V curve, the PSO with large swarm size or generation number has a slow response compared with the conventional P&O algorithm. On the other hand, small swarm size or generation number may lead to an inaccurate solution, which is far from the GMPP.

The proposed method combines the merits from the conventional P&O and from the PSO methods. Before performing an online search, the voltage is initialized by the

MPPE, which is a soft computing approach used to estimate the value of V_{gmp}. The MPPE narrows the search range for the MPPR and, at the same time, reduces the probability of trapping into local best. In the MPPR, variable perturbation steps not only increase the tracking speed, but also prevent oscillations at a steady state.

5.6.3 The Performance of The Proposed MPPT Algorithm in a PV System under Rapidly Changing Environmental Conditions

To evaluate a PV array working under rapidly changing environmental conditions, six tests are organized as shown in Table 5.5. Take test 1 for example, the total simulation time is divided into four subintervals, in which the environmental factors are set as: I, II, III, and IV. Figure 5.18 shows the time plot of the output power obtained with the proposed method for Test 1 - Test 6. As rapid isolation changes are detected ($\Delta G > \epsilon_u$), the algorithm calls the MPPE function. It can be seen that the V_{ref} jumps to a value closed to the V_{gmp} at the beginning of every subintervals. The variable-step MPPR then adjusts the operating point so as to obtain a higher output power. These tests show that the proposed algorithm gives a good guess for the V_{gmp} under rapidly changing environmental conditions.

Table 5.5: Testing sets for a PV array under rapidly changing environmental conditions.

Time (s)	$0 \leqslant t \leqslant 0.5$	$0.5 \leqslant t \leqslant 1$	$1 \leqslant t \leqslant 1.5$	$1.5 \leqslant t \leqslant 2$
Test 1	I	II	III	IV
Test 2	V	VI	V	VI
Test 3	VII	VIII	VII	VIII
Test 4	V	II	V	II
Test 5	V	VII	V	VII
Test 6	VIII	I	VIII	I

5.6.4 The Performance of The Proposed MPPT Algorithm in a PV System under Gradually Changing Environmental Conditions

The level of irradiance may be changed gradually during a particular period of time. Figure 5.19 shows an example for the gradually changing environmental conditions. The temperature is assumed to be stable at 25 ℃, while the level of irradiance is set as shown in Figure 5.20 (a). During 0 - 2 s, the G_1 increases from 500 W/m^2 to 1000 W/m^2, and the other PV modules receives 1000 W/m^2. By varying the operating voltage, the corresponding P-V curve is illustrated in Figure 5.19. When the G_1 is in

the range between 500 W/m^2 and 600 W/m^2, the V_{gmp} is around 35 V. The height of the right peak rises with the increase of G_1. As the G_1 is up to 650 W/m^2, the right peak is higher than the left one and the V_{gmp} moves to a value about 52 V. For this case, most of the conventional online MPPT method (e.g. P&O and IncCond) may fail to track the GMPP.

The proposed model-based two-stage MPPT method applies the value ΔG to detect the gradually changing environmental conditions. As the conditions are recognized, the algorithm calls the MPPE for every 6 control cycles. Figures 5.20 (b) and (c) show the time plot of output power P_{pva}, reference voltage V_{ref} and operating voltage V_{pva}. Before 0.8 s, the V_{ref} is kept around 35 V, which is the voltage of the first peak. After that, it jumps to 52 V. That indicates the algorithm has recognized the changes on the V_{gmp} and has used the MPPE to give a good initial point for the MPPR method.

5.7 Summary

By combining the offline Weightless Swarm Algorithm (WSA) with the online Adaptive Perturb & Observe (APO) method, a two-step MPPT method with a simple and straightforward approximate PV electrical model has been successfully developed.

After briefly outlining the basic procedure of the applied Maximum Power Point Estimation (MPPE) and Maximum Power Point Revision method (MPPR), it is then implemented in the PSIM simulation environment. The simulation results show that the proposed MPPT method can efficiently track the GMPP of the P-V characteristics curves under rapidly and gradually changing testing environments.

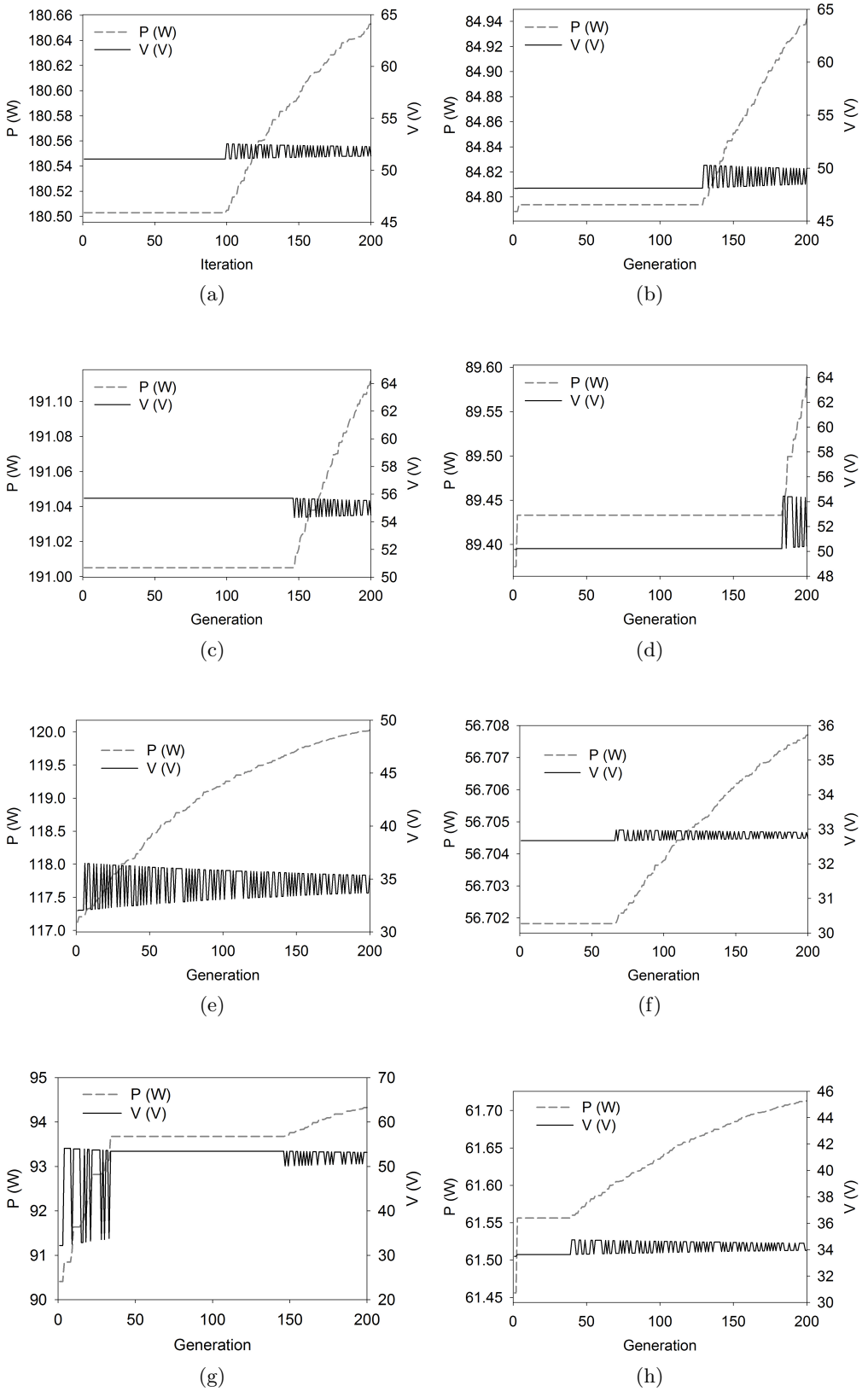

Figure 5.13: Evolution performance of the MPPE under various testing environment sets: (a) I (b) II (c) III (d) IV (e) V (f) VI (g) VII (h) VIII.

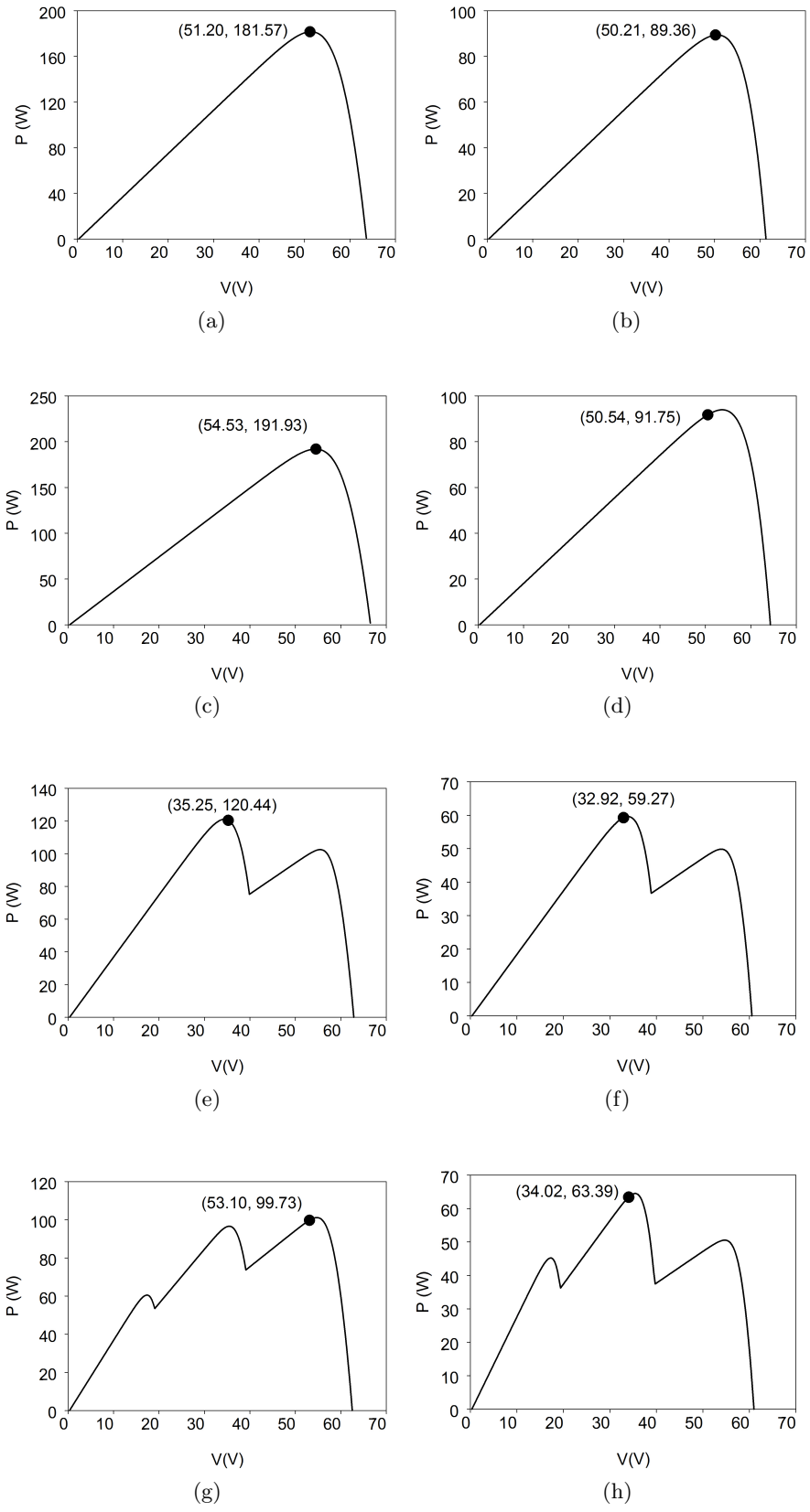

Figure 5.14: Estimated GMPPs on the P-V curve for various testing environment sets: (a) I (b) II (c) III (d) IV (e) V (f) VI (g) VII (h) VIII.

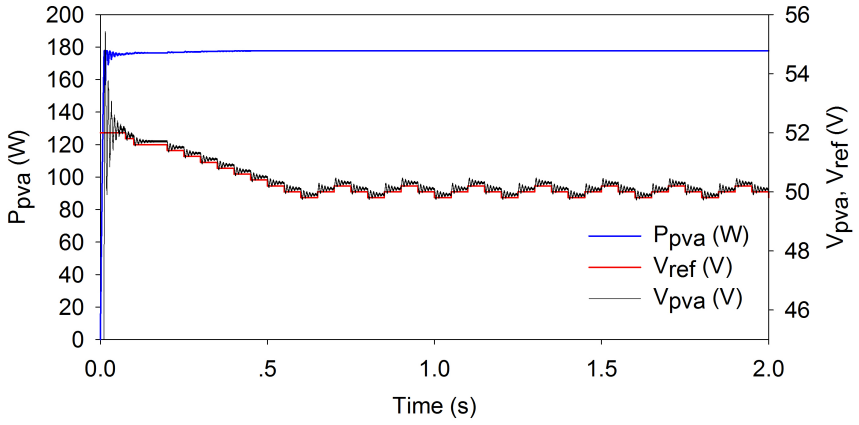

(a)

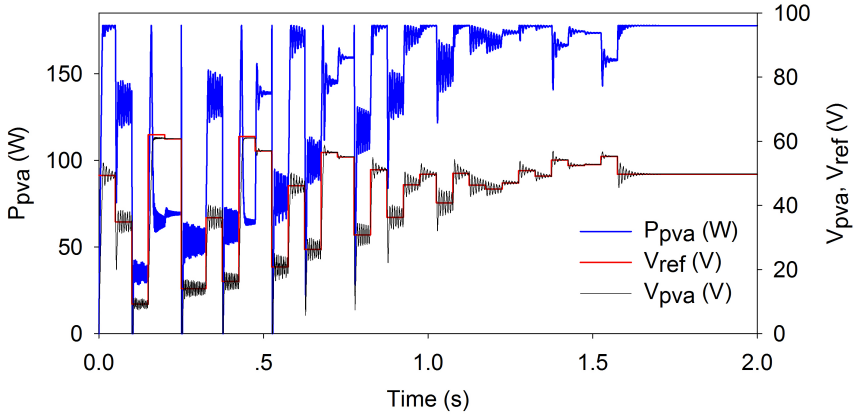

(b)

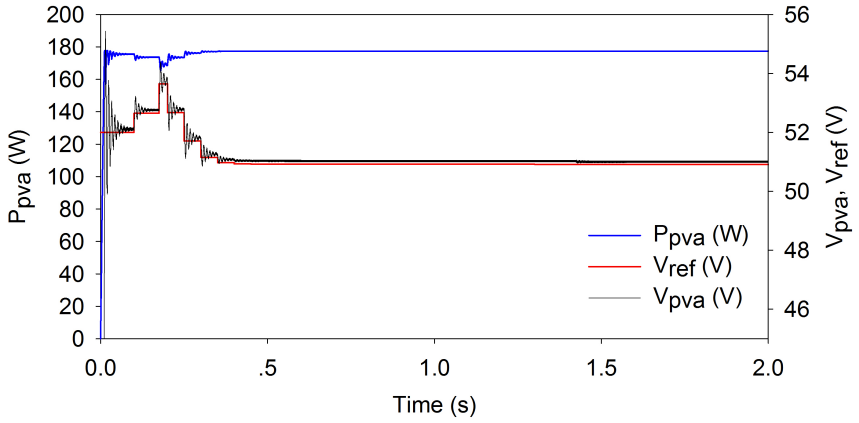

(c)

Figure 5.15: Time plot of the output power obtained with (a) P&O method under the environment set I (perturbation step = 0.2 V, initial voltage = 52 V); (b) PSO (swarm size = 5 particles, maximum generation = 6, $c_1 = c_2 = 2$, $w = 0.5$); (c) proposed method.

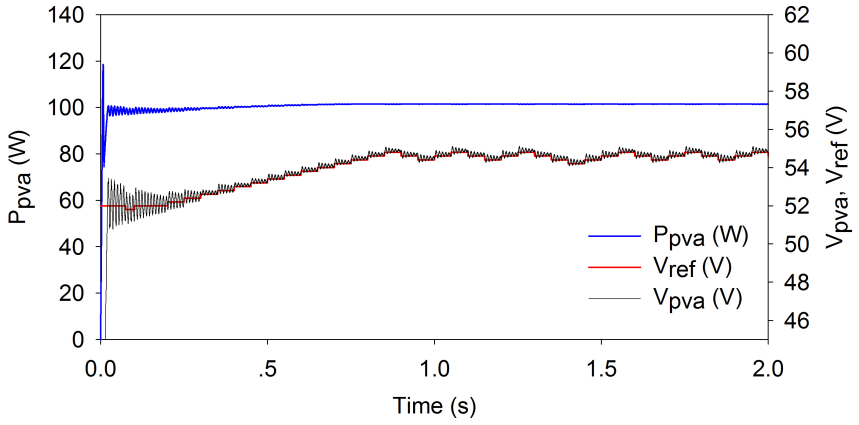

(a)

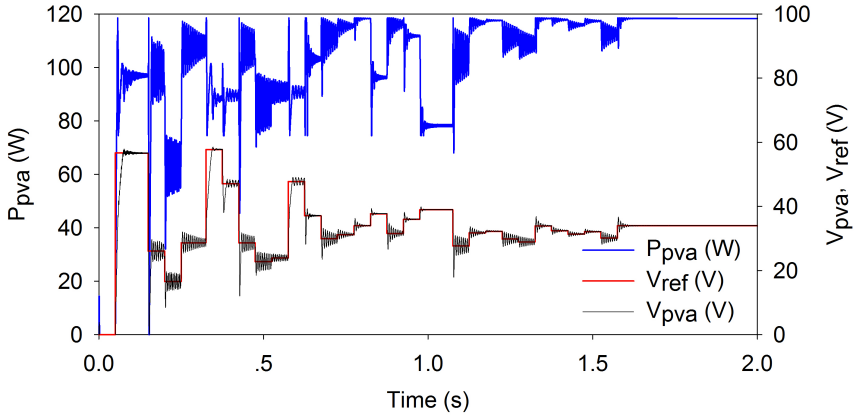

(b)

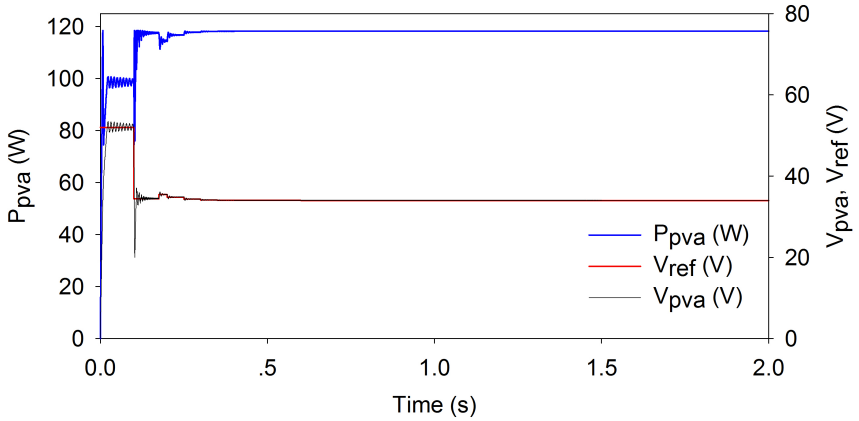

(c)

Figure 5.16: Time plot of the output power obtained with (a) P&O method under the environment set V (perturbation step = 0.2 V, initial voltage = 52 V); (b) PSO (swarm size = 5 particles, maximum generation = 6, $c_1 = c_2 = 2$, $w = 0.5$); (c) proposed method.

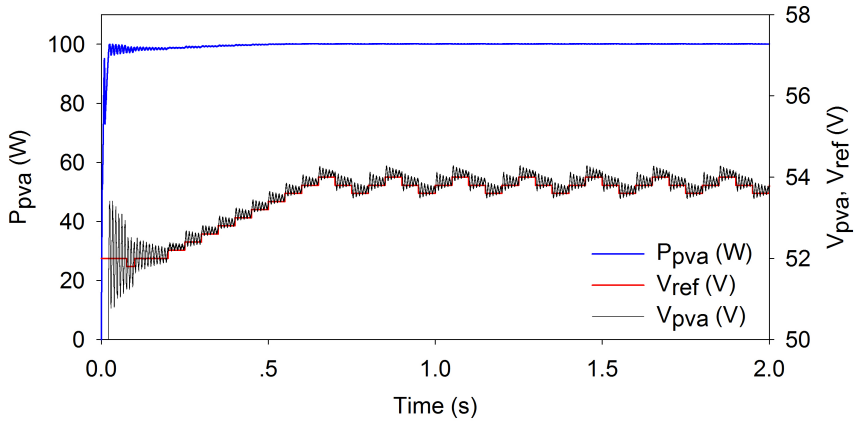

(a)

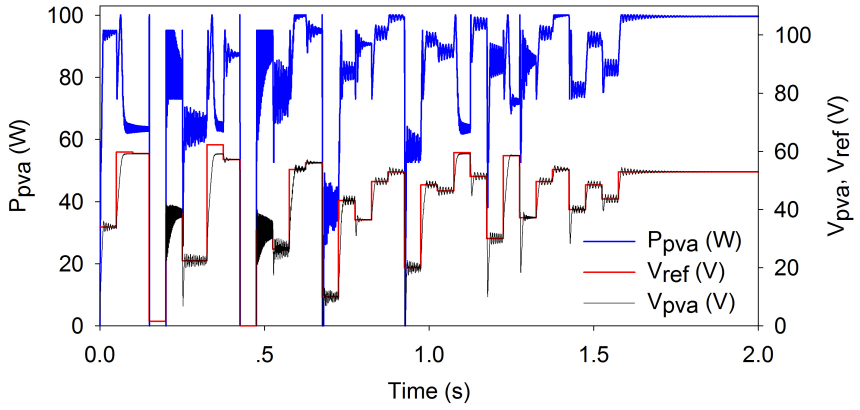

(b)

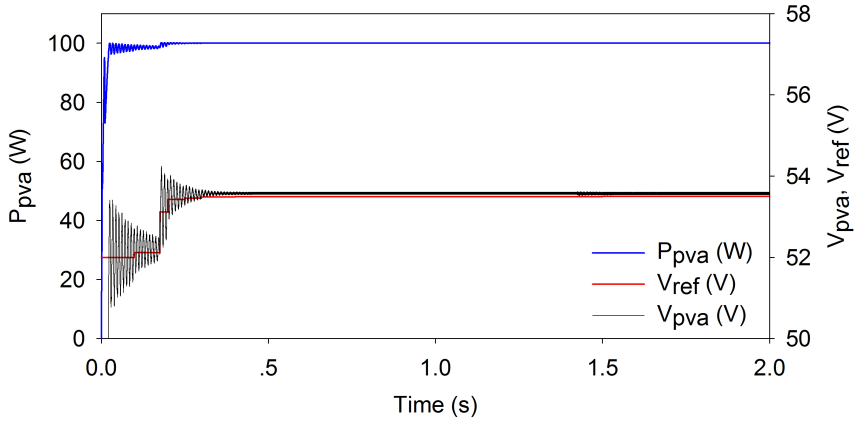

(c)

Figure 5.17: Time plot of the output power obtained with (a) P&O method under the environment set VII (perturbation step = 0.2 V, initial voltage = 52 V); (b) PSO (swarm size = 5 particles, maximum generation = 6, $c_1 = c_2 = 2$, $w = 0.5$); (c) proposed method.

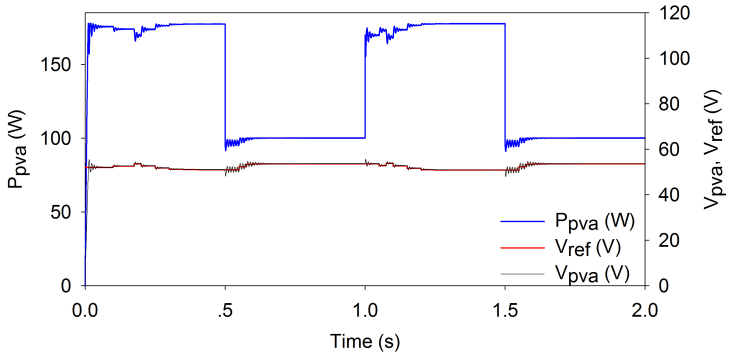

(a)

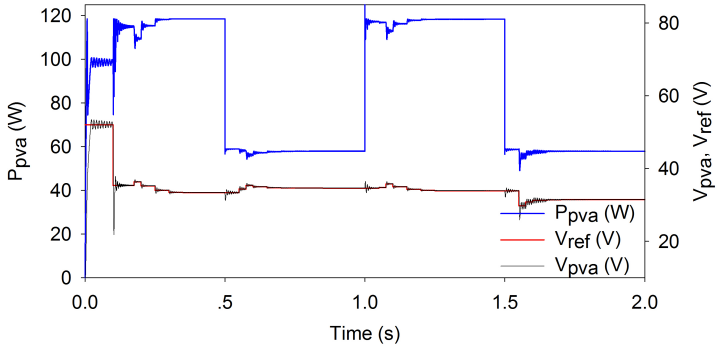

(b)

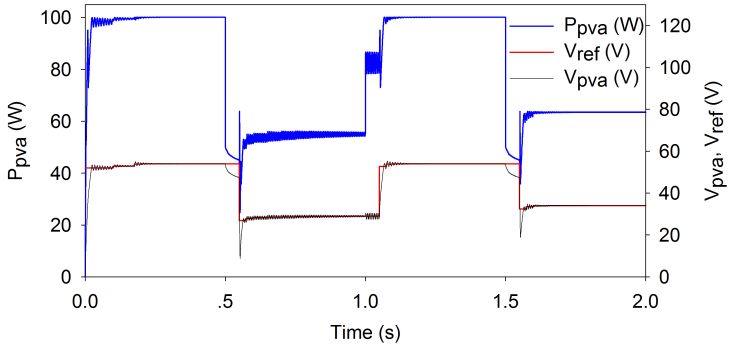

(c)

Figure 5.18: Time plot of the output power obtained with the proposed method in different tests: (a) Test 1; (b) Test 2; (c) Test 3; (d) Test 4; (e) Test 5; (f) Test 6.

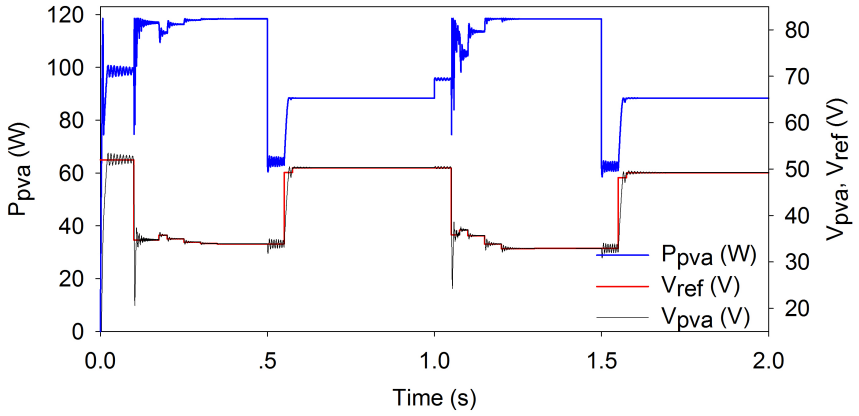

(d)

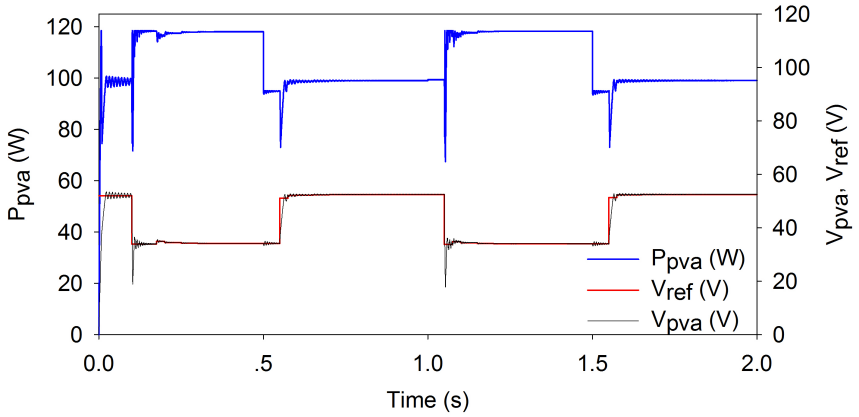

(e)

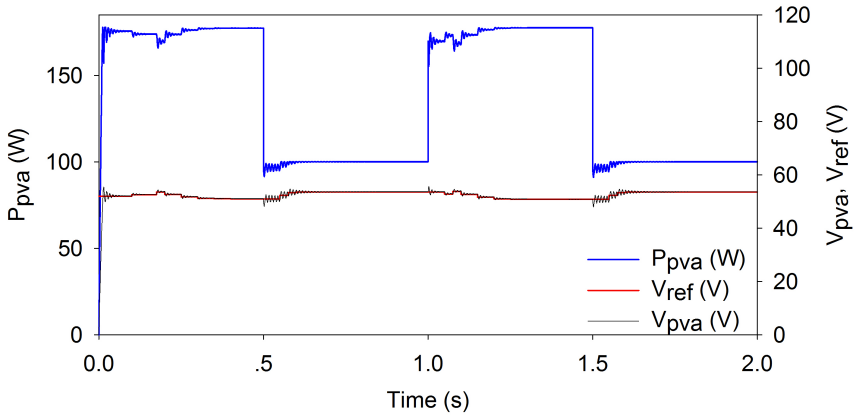

(f)

Figure 5.18: Time plot of the output power obtained with the proposed method in different tests: (a) Test 1; (b) Test 2; (c) Test 3; (d) Test 4; (e) Test 5; (f) Test 6.

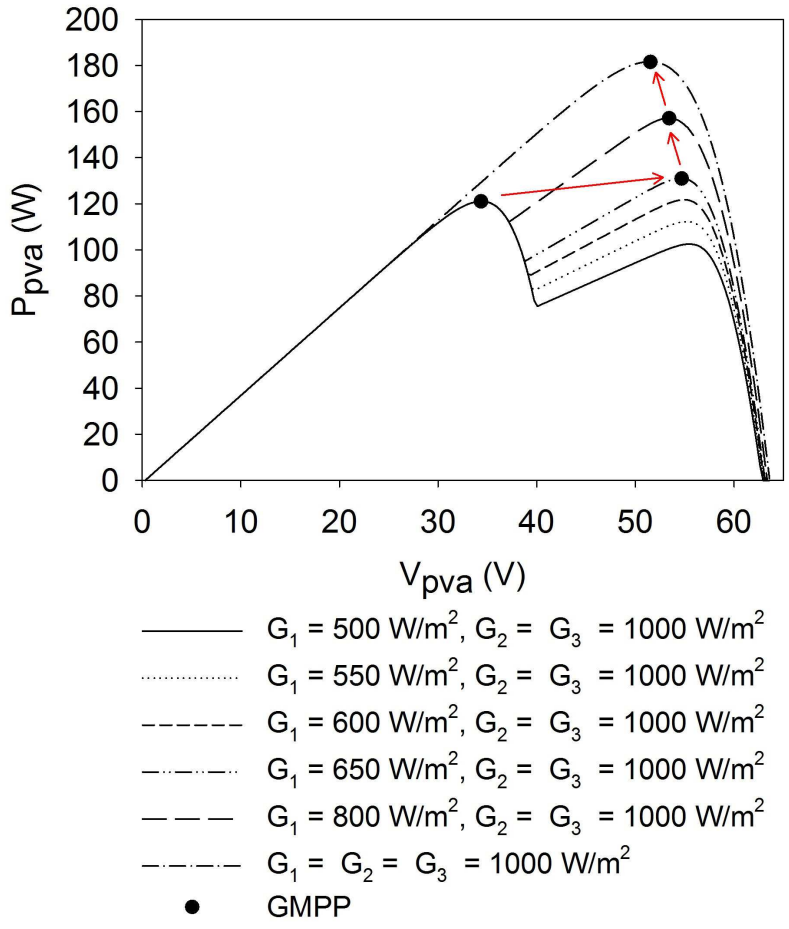

Figure 5.19: The P-V curve of a PV array receiving gradually changing insolation.

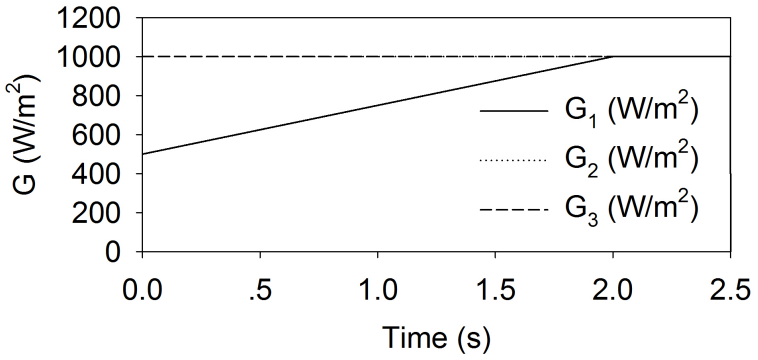

(a)

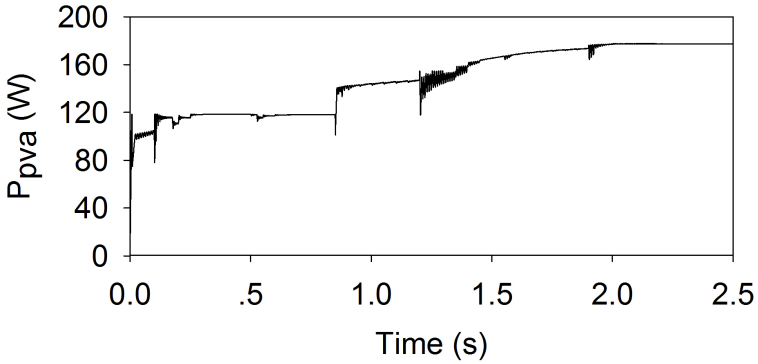

(b)

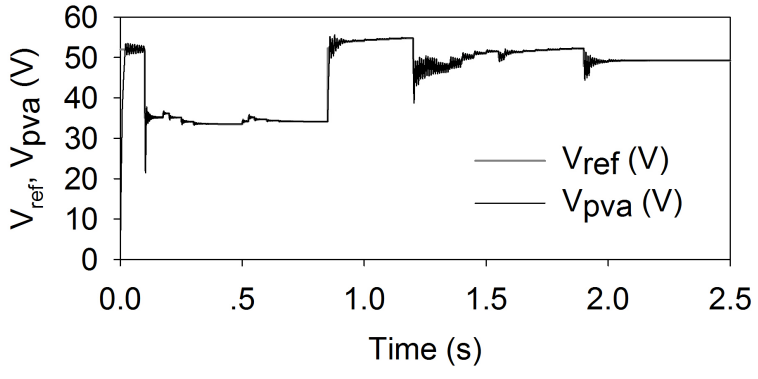

(c)

Figure 5.20: A PV array receiving gradually changing insolation: (a) irradiance G; (b) output power P_{pva}; (c) reference voltage V_{ref} and operating voltage V_{pva}.

Chapter 6

Conclusions and Future Work

In this thesis, the problems of parameter estimation and Maximum Power Point Tracking (MPPT) have been investigated for Photovoltaic (PV) systems. Several artificial intelligence optimization approaches are analyzed and are used to solve the two problems. The applied algorithms are summarized as follows:

- The Cuckoo Search (CS) algorithm has been applied to estimate the parameters for PV electrical models. The CS algorithm is based on the cuckoo breeding behavior. Instead of conventional isotropic random walks, the algorithm uses Lévy flights. The simulation results showed that CS algorithm outperforms Genetic Algorithm (GA) [18], Chaos Particle Swarm Algorithm (CPSO) [17], and Pattern Search (PS) [74] methods. At a certain irradiance level, the CS obtained slightly lower RMSE for model parameters, recording 0.0010 in numerical value, and its convergence speed was slightly faster than the CPSO. Moreover, the validity of the CS algorithm was evaluated using KC200GT PV module operating under different environmental conditions. In statistical analysis, the CS algorithm recorded the lowest RMSE value compared with other algorithms such as the GA, CPSO and PS.

- The Parallel Particle Swarm Optimization (PPSO) has been implemented to speed up the parameter estimation process for different PV electrical models. It was implemented in Open Computing Language (OpenCL) and can be executed with a wide range of multi-core computing devices. In order to make a comprehensive comparison, the parameters were estimated by the other methods, such as Least Square Optimization (LSO) [16], PS, and Simulated Annealing (SA) algorithms [74]. From these test results, the mean absolute error obtained

by the PPSO with double diode cell model achieves the lowest value, recording 6.6415E-4, which is 51.85% lower than the SA with the same PV electrical model, and is approximately 3 % lower than the PPSO with the single diode cell model. The PPSO-based parameter estimation method did not only record lower error values, but also showed speed improvements. The simulation results showed that the PPSO with 2048 particles is capable of accelerating the computational speed by at least 64% on the used computing platforms.

- The Weightless Swarm Algorithm (WSA) has been proposed to estimate the Global Maximum Power Point (GMPP) locus with an approximate PV electrical model. It is capable of predicting a PV array under either the uniform insolation conditions or the partial shading conditions. By means of alternative use of the WSA-based Maximum Power Point Estimation (MPPE) and an Adaptive Perturb & Observe (APO) based Maximum Power Point Revision (MPPR), the two-stage MPPT method first gives a good initial operating point and the accuracy is further improved online as the changes of environments are detected. To verify the efficiency of the proposed method, an MPPT system composed of a SEPIC and PV generator was implemented in PSIM. The results showed that the model-based two-stage method combines the merits of both the direct and indirect MPPT methods: the dynamic response of the proposed MPPT method is quicker than that of the conventional P&O and PSO methods. Moreover, the WSA-based MPPE method prevented the operating point stay stuck at a local best value, and the output power did not oscillate around the GMPP.

To sum up, our research effort has been taken in developing and implementing new algorithms to solve parameter estimation and MPPT methods. The proposed methods have been verified from the measured data and simulation experiments. The CS algorithm minimizes the errors of parameter estimation while the PPSO further enhance the computational efficiency under a parallel computing environment. The proposed model-based two-stage MPPT method guarantees high accuracy and reliability of tracking performance.

Although the proposed methods achieved promising results with respect to the investigated problems, there are several aspects that can be further investigated:

- The performance of the artificial intelligence optimization algorithm significantly depends on the values of algorithm parameters. An optimal parameter setting will

improve performance in terms of the convergence speed. Therefore, a self-tuning, which is the process of tuning an algorithm to find the best parameter settings, is required to enable the algorithm to perform the best for a given problem.

- Since branching is difficult for all the computing devices, especially GPUs, the process of updating positions and velocities of particles in the PPSO has not been parallelized. On the other hand, like the WSA, the inertia weight w as well as branching process for bounds checking can be ignored to further improve the computational efficiency. This can be investigated in our future work.

- The performance of the proposed parameter estimation and MPPT methods will be explored on the TI's Piccolo F28035 based Solar Explorer Development Kit. The experimental results obtained from the kit will further verify the feasibility of the proposed MPPT method.

Appendix A

PV Physical Model Adopted in PSIM

By using the parameters extracted at the STCs, the I-V characteristics of a PV module under nonstandard operating conditions are calculated via the following equations:

$$I = I_{ph} - I_D - I_R \tag{A.1}$$

$$I_{ph} = I_{scn} \cdot \frac{G}{G_n} - K_i \cdot (T - T_n) \tag{A.2}$$

$$I_D = I_{o1} \cdot (e^{\frac{qV_d}{A_1 kT}} - 1) \tag{A.3}$$

$$I_{o1} = I_{on1} \cdot \left(\frac{G}{G_n}\right)^3 \cdot e^{\left(\frac{qE_g}{A_1 k}\right)\cdot\left(\frac{1}{T} - \frac{1}{T_n}\right)} \tag{A.4}$$

$$I_R = \frac{V_D}{R_{pm}} \tag{A.5}$$

$$V_D = \frac{V}{N_s} + I \cdot R_{sm} \tag{A.6}$$

where G is the solar irradiance, T is the cell temperature, I_{ph} is the photocurrent, I_o is the reserve saturation current of the diode, I_{sc} is the short circuit current, R_{sm} is the series resistance, R_{pm} is the shunt resistance, k is Boltzmann constant, q is electron charge, N_s is the number of series connected cell in the PV module, K_i is the short circuit current coefficient, I_R is the current flowing through the resistance, A_1 is the ideality factor, E_g is the band gap energy, V_D and I_D represent the voltage and current flowing through the diode respectively. I_{on1}, I_{scn}, G_n and T_n denote the I_{o1}, I_{sc}, G, and T measured in the standard testing conditions.

Appendix B

The Experimental I-V Data of The R.T.C. France PV Cell

Measurement	G	T	$\widehat{I}$	$\widehat{V}$
1	1000	33	0.7640	-0.2057
2	1000	33	0.7620	-0.1291
3	1000	33	0.7605	-0.0588
4	1000	33	0.7605	0.0057
5	1000	33	0.7600	0.0646
6	1000	33	0.7590	0.1185
7	1000	33	0.7570	0.1678
8	1000	33	0.7570	0.2132
9	1000	33	0.7555	0.2545
10	1000	33	0.7540	0.2924
11	1000	33	0.7505	0.3269
12	1000	33	0.7465	0.3585
13	1000	33	0.7385	0.3873
14	1000	33	0.7280	0.4137
15	1000	33	0.7065	0.4373
16	1000	33	0.6755	0.4590
17	1000	33	0.6320	0.4784
18	1000	33	0.5730	0.4960
19	1000	33	0.4990	0.5119
20	1000	33	0.4130	0.5265
21	1000	33	0.3165	0.5398
22	1000	33	0.2120	0.5521
23	1000	33	0.1035	0.5633
24	1000	33	-0.0100	0.5736
25	1000	33	-0.1230	0.5833
26	1000	33	-0.2100	0.5900

Appendix C

The Experimental I-V Data of The Photowatt-PWP 201 PV Module

Measurement	G	T	$\widehat{I}$	$\widehat{V}$
1	1000	45	1.0315	0.1248
2	1000	45	1.03	1.8093
3	1000	45	1.026	3.3511
4	1000	45	1.022	4.7622
5	1000	45	1.018	6.0538
6	1000	45	1.0155	7.2364
7	1000	45	1.014	8.3189
8	1000	45	1.01	9.3097
9	1000	45	1.0035	10.2163
10	1000	45	0.988	11.0449
11	1000	45	0.963	11.8018
12	1000	45	0.9255	12.4929
13	1000	45	0.8725	13.1231
14	1000	45	0.8075	13.6983
15	1000	45	0.7265	14.2221
16	1000	45	0.6345	14.6995
17	1000	45	0.5345	15.1346
18	1000	45	0.4275	15.5311
19	1000	45	0.3185	15.8929
20	1000	45	0.2085	16.2229
21	1000	45	0.101	16.5241
22	1000	45	-0.008	16.7987
23	1000	45	-0.111	17.0499
24	1000	45	-0.209	17.2793
25	1000	45	-0.303	17.4885

Appendix D

The Experimental I-V Data of The KC200GT PV Module

Measurement	G	T	$\widehat{I}$	$\widehat{V}$
1	200	25	1.5754	0.0409
2	200	25	1.5754	1.0472
3	200	25	1.5754	2.0534
4	200	25	1.5754	3.0707
5	200	25	1.5754	4.0769
6	200	25	1.5754	4.9957
7	200	25	1.5754	6.0129
8	200	25	1.5754	7.0192
9	200	25	1.5754	8.0255
10	200	25	1.5754	9.0427
11	200	25	1.5754	10.0490
12	200	25	1.5754	11.0662
13	200	25	1.5754	11.9740
14	200	25	1.5754	12.9912
15	200	25	1.5754	13.9975
16	200	25	1.5754	15.0147
17	200	25	1.5754	16.0210
18	200	25	1.5754	17.0272
19	200	25	1.5754	18.0445
20	200	25	1.5754	19.0507
21	200	25	1.5754	20.0679
22	200	25	1.5754	21.0742
23	200	25	1.5568	22.0805
24	200	25	1.5358	22.9993
25	200	25	1.4962	24.0165
26	200	25	1.4589	25.0227
27	200	25	1.3982	26.0290
28	200	25	1.2817	27.0462
29	200	25	1.0462	28.0525
30	200	25	0.7524	29.0697
31	200	25	0.3607	30.0760

32	400	25	3.2402	0.0409
33	400	25	3.2402	1.0472
34	400	25	3.2402	2.0534
35	400	25	3.2402	3.0707
36	400	25	3.2215	4.1754
37	400	25	3.2215	4.9957
38	400	25	3.2215	6.0129
39	400	25	3.2215	7.0192
40	400	25	3.2215	8.0255
41	400	25	3.2215	9.0427
42	400	25	3.2215	10.0490
43	400	25	3.2215	11.0662
44	400	25	3.2005	12.0724
45	400	25	3.2005	13.0787
46	400	25	3.2005	13.9100
47	400	25	3.2005	15.0147
48	400	25	3.1819	16.0210
49	400	25	3.1819	17.0272
50	400	25	3.1819	18.0445
51	400	25	3.1819	19.0507
52	400	25	3.1619	20.0679
53	400	25	3.1609	20.9867
54	400	25	3.1609	21.9930
55	400	25	3.1422	22.9993
56	400	25	3.1422	24.0165
57	400	25	3.0839	25.0227
58	400	25	2.9860	26.0290
59	400	25	2.8298	26.9478
60	400	25	2.4964	28.0525
61	400	25	2.1047	29.0697
62	400	25	1.4775	30.0760
63	400	25	0.5962	31.0823
64	600	25	4.8653	0.0409
65	600	25	4.8653	1.0472
66	600	25	4.8653	2.0534
67	600	25	4.8653	3.0707
68	600	25	4.8653	4.0769
69	600	25	4.8653	5.0941
70	600	25	4.8653	6.0129
71	600	25	4.8453	7.0192
72	600	25	4.8466	8.0255
73	600	25	4.8466	9.0427
74	600	25	4.8466	10.0490
75	600	25	4.8280	11.0662
76	600	25	4.8280	12.0724
77	600	25	4.8070	13.0787
78	600	25	4.8070	14.0959
79	600	25	4.8070	14.9163
80	600	25	4.8070	16.0210

81	600	25	4.8070	17.0272
82	600	25	4.7883	18.0445
83	600	25	4.7883	19.0507
84	600	25	4.7883	20.0679
85	600	25	4.7487	21.0742
86	600	25	4.7487	22.0805
87	600	25	4.7487	23.0977
88	600	25	4.7300	24.0165
89	600	25	4.6694	25.0227
90	600	25	4.5715	26.0290
91	600	25	4.4153	27.0462
92	600	25	4.0819	28.0525
93	600	25	3.4756	29.0697
94	600	25	2.7692	30.0760
95	600	25	1.9275	30.9948
96	600	25	0.5962	32.0010
97	800	25	6.5300	0.0409
98	800	25	6.5300	1.0472
99	800	25	6.5300	2.0534
100	800	25	6.4927	3.0707
101	800	25	6.4927	4.0769
102	800	25	6.4927	4.9082
103	800	25	6.4927	6.0129
104	800	25	6.4927	7.0192
105	800	25	6.4530	8.0255
106	800	25	6.4530	9.0427
107	800	25	6.4530	10.0490
108	800	25	6.4530	11.0662
109	800	25	6.4530	12.0724
110	800	25	6.4134	13.0787
111	800	25	6.4134	14.0959
112	800	25	6.4134	14.9163
113	800	25	6.4134	16.0210
114	800	25	6.4134	17.0272
115	800	25	6.3948	18.0445
116	800	25	6.3948	19.0507
117	800	25	6.3948	20.0679
118	800	25	6.3551	21.0742
119	800	25	6.3551	22.0805
120	800	25	6.3551	22.9118
121	800	25	6.3155	24.0165
122	800	25	6.2759	25.0227
123	800	25	6.2176	26.0290
124	800	25	6.0031	27.0462
125	800	25	5.5717	28.0525
126	800	25	4.9049	29.0697
127	800	25	4.0049	30.0760
128	800	25	2.7319	31.0823
129	800	25	1.0671	32.0995

130	1000	25	8.1761	0.0409
131	1000	25	8.1761	1.0472
132	1000	25	8.1761	2.0534
133	1000	25	8.1364	3.0707
134	1000	25	8.1364	4.0769
135	1000	25	8.1364	4.9082
136	1000	25	8.1178	6.0129
137	1000	25	8.1178	7.0192
138	1000	25	8.1178	8.0255
139	1000	25	8.0781	9.0427
140	1000	25	8.0781	10.0490
141	1000	25	8.0781	11.0662
142	1000	25	8.0781	11.9740
143	1000	25	8.0595	12.9912
144	1000	25	8.0595	13.9975
145	1000	25	8.0385	15.0147
146	1000	25	8.0385	16.0210
147	1000	25	8.0199	17.0272
148	1000	25	8.0199	18.0445
149	1000	25	8.0012	19.0507
150	1000	25	7.9802	20.0679
151	1000	25	7.9802	21.0742
152	1000	25	7.9616	22.0805
153	1000	25	7.9219	22.9993
154	1000	25	7.9219	24.0165
155	1000	25	7.8823	25.0227
156	1000	25	7.7844	26.0290
157	1000	25	7.5699	27.0462
158	1000	25	7.1385	28.0525
159	1000	25	6.4717	29.0697
160	1000	25	5.4155	30.0760
161	1000	25	3.8091	31.1807
162	1000	25	2.1443	32.0995
163	1000	25	0.4400	32.9198
164	1000	50	8.2600	0.0761
165	1000	50	8.2410	1.0405
166	1000	50	8.2410	2.0145
167	1000	50	8.2400	3.0656
168	1000	50	8.2214	3.9625
169	1000	50	8.2214	3.9625
170	1000	50	8.2214	4.9268
171	1000	50	8.2214	6.0648
172	1000	50	8.2014	7.0388
173	1000	50	8.2014	8.0031
174	1000	50	8.1818	8.9771
175	1000	50	8.1618	9.9511
176	1000	50	8.1618	10.9251
177	1000	50	8.1418	12.0534
178	1000	50	8.1422	13.0274

179	1000	50	8.1222	14.0014
180	1000	50	8.1235	14.9754
181	1000	50	8.1049	15.9398
182	1000	50	8.1049	16.9138
183	1000	50	8.0839	18.0517
184	1000	50	8.0653	19.0161
185	1000	50	8.0257	19.9901
186	1000	50	7.9861	20.9641
187	1000	50	7.9465	21.9381
188	1000	50	7.8300	22.9025
189	1000	50	7.4969	24.0404
190	1000	50	6.9891	25.0144
191	1000	50	6.2065	25.9788
192	1000	50	5.2072	26.9528
193	1000	50	3.8958	27.9268
194	1000	50	1.9601	29.0551
195	1000	50	0.0221	29.7880
196	1000	75	8.3378	0.0761
197	1000	75	8.3192	0.9633
198	1000	75	8.3192	1.9373
199	1000	75	8.3006	2.9885
200	1000	75	8.3006	3.9625
201	1000	75	8.2796	5.0136
202	1000	75	8.2796	5.9876
203	1000	75	8.2400	6.9520
204	1000	75	8.2400	7.9260
205	1000	75	8.2400	8.9771
206	1000	75	8.2400	9.9511
207	1000	75	8.2027	10.9251
208	1000	75	8.2027	11.9763
209	1000	75	8.2027	12.9503
210	1000	75	8.1818	14.0786
211	1000	75	8.1235	14.9754
212	1000	75	8.1235	15.9398
213	1000	75	8.1049	16.9909
214	1000	75	8.0443	17.9650
215	1000	75	7.9465	18.9390
216	1000	75	7.7718	19.9901
217	1000	75	7.3199	20.9641
218	1000	75	6.7539	21.9381
219	1000	75	5.7942	23.0664
220	1000	75	4.6994	24.0404
221	1000	75	3.3088	25.0144
222	1000	75	1.6061	25.9788
223	1000	75	0.0012	26.8756

Bibliography

[1] Tomas Markvart. *Solar Electricity.* John Wiley & Sons, New York, 2 edition, 2000.

[2] Roger A. Messenger and Jerry Ventre. *Photovoltaic Systems Engineering.* CRC Press, 2nd edition, 2004.

[3] *Technology Roadmap: Solar Photovoltaic Energy.* International Energy Agency, 2010.

[4] *Solar Photovoltaics Technology Brief.* International Renewable Energy Agency, 2013.

[5] *PVPS Report Snapshot of Global PV 1992-2013: Preliminary Trends Information from the IEA PVPS Programme.* International Energy Agency, 2013.

[6] Jieming Ma, Ka Lok Man, T. O. Ting, Nan Zhang, Chi-Un Lei, and Ngai Wong. Low-cost global mppt scheme for photovoltaic systems under partially shaded conditions. In *IEEE International Symposium on Circuits and Systems (ISCAS)*, pages 245–248, 2013.

[7] Nabil A. Ahmed and Masafumi Miyatake. A novel maximum power point tracking for photovoltaic applications under partially shaded insolation conditions. *Electric Power Systems Research*, 78(5):777–784, 2008.

[8] Jieming Ma, Ka Lok Man, T. O. Ting, Nan Zhang, Chi-Un Lei, and Ngai Wong. A hybrid mppt method for photovoltaic systems via estimation and revision method. In *IEEE International Symposium on Circuits and Systems (ISCAS)*, pages 241–244, 2013.

[9] Mohammadmehdi Seyedmahmoudian, Saad Mekhilef, Rasoul Rahmani, Rubiyah Yusof, and Ehsan Renani. Analytical modeling of partially shaded photovoltaic systems. *Energies*, 6(1):128–144, 2013.

[10] Chen Liang-Rui, Tsai Chih-Hui, Lin Yuan-Li, and Lai Yen-Shin. A biological swarm chasing algorithm for tracking the pv maximum power point. *Energy Conversion, IEEE Transactions on*, 25(2):484–493, 2010.

[11] H. Patel and V. Agarwal. Maximum power point tracking scheme for pv systems operating under partially shaded conditions. *IEEE Transactions on Industrial Electronics*, 55(4):1689–1698, 2008.

[12] Xin-She Yang. *Nature-Inspired Metaheuristic Algorithm.* Luniver Press, 2nd edition, 2010.

[13] James Kennedy, Russell C. Eberhart, and Yuhui Shi. *Swarm Intelligence.* Morgan Kaufmann Publishers, 2001.

[14] Xin-She Yang and Suash Deb. Cuckoo search via levy flights. In *Proc. of World Congress on Nature & Biologically Inspired Computing*, pages 210–214. India. IEEE Publications, 2009.

[15] J. Kennedy and R. Eberhart. Particle swarm optimization. In *IEEE International Conference on Neural Networks*, volume 4, pages 1942–1948, 1995.

[16] T. Easwarakhanthan, J. Bottin, I. Bouhouch, and C. Boutrit. Nonlinear minimization algorithm for determining the solar cell parameters with microcomputers. *International Journal of Solar Energy*, 4(1):1–12, 1986.

[17] Huang Wei, Jiang Cong, Xue Lingyun, and Song Deyun. Extracting solar cell model parameters based on chaos particle swarm algorithm. In *2011 International Conference on Electric Information and Control Engineering (ICEICE)*, pages 398–402, 2011.

[18] A. Jervase Joseph, Bourdoucen Hadj, and Al-Lawati Ali. Solar cell parameter extraction using genetic algorithms. *Measurement Science and Technology*, 12(11):1922, 2001.

[19] M. F. AlHajri, K. M. El-Naggar, M. R. AlRashidi, and A. K. Al-Othman. Optimal extraction of solar cell parameters using pattern search. *Renewable Energy*, 44(0):238–245, 2012.

[20] U.S. DOE. *Annual Energy Review 2011.* Energy Information Administration (EIA), 2012.

[21] M. G. Villalva, J. R. Gazoli, and E. R. Filho. Comprehensive approach to modeling and simulation of photovoltaic arrays. *IEEE Transactions on Power Electronics*, 24(5):1198–1208, 2009.

[22] M. U. Siddiqui and M. Abido. Parameter estimation for five- and seven-parameter photovoltaic electrical models using evolutionary algorithms. *Applied Soft Computing*, 13(12):4608–4621, 2013.

[23] K. Ishaque, Z. Salam, M. Amjad, and S. Mekhilef. An improved particle swarm optimization (pso)-based mppt for pv with reduced steady-state oscillation. *IEEE Transactions on Power Electronics*, 27(8):3627–3638, 2012.

[24] M. Miyatake, M. Veerachary, F. Toriumi, N. Fujii, and H. Ko. Maximum power point tracking of multiple photovoltaic arrays: A pso approach. *IEEE Transactions on Aerospace and Electronic Systems*, 47(1):367–380, 2011.

[25] Nguyen Dzung and B. Lehman. An adaptive solar photovoltaic array using model-based reconfiguration algorithm. *IEEE Transactions on Industrial Electronics*, 55(7):2644–2654, 2008.

[26] Nguyen Dzung and B. Lehman. A reconfigurable solar photovoltaic array under shadow conditions. In *Twenty-Third Annual IEEE Applied Power Electronics Conference and Exposition*, pages 980–986, 2008.

[27] Jee-Hoon Jung and Shehab Ahmed. Real-time simulation model development of single crystalline photovoltaic panels using fast computation methods. *Solar Energy*, 86(6):1826–1837, 2012.

[28] Ali Naci Celik and Nasr Acikgoz. Modelling and experimental verification of the operating current of mono-crystalline photovoltaic modules using four- and five-parameter models. *Applied Energy*, 84(1):1–15, 2007.

[29] C. Carrero, J. Amador, and S. Arnaltes. A single procedure for helping pv designers to select silicon pv modules and evaluate the loss resistances. *Renewable Energy*, 32(15):2579–2589, 2007.

[30] Chih-Tang Sah, R. N. Noyce, and W. Shockley. Carrier generation and recombination in p-n junctions and p-n junction characteristics. *Proceedings of the IRE*, 45(9):1228–1243, 1957.

[31] Kensuke Nishioka, Nobuhiro Sakitani, Yukiharu Uraoka, and Takashi Fuyuki. Analysis of multicrystalline silicon solar cells by modified 3-diode equivalent circuit model taking leakage current through periphery into consideration. *Solar Energy Materials and Solar Cells*, 91(13):1222–1227, 2007.

[32] France Lasnier and Tony Gan Ang. *Photovoltaic Engineering Handbook*. Institute of Physics Publishing, 1990.

[33] Luis Castaner and Santiago Silvestre. *Modelling Photovoltaic Systems Using PSpice*. John Wiley & Sons Ltd., 2002.

[34] Y. Mahmoud, W. Xiao, and H. H. Zeineldin. A simple approach to modeling and simulation of photovoltaic modules. *IEEE Transactions on Sustainable Energy*, 3(1):185–186, 2012.

[35] T.U. Townsend. *A Method for Predicting the Long-Term Performance of Directly-Coupled Photovoltaic Systems*. Thesis, 1989.

[36] J. A. Duffie and W. A. Beckman. *Solar Engineering of Thermal Processes*. Wiley & Sons, Inc., New York, 2nd edition, 1991.

[37] A. Chatterjee, A. Keyhani, and D. Kapoor. Identification of photovoltaic source models. *IEEE Transactions on Energy Conversion*, 26(3):883–889, 2011.

[38] Soon Jing Jun and Low Kay-Soon. Photovoltaic model identification using particle swarm optimization with inverse barrier constraint. *Power Electronics, IEEE Transactions on*, 27(9):3975–3983, 2012.

[39] T. Tafticht and K. Agbossou. Development of a mppt method for photovoltaic systems. In *Canadian Conference on Electrical and Computer Engineering*, volume 2, 2004.

[40] Mohammad H. Moradi and Ali Reza Reisi. A hybrid maximum power point tracking method for photovoltaic systems. *Solar Energy*, 85(11):2965–2976, 2011.

[41] L. V. Hartmann, M. A. Vitorino, M. B. R. Correa, and A. M. N. Lima. Combining model-based and heuristic techniques for fast tracking the maximum-power point of photovoltaic systems. *IEEE Transactions on Power Electronics*, 28(6):2875–2885, 2013.

[42] Geoff Walker. Evaluating mppt converter topologies using a matlab pv model. *Journal of Electrical and Electronics Engineering*, 21:49–55, 2001.

[43] M. G. J. Xiao, Weidongand Lind, W. G. Dunford, and A. Capel. Real-time identification of optimal operating points in photovoltaic power systems. *IEEE Transactions on Industrial Electronics*, 53(4):1017–1026, 2006.

[44] Kashif Ishaque, Zainal Salam, and Hamed Taheri. Simple, fast and accurate two-diode model for photovoltaic modules. *Solar Energy Materials and Solar Cells*, 95(2):586–594, 2011.

[45] F. J. Garcia Sanchez, A. Ortiz-Conde, and J. J. Liou. Calculating double-exponential diode model parameters from previously extracted single-exponential model parameters. *Electronics Letters*, 31(1):71–72, 1995.

[46] M. Wolf, G. T. Noel, and Richard J. Stirn. Investigation of the double exponential in the current-voltage characteristics of silicon solar cells. *IEEE Transactions on Electron Devices*, 24(4):419–428, 1977.

[47] V. Quaschning and R. Hanitsch. Numerical simulation of photovoltaic generators with shaded cells. In *Universities Power Engineering Conference*, volume 30, pages 583–586, 1995.

[48] D. S. H. Chan and J. C. H. Phang. Analytical methods for the extraction of solar-cell single- and double-diode model parameters from i-v characteristics. *IEEE Transactions on Electron Devices*, 34(2):286–293, 1987.

[49] M. U. Siddiqui and M. Abido. Parameter estimation for five- and seven-parameter photovoltaic electrical models using evolutionary algorithms. *Applied Soft Computing*, 13(12):4608–4621, 2013.

[50] Valerio Lo Brano and Giuseppina Ciulla. An efficient analytical approach for obtaining a five parameters model of photovoltaic modules using only reference data. *Applied Energy*, 111(0):894–903, 2013.

[51] Valerio Lo Brano, Aldo Orioli, and Giuseppina Ciulla. On the experimental validation of an improved five-parameter model for silicon photovoltaic modules. *Solar Energy Materials and Solar Cells*, 105(0):27–39, 2012.

[52] Valerio Lo Brano, Aldo Orioli, Giuseppina Ciulla, and Alessandra Di Gangi. An improved five-parameter model for photovoltaic modules. *Solar Energy Materials and Solar Cells*, 94(8):1358–1370, 2010.

[53] James Vere Beck and Keneth J. Arnold. *Parameter Estimation in Engineering and Science Parameter*. Wiley series in probability and mathematical statistics, New York, 1977.

[54] Kashif Ishaque, Zainal Salam, Hamed Taheri, and Amir Shamsudin. A critical evaluation of ea computational methods for photovoltaic cell parameter extraction based on two diode model. *Solar Energy*, 85(9):1768–1779, 2011.

[55] Kashif Ishaque, Zainal Salam, Saad Mekhilef, and Amir Shamsudin. Parameter extraction of solar photovoltaic modules using penalty-based differential evolution. *Applied Energy*, 99(0):297–308, 2012.

[56] D. S. H. Chan and J. C. H. Phang. Analytical methods for the extraction of solar-cell single- and double-diode model parameters from i-v characteristics. *IEEE Transactions on Electron Devices*, 34(2):286–293, 1987.

[57] J. C. H. Phang, D. S. H. Chan, and J. R. Phillips. Accurate analytical method for the extraction of solar cell model parameters. *Electronics Letters*, 20(10):406–408, 1984.

[58] W. De Soto, S. A. Klein, and W. A. Beckman. Improvement and validation of a model for photovoltaic array performance. *Solar Energy*, 80(1):78–88, 2006.

[59] Adelmo Ortiz-Conde, Francisco J. Garca Snchez, and Juan Muci. New method to extract the model parameters of solar cells from the explicit analytic solutions of their illuminated iv characteristics. *Solar Energy Materials and Solar Cells*, 90(3):352–361, 2006.

[60] M. A. de Blas, J. L. Torres, E. Prieto, and A. Garca. Selecting a suitable model for characterizing photovoltaic devices. *Renewable Energy*, 25(3):371–380, 2002.

[61] R. Gottschalg, M. Rommel, D. G. Infield, and M. J. Kearney. The influence of the measurement environment on the accuracy of the extraction of the physical parameters of solar cells. *Measurement Science and Technology*, 10(9):796, 1999.

[62] H. Mullejans, J. Hyvarinen, J. Karila, and E. D. Dunlop. Reliability of the routine 2-diode model fitting of pv modules. In *19th European Photovoltaic Solar Energy Conference*, page 2459, 2004.

[63] J. Appelbaum, A. Chait, and D. Thompson. Parameter estimation and screening of solar cells. *Progress in Photovoltaics: Research and Applications*, 1(2):93–106, 1993.

[64] P. Wolf and V. Benda. Identification of pv solar cells and modules parameters by combining statistical and analytical methods. *Solar Energy*, 93(0):151–157, 2013.

[65] R Gottschalg, M Rommel, DG Infield, and H Ryssel. Comparison of different methods for the parameter determination of the solar cells double exponential equation. *Proceedings of the 14th European Photovoltaic Solar Energy Conference (PVSEC), Barcelona, Spain*, pages 321–324, 1997.

[66] *PSIM Users Guide*. Powersim Inc., 2010.

[67] H. Bayhan and M. Bayhan. A simple approach to determine the solar cell diode ideality factor under illumination. *Solar Energy*, 85(5):769–775, 2011.

[68] GH Yordanov, OM Midtgrd, and TO Saetre. Two-diode model revisited: Parameters extraction from semi-log plots of iv data. *25th European Photovoltaic Solar Energy Conference*, 2010.

[69] R. C. Eberhart and Shi Yuhui. Particle swarm optimization: developments, applications and resources. In *Proceedings of the 2001 Congress on Evolutionary Computation*, volume 1, pages 81–86, 2001.

[70] M. Clerc and J. Kennedy. The particle swarm - explosion, stability, and convergence in a multidimensional complex space. *IEEE Transactions on Evolutionary Computation*, 6(1):58–73, 2002.

[71] Soon Jing Jun and Low Kay-Soon. Photovoltaic model identification using particle swarm optimization with inverse barrier constraint. *IEEE Transactions on Power Electronics*, 27(9):3975–3983, 2012.

[72] Meiying Ye, Xiaodong Wang, and Yousheng Xu. Parameter extraction of solar cells using particle swarm optimization. *Journal of Applied Physics*, 105(9):094502–8, 2009.

[73] N. Rajasekar, Neeraja Krishna Kumar, and Rini Venugopalan. Bacterial foraging algorithm based solar pv parameter estimation. *Solar Energy*, 97(0):255–265, 2013.

[74] K. M. El-Naggar, M. R. AlRashidi, M. F. AlHajri, and A. K. Al-Othman. Simulated annealing algorithm for photovoltaic parameters identification. *Solar Energy*, 86(1):266–274, 2012.

[75] Kashif Ishaque, Zainal Salam, Saad Mekhilef, and Amir Shamsudin. Parameter extraction of solar photovoltaic modules using penalty-based differential evolution. *Applied Energy*, 99(0):297–308, 2012.

[76] W. T. da Costa, J. F. Fardin, D. S. L. Simonetti, and L. de V. B. M. Neto. Identification of photovoltaic model parameters by differential evolution. In *IEEE International Conference on Industrial Technology (ICIT)*, pages 931–936, 2010.

[77] Jieming Ma, T. O. Ting, Ka Lok Man, Nan Zhang, Sheng-Uei Guan, and Prudence W. H. Wong. Parameter estimation of photovoltaic models via cuckoo search. *Journal of Applied Mathematics*, 2013:8, 2013.

[78] J. T. Bialasiewicz. Renewable energy systems with photovoltaic power generators: Operation and modeling. *Industrial Electronics, IEEE Transactions on*, 55(7):2752–2758, 2008.

[79] Pallavee Bhatnagar and R. K. Nema. Maximum power point tracking control techniques: State-of-the-art in photovoltaic applications. *Renewable and Sustainable Energy Reviews*, 23(0):224–241, 2013.

[80] Emilio Mamarelis, Giovanni Petrone, and Giovanni Spagnuolo. A two-steps algorithm improving the p&o steady state mppt efficiency. *Applied Energy*, 113(0):414–421, 2014.

[81] E. Roman, R. Alonso, P. Ibanez, S. Elorduizapatarietxe, and D. Goitia. Intelligent pv module for grid-connected pv systems. *IEEE Transactions on Industrial Electronics*, 53(4):1066–1073, 2006.

[82] K. Kobayashi, I. Takano, and Y. Sawada. A study on a two stage maximum power point tracking control of a photovoltaic system under partially shaded insolation conditions. In *IEEE Power Engineering Society General Meeting*, volume 4, page 2617 Vol. 4, 2003.

[83] V. Salas, E. Olas, A. Barrado, and A. Lzaro. Review of the maximum power point tracking algorithms for stand-alone photovoltaic systems. *Solar Energy Materials and Solar Cells*, 90(11):1555–1578, 2006.

[84] Hua Chihchiang, Lin Jongrong, and Shen Chihming. Implementation of a dsp-controlled photovoltaic system with peak power tracking. *IEEE Transactions on Industrial Electronics*, 45(1):99–107, 1998.

[85] HS-H Chung, KK Tse, SY Ron Hui, CM Mok, and MT Ho. A novel maximum power point tracking technique for solar panels using a sepic or cuk converter. *Power Electronics, IEEE Transactions on*, 18(3):717–724, 2003.

[86] N. Femia, G. Petrone, G. Spagnuolo, and M. Vitelli. Optimization of perturb and observe maximum power point tracking method. *Power Electronics, IEEE Transactions on*, 20(4):963–973, 2005.

[87] K. H. Hussein, I. Muta, T. Hoshino, and M. Osakada. Maximum photovoltaic power tracking: an algorithm for rapidly changing atmospheric conditions. *IEE Proceedings of Generation, Transmission and Distribution*, 142(1):59–64, 1995.

[88] Chun Seunghyun and A. Kwasinski. Analysis of classical root-finding methods applied to digital maximum power point tracking for sustainable photovoltaic energy generation. *IEEE Transactions on Power Electronics*, 26(12):3730–3743, 2011.

[89] Chun Seunghyun and A. Kwasinski. Modified regula falsi optimization method approach to digital maximum power point tracking for photovoltaic application. In *Twenty-Sixth Annual IEEE Applied Power Electronics Conference and Exposition (APEC)*.

[90] H. E. S. A. Ibrahim, F. F. Houssiny, H. M. Z. El-Din, and M. A. El-Shibini. Microcomputer controlled buck regulator for maximum power point tracker for dc pumping system operates from photovoltaic system. In *1999 IEEE International Fuzzy Systems Conference Proceedings*, volume 1, pages 406–411 vol.1, 1999.

[91] S. Kurokami and N. Takehara. Power control apparatus and method and power generating system using them, 1997.

[92] M. Veerachary, T. Senjyu, and K. Uezato. Voltage-based maximum power point tracking control of pv system. *IEEE Transactions on Aerospace and Electronic Systems*, 38(1):262–270, 2002.

[93] Yu-yun Chen and Yong-kui Man. Constant current-based maximum-power-point tracking for photovoltaic power systems. In *Control and Decision Conference*, pages 3422–3425, 2009.

[94] Jieming Ma, Ka Lok Man, TO Ting, Hyunshin Lee, Taikyeong Jeong, Jong-Kug Sean, Sheng-Uei Guan, and Prudence WH Wong. *Insight of Direct Search Methods and Module-Integrated Algorithms for Maximum Power Point Tracking (MPPT) of Stand-Alone Photovoltaic Systems*, pages 463–471. Springer, 2012.

[95] Pallavee Bhatnagar and R. K. Nema. Maximum power point tracking control techniques: State-of-the-art in photovoltaic applications. *Renewable and Sustainable Energy Reviews*, 23(0):224–241, 2013.

[96] Kashif Ishaque, Zainal Salam, and George Lauss. The performance of perturb and observe and incremental conductance maximum power point tracking method under dynamic weather conditions. *Applied Energy*, 119(0):228–236, 2014.

[97] Xiao Weidong and W. G. Dunford. A modified adaptive hill climbing mppt method for photovoltaic power systems. In *IEEE 35th Annual Power Electronics Specialists Conference*, volume 3, pages 1957–1963 Vol.3.

[98] Richard L. Burden and J. Douglas Faires. *Numerical Analysis*. Cengage Learning, 2010.

[99] John H. Mathews and Kurtis D. Fink. *Numerical Methods Using MATLAB*. Person Eduation, Inc., 4th edition, 2004.

[100] Review of the maximum power point tracking algorithms for stand-alone photovoltaic systems. *Solar Energy Materials and Solar Cells*, 90(11):1555 – 1578, 2006.

[101] T. Esram and P. L. Chapman. Comparison of photovoltaic array maximum power point tracking techniques. *IEEE Transactions on Energy Conversion*, 22(2):439–449, 2007.

[102] T. Noguchi, S. Togashi, and R. Nakamoto. Short-current pulse based adaptive maximum-power-point tracking for photovoltaic power generation system. In *IEEE International Symposium on Industrial Electronics*, volume 1, pages 157–162 vol.1, 2000.

[103] Kashif Ishaque and Zainal Salam. A review of maximum power point tracking techniques of pv system for uniform insolation and partial shading condition. *Renewable and Sustainable Energy Reviews*, 19(0):475–488, 2013.

[104] S. Daraban, D. Petreus, and C. Morel. A novel global mppt based on genetic algorithms for photovoltaic systems under the influence of partial shading. In *39th Annual Conference of the IEEE Industrial Electronics Society*, pages 1490–1495, 2013.

[105] Jubaer Ahmed and Zainal Salam. A maximum power point tracking (mppt) for pv system using cuckoo search with partial shading capability. *Applied Energy*, 119(0):118–130, 2014.

[106] Xing Jie and Xiao Deyun. New metropolis coefficients of particle swarm optimization. In *Chinese Control and Decision Conference*, pages 3518–3521, 2008.

[107] Xin-She Yang and Suash Deb. Engineering optimisation by cuckoo search. *Int. J. Mathematical Modelling and Numerical Optimisation*, 1(4):330–343, 2010.

[108] Kashif Ishaque, Zainal Salam, Amir Shamsudin, and Muhammad Amjad. A direct control based maximum power point tracking method for photovoltaic system under partial shading conditions using particle swarm optimization algorithm. *Applied Energy*, 99(0):414–422, 2012.

[109] Mohammad Faridun Naim Tajuddin, Shahrin Md Ayob, Zainal Salam, and Mohd Sazli Saad. Evolutionary based maximum power point tracking technique using differential evolution algorithm. *Energy and Buildings*, 67(0):245–252, 2013.

[110] Badia Amrouche, Abderrezak Guessoum, and Maiouf Belhamel. A simple behavioural model for solar module electric characteristics based on the first order system step response for mppt study and comparison. *Applied Energy*, 91(1):395–404, 2012.

[111] Aldo Orioli and Alessandra Di Gangi. A procedure to calculate the five-parameter model of crystalline silicon photovoltaic modules on the basis of the tabular performance data. *Applied Energy*, 102(0):1160–1177, 2013.

[112] J. P. Charles, G. Bordure, A. Khoury, and P. Mialhe. Consistency of the double exponential model with physical mechanisms of conduction for a solar cell under illumination. *Journal of Physics D: Applied Physics*, 18(11):2261, 1985.

[113] H. Bayhan and A. Sertap Kavasoglu. Exact Analytical Solution of the Diode Ideality Factor of a pn Junction Device Using Lambert W-function Model. *Turkish Journal of Physics*, 31:7–10, January 2007.

[114] Alireza Askarzadeh and Alireza Rezazadeh. Parameter identification for solar cell models using harmony search-based algorithms. *Solar Energy*, 86(11):3241–3249, 2012.

[115] K. Bouzidi, M. Chegaar, and N. Nehaoua. New method to extract theparameters of solar cells from their illuminated i-v curve. In *4th International Conference on Computer Integrated Manufacturing*, 2007.

[116] Rosario Nunzio Mantegna. Fast, accurate algorithm for numerical simulation of lvy stable stochastic processes. *Physical Review E*, 49(5):4677–4683, 1994. PRE.

[117] AmirHossein Gandomi, Xin-She Yang, and AmirHossein Alavi. Cuckoo search algorithm: a metaheuristic approach to solve structural optimization problems. *Engineering with Computers*, 29(1):17–35, 2013.

[118] X. Yang. Cuckoo search algorithm (source code). `http://www.mathworks.com/matlabcentral/fileexchange/29809-cuckoo-search-cs-algorithm`.

[119] Pinar Civicioglu and Erkan Besdok. A conceptual comparison of the cuckoo-search, particle swarm optimization, differential evolution and artificial bee colony algorithms. *Artificial Intelligence Review*, 39(4):315–346, 2013.

[120] M. Bashahu and P. Nkundabakura. Review and tests of methods for the determination of the solar cell junction ideality factors. *Solar Energy*, 81(7):856–863, 2007.

[121] The MathWorks Inc. Optimization toolbox. `http://www.mathworks.com/products/optimization/index.html`.

[122] B. Birge. Particle swarm optimization toolbox. `http://www.mathworks.com/matlabcentral/fileexchange/7506-particleswarm-optimization-toolbox`.

[123] Benedict Gaster, Lee Howes, David R. Kaeli, Perhaad Mistry, and Dana Schaa. *Heterogeneous Computing with OpenCL: Revised OpenCL*. Morgan Kaufmann Publishers, 2nd edition, 2012.

[124] Luca Mussi, Fabio Daolio, and Stefano Cagnoni. Evaluation of parallel particle swarm optimization algorithms within the cuda architecture. *Information Sciences*, 181(20):4642–4657, 2011.

[125] Benedict Gaster, Lee Howes, David R. Kaeli, Perhaad Mistry, and Dana Schaa. *Heterogeneous Computing with OpenCL*. Elsevier, 2nd edition, 2012.

[126] G. Venter and J. Sobieszczanski-Sobieski. Multidisciplinary optimization of a transport aircraft wing using particle swarm optimization. *Structural and Multidisciplinary Optimization*, 26(1-2):121–131, 2004.

[127] D. H. Wolpert and W. G. Macready. No free lunch theorems for optimization. *IEEE Transactions on Evolutionary Computation*, 1(1):67–82, 1997.

[128] Dezso Sera. *Real-time Modelling, Diagnostics and Optimised MPPT for Residential PV systems*. Thesis, 2009.

[129] H Haeberlin, L Borgna, M Kaempfer, and U Zwahlen. Measurement of dynamic mpp-tracking efficiency at grid-connected pv inverters. In *21st Europe PV Conference*.

[130] Kashif Ishaque, Zainal Salam, and Syafaruddin. A comprehensive matlab simulink pv system simulator with partial shading capability based on two-diode model. *Solar Energy*, 85(9):2217–2227, 2011.

[131] Jieming Ma, Ka Lok Man, T. O. Ting, Nan Zhang, Sheng-Uei Guan, and Prudence W. H. Wong. Approximate single-diode photovoltaic model for efficient i-v characteristics estimation. *The Scientific World Journal*, 2013:7, 2013.

[132] M. A. S. Masoum, H. Dehbonei, and E. F. Fuchs. Theoretical and experimental analyses of photovoltaic systems with voltageand current-based maximum power-point tracking. *IEEE Transactions on Energy Conversion*, 17(4):514–522, 2002.

[133] L. Cristaldi, M. Faifer, M. Rossi, and S. Toscani. An improved model-based maximum power point tracker for photovoltaic panels. *IEEE Transactions on Instrumentation and Measurement*, 63(1):63–71, 2014.

[134] Wang Xiaolei, Jiang Huai-zhen, Yang Liang, and Yan Pan. A new method of mppt control based on the model of photovoltaic array. In *Power and Energy Engineering Conference (APPEEC), 2011 Asia-Pacific*, pages 1–3.

[135] Lei Pan, Wei Gong, and Yinghong Wang. Maximum power point tricking control of solar photovoltaic power generation system based on model reference adaptive. In *International Conference on Sustainable Power Generation and Supply*, pages 1–5.

[136] Amit Jain, Sandeep Sharma, and Avinashi Kapoor. Solar cell array parameters using lambert w-function. *Solar Energy Materials and Solar Cells*, 90(1):25–31, 2006.

[137] Amit Jain and Avinashi Kapoor. Exact analytical solutions of the parameters of real solar cells using lambert w-function. *Solar Energy Materials and Solar Cells*, 81(2):269–277, 2004.

[138] Jee-Hoon Jung and Shehab Ahmed. Real-time simulation model development of single crystalline photovoltaic panels using fast computation methods. *Solar Energy*, 86(6):1826–1837, 2012.

[139] Cleve Moler. *Numerical Computing with MATLAB*. SIAM, 2004.

[140] M. G. Villalva, J. R. Gazoli, and E. R. Filho. Comprehensive approach to modeling and simulation of photovoltaic arrays. *IEEE Transactions on Power Electronics*, 24(5):1198–1208, 2009.

[141] Lele Peng, Yize Sun, Zhuo Meng, Yuling Wang, and Yang Xu. A new method for determining the characteristics of solar cells. *Journal of Power Sources*, 227(0):131–136, 2013.

[142] Won Young Yang, Wenwu Cao Cao, Tae-Sang Chung, and John Morris. *Applied numerical methods using MATLAB*. John Wiley & Sons, Inc, 2005.

[143] Guihua Liu, Panbao Wang, Wei Wang, and Qi Wang. *MPPT Algorithm Under Partial Shading Conditions*, pages 91–98. Springer, 2012.

[144] K. Deb, A. Pratap, S. Agarwal, and T. Meyarivan. A fast and elitist multiobjective genetic algorithm: Nsga-ii. *IEEE Transactions on Evolutionary Computation*, 6(2):182–197, 2002.

[145] Yao Xin, Liu Yong, and Lin Guangming. Evolutionary programming made faster. *IEEE Transactions on Evolutionary Computation*, 3(2):82–102, 1999.

[146] J. Brest, S. Greiner, B. Boskovic, M. Mernik, and V. Zumer. Self-adapting control parameters in differential evolution: A comparative study on numerical benchmark problems. *IEEE Transactions on Evolutionary Computation*, 10(6):646–657, 2006.

[147] Anula Khare and Saroj Rangnekar. A review of particle swarm optimization and its applications in solar photovoltaic system. *Applied Soft Computing*, 13(5):2997–3006, 2013.

[148] T. O. Ting, Ka Lok Man, Sheng-Uei Guan, Mohamed Nayel, and Kaiyu Wan. *Weightless Swarm Algorithm (WSA) for Dynamic Optimization Problems*, volume 7513 of *Lecture Notes in Computer Science*, book section 60, pages 508–515. Springer Berlin Heidelberg, 2012.

[149] T. O. Ting, Ka Lok Man, Sheng-Uei Guan, JK Seon, TT Jeong, and Prudence WH Wong. Maximum power point tracking (mppt) via weightless swarm algorithm (wsa) on cloudy days. In *IEEE Asia Pacific Conference on Circuits and Systems (APCCAS)*, pages 336–339, 2012.

[150] Daniel W. Hart. *Power Electronics*. McGraw-Hill, 2010.

[151] M. Veerachary and H. Khas. PSIM circuit-oriented simulator model for the nonlinear photovoltaic sources. *IEEE Transactions on Aerospace Electronic Systems*, 42:735–740, April 2006.

[152] Wei Gu. *Designing A SEPIC Converter*. National Semiconductor, 2007.